PRECISE ORBIT DETERMINATION OF LOW EARTH ORBITERS WITH A SINGLE GPS RECEIVER-BASED, GEOMETRIC STRATEGY

SUNIL BISNATH

February 2004

TECHNICAL REPORT NO. 220

PRECISE ORBIT DETERMINATION OF LOW EARTH ORBITERS WITH A SINGLE GPS RECEIVER-BASED, GEOMETRIC STRATEGY

Sunil Bisnath

Department of Geodesy and Geomatics Engineering
University of New Brunswick
P.O. Box 4400
Fredericton, N.B.
Canada
E3B 5A3

February 2004

PREFACE

This technical report is a reproduction of a dissertation submitted in partial fulfillment of the requirements for the degree of Doctor of Philosophy in the Department of Geodesy and Geomatics Engineering, February 2004. The research was supervised by Dr. Richard Langley, and funding was provided by NSERC, the Natural Sciences and Engineering Research Council of Canada with additional support from GEOIDE, the Geomatics for Informed Decisions Network of Centres of Excellence.

As with any copyrighted material, permission to reprint or quote extensively from this report must be received from the author. The citation to this work should appear as follows:

Bisnath, S. (2004). Precise Orbit Determination of Low Earth Orbiters with a Single GPS Receiver-Based, Geometric Strategy. Ph.D. dissertation, Department of Geodesy and Geomatics Engineering Technical Report No. 220, University of New Brunswick, Fredericton, New Brunswick, Canada, 143 pp.

ABSTRACT

One application of the Global Positioning System (GPS) involves placing GPS receivers aboard earth orbiting space vehicles to provide *in situ* tracking information to aid in platform precise orbit determination (POD). In the mid-1990s, the most advanced high-precision form of GPS-based orbits was being produced by hybrid classical orbit determination and GPS-based techniques. Given the inherent complexity and computational cost of producing dynamics-based orbits, I began studying if a GPS-only orbit could be determined and if so, how accurate and precise it could be.

A much less complex, direct and therefore very efficient approach became apparent after iteration: to use an augmented form of undifferenced GPS positioning by processing simultaneous measurements from the LEO receiver and precise GPS satellite ephemerides and clock offsets. Pseudorange observables are used to provide coarse position solutions and time-differenced, carrier phase observables are used to provide precise position change. To avoid constantly changing GPS satellite-to-receiver pairs, carrier smoothing of the pseudoranges is performed in the position domain. The resulting solution represents a kinematic, sequential, least-squares filter / smoother. The stand-alone positioning mode coupled with the fundamental dynamics-free nature of the processing engine resulted in solidifying the two foundations the final geometric strategy filter is based on.

The thesis question has been answered positively: LEO POD with a GPS-only solution utilising a single GPS receiver is possible. The processed results show that near-decimetre-level accuracy is attainable when compared against high-calibre hybrid

dynamics / GPS orbits for the CHAMP satellite. A number of refinements and additions to this research have also been proposed.

ACKNOWLEDGEMENTS

I would like to thank my advisor, Richard Langley, for giving me the opportunity to perform this research and to enter the scientific community.

I thank the great group of lifelong friends that I have made during the Ph.D. years, who are as diverse as they are interesting. Fredericton has been a doorway to the world.

This dissertation is dedicated to my family: Janki, Dulcie, Diana, Ann, Carol, Troy, and Alyssa, without whom I would not have found the courage and persistence to travel this road.

TABLE OF CONTENTS

LIST OF FIGURES

LIST OF TABLES

LIST OF SYMBOLS

A	(various)	design (measurement partials) matrix
C	(various)	variance-covariance matrix
E	(deg)	eccentric anomaly
F	($kg \cdot m^3/s^2$)	force vector
F	(various)	forward filter weight matrix
G	(various)	true observation matrix
GM	(m^3/s^2)	earth's gravitational constant
I	(m)	ionospheric delay or advance
M	(deg)	mean anomaly
M	(m)	pseudorange multipath
N	(unitless)	carrier phase integer ambiguity
P	(m)	pseudorange measurement
P	(m/s^2)	perturbing accelerations
P	(various)	weight matrix
R	(various)	reverse filter weight matrix
T	(m)	tropospheric delay
T_{rel}	(s)	periodic relativity
X	(various)	state vector
Y	(various)	observation vector
a	(m)	semi-major axis
c	(m/s)	vacuum speed of light
dTRK	(m)	pseudorange dynamics-induced tracking error
dtrk	(m)	carrier phase dynamics-induced tracking error
e	(unitless)	eccentricity
e	(m)	pseudorange random noise
i	(deg)	inclination
k	(various)	Lagrange correlates vector
m	(m)	carrier phase multipath

n	(rad/s)	mean motion
pm	(m)	pseudo-multipath
r	(m)	geocentric position vector
v	(various)	residual vector
w	(various)	misclosure vector
Φ	(m)	carrier phase measurement
Ω	(deg)	right ascension of ascending node
$\delta\mathbf{x}$	(various)	corrections vector
ε	(m)	carrier phase random noise
λ	(m)	GPS signal wavelength
ρ	(m)	geometric range
σ	(various)	standard deviation
τ	(s)	time constant in dynamic model
ω	(deg)	argument of perigee
$\nabla\Delta$	(unitless)	btw. transmitter and btw. receiver double difference
ℓ	(various)	observation vector

1. INTRODUCTION

The Global Positioning System (GPS) was initially developed by the United States Department of Defense to provide global timing, positioning and navigation capabilities to U.S. and allied forces. The basic operation of GPS involves the measurement, with a GPS receiver, of electromagnetic waves transmitted by the earth-orbiting GPS satellite constellation and the computation of the travel time of these received signals. The time measurements are converted to distance measurements, which can then be used to trilaterate the unknown position and time of the receiver from the known positions of the satellite transmitters and signal transmit times. A number of excellent books describe the principles of GPS; some examples are, for introductions: Wells *et al.* [1987] and El-Rabbany [2002]; to describe the fundamental GPS operation and processing equations: Leick [1995], Hofmann-Wellenhof *et al.* [2001], Teunissen and Kleusburg [1998] and Misra and Enge [2001]; and to describe fundamental operation and application areas: Janiczek [1980] and Parkinson and Spilker [1996].

Given the original purpose of GPS, a vast array of additional applications and processing schemes have been and are being devised. One such application involves placing GPS receivers aboard earth orbiting space vehicles to provide tracking information (*in situ* range, range-rate, position, and velocity) to aid in platform orbit determination. The determination of artificial satellite orbits has been intensely studied for the past half-century and this progress is well represented in many books including Escobal [1976], Roy [1982], and recently Montenbruck and Gill [2000]. In the early development of GPS, it was observed that the precise, global coverage and ease of use of GPS could significantly improve the determination of orbits of Low Earth Orbiters

(LEOs). One of the first prediction scenarios was using GPS to track the U.S. Space Shuttle [Van Leeuwen *et al.*, 1980], with the first civilian satellite to carry a receiver being Landsat 4 in 1982 [Birmingham, *et al.*, 1983].

As the need for more precise, time-stamped locations of LEOs has grown in recent years, the demand for GPS-based solutions has grown as well. On the Spaceborne GPS (SGPS) Internet site that I created and maintained [Bisnath, 1999] at the University of New Brunswick (UNB), an attempt was made to provide a log of civilian SGPS launches and applications. These applications have been classified as: real-time orbit determination; precise (post-processed) orbit determination (POD); attitude determination; relative positioning; and time synchronization. Dozens of SGPS receivers are presently in orbit with more planned involving innovative applications.

1.1. Research Motivation and Thesis Statement

In the mid 1990s, UNB was contracted by the Canadian Space Agency to investigate the use of GPS for space applications. One of these contracts pertained to the use of GPS for orbit determination of a small or micro-satellite. I co-authored the report [Bisnath and Langley, 1996], a by-product of which was the SGPS Internet site previously described. This contract fuelled my interest in GPS-based orbit determination research.

At the time, the most advanced high-precision form of GPS-based orbits was being produced by a hybrid classical orbit determination and GPS-based technique called "reduced dynamics" developed at the Jet Propulsion Laboratory (JPL) (see, *e.g.*, Wu *et al.* [1991] and Wu and Melbourne [1993]). This strategy provides a Kalman filter

mechanism to near-optimally combine the classical technique's complex dynamic models describing the LEO motion and the relative carrier phase-based measurements of position provided by GPS. (A more detailed account of this technique is given in Chapter 2.) Given that this strategy appears to be an ultimate solution: improvements in orbit accuracy can come only from improved dynamics, more precise GPS measurements, or improved tuning of the Kalman filter, and not an improvement over the orbit determination strategy itself, I began to look elsewhere for research advancement.

One area of interest was situations where GPS provided more accurate, yet less precise orbit positions over dynamic models. Especially at lower altitudes (*e.g.*, less than approximately 1000 km), the low resolution of geopotential and drag models meant that *oversmoothing* of LEO trajectories were of concern. Also, given the inherent complexity and computational cost of producing dynamics-based orbits, I began studying if a GPS-only orbit could be determined and if so, how accurate and precise could it be. The question posed was: Can precise orbit determination of a LEO be accomplished with a GPS-only solution? With the removal of the intentional GPS satellite clock degradation referred to as Selective Availability (SA) by the United States government, the thesis question became: Is POD of LEOs possible with a GPS-only solution and a single spaceborne GPS receiver? That is, all POD strategies were based on the use of spaceborne and terrestrial receivers jointly producing relative LEO positions and the removal of SA, as will be explained in Chapter 5, allowed for this situation to change. Given the nature of the processing strategy developed, as will be explained in Chapter 3, the technique discussed in this dissertation can be generalized to pertain to all platforms, even though LEOs were the primary focus of this research.

1.2. CONTRIBUTIONS OF THIS RESEARCH

The primary and overriding contribution of the research reported here is that the thesis question is answered – positively: LEO POD is possible with a single GPS receiver aboard the LEO. This answer is given with a number of caveats that are provided in the body of the dissertation. Quantitative descriptions of the precision and accuracy of these orbits and required processing costs are also provided.

A GPS data processing strategy has been devised to address the thesis statement outlined. The technique, referred to as the geometric strategy for POD, represents the novel combination and application of existing algorithms and research, along with recent technological improvements and advances in GPS measurement collection.

A simulation capability was developed to prove that the concept of a GPS-only POD solution was possible. This solution error simulator was created in software as the first stage of fulfilling the goal of the thesis.

The algorithms and processing software were developed to compute POD solutions. The derived positioning filter was realised in software, along with numerous other preprocessing, processing, and post-processing modules.

This research allowed UNB to participate in international studies of the use of GPS in precise orbit determination under the auspices of the International GPS Service (IGS), and cooperate with the Deutsches Zentrum für Luft- und Raumfahrt (DLR).

The other result of the research, aside from the developed processing software, has been the generation of numerous papers, presentations, and reports, many of which are referred to in this dissertation.

1.3. OUTLINE OF DISSERTATION

The outline of the remainder of the dissertation is now provided. The logical progression of thought is presented as clearly and concisely as possible, though the rapid advancement of GPS technology and research means that the state of the art and research environment changed significantly over the course of this research. Therefore some material is presented chronologically to provide greater understanding as to the methodology followed. Where necessary, appendices provide additional information concerning mathematical derivation and practicalities of the developed software.

Chapter 2 reviews the principles of classical orbit determination and contemporary methods of precise orbit determination with GPS. Attention is given to the boon that GPS has become in terms of an additional or sole position-tracking sensor.

This concise examination assists in the creation of the UNB geometric strategy presented in Chapter 3. The logical development of the strategy, separate from existing strategies, but based on previously developed GPS data processing algorithms and technological changes is given. Detailed derivations of the generic positioning filter and the specific LEO POD models are provided.

In Chapter 4, the proof of concept study for the processing approach is presented. It was an elementary investigation designed to determine if the use of the developed

processing strategy was feasible. The approach relies on the law of propagation of error and simulated LEO / GPS satellites / reference GPS receivers geometry and precision.

The rationale for the revised (present) processing strategy is given in Chapter 5. Descriptions of the updated algorithms and a detailed account of the software realisation is also provided. The changes in the strategy allow for not only a more streamlined POD process, but for a solidifying of the underlying processing philosophy.

Chapter 6 contains the processing results from the geometric strategy processor. Numerous datasets were investigated, but the processing centred on a number of datasets from the CHAMP satellite. Analysis and resulting software modifications are presented, as well as descriptions of the precision and accuracy of the determined orbits.

Chapter 7 gives conclusions, recommendations for further research, and provides a discussion of the potential of this form of GPS data processing for spaceborne applications and for other platforms.

Finally, a complete reference list is provided in Chapter 8.

2. REVIEW OF CONTEMPORARY LOW EARTH ORBITER PRECISE ORBIT DETERMINATION STRATEGIES

The goal of determining the path, trajectory, or orbit of a heavenly body, that is astrodynamics, represents one of the oldest realms of science. No attempt is made here to review the long and interesting history of the developments in this field. Rather an attempt is made in section 2.1 to describe the fundamentals of orbit determination. And section 2.2 describes the great aid that GPS measurements have brought to this determination process by comparing GPS measurements against those from conventional tracking techniques, and details the forms of GPS-based precise orbit determination in existence at the outset of this dissertation research.

2.1. CLASSICAL ORBIT DETERMINATION

In astrodynamics, orbit determination refers to deriving orbital parameters from observations [Seeber, 1993]. More specifically, satellite orbit determination refers to the reduction of tracking measurements of a spacecraft that are influenced by both random and systematic errors, using a mathematical force model that is not exact, to derive the best estimate of the orbital parameters which fully describe the spacecraft's motion at any other time (after Tapley [1989]). To ease computational complexity, this problem has traditionally been subdivided into two components (*e.g.*, Escobal [1976]): preliminary orbit determination and differential correction of orbits (or orbit improvement [Roy, 1982]).

2.1.1. Stages of Orbit Determination

The first phase of orbit determination consists of determining an approximate orbit from a minimum set of observations of the spacecraft. This represents two-body motion in celestial mechanics. That is, only the mutual attraction of the two bodies, assumed to be point masses, is taken into account. Mathematically, from Newton's second law of motion and law of gravitation the following second-order differential vector equations can be developed:

$$\ddot{\mathbf{r}} = -\frac{GM}{r^3}\mathbf{r}, \tag{2.1}$$

where $\ddot{\mathbf{r}}$ is the acceleration vector of the spacecraft, GM is the earth's gravitational constant, and $\mathbf{r}$ is the geocentric position vector of the spacecraft. The solution of equations (2.1) requires six constants of integration: three for the first integration (velocity constants) and three for the second integration (position constants). These constants are the elements of the orbit, also referred to as the spacecraft state vector:

$$\left(x_{t_0}, y_{t_0}, z_{t_0}, \dot{x}_{t_0}, \dot{y}_{t_0}, \dot{z}_{t_0}\right) \tag{2.2}$$

evaluated for some specific epoch t_0. The state can be represented by a variety of parameter representations (see, *e.g.*, Escobal [1976]) including the familiar Keplerian elements

$$\left(a_{t_0}, e_{t_0}, i_{t_0}, \Omega_{t_0}, \omega_{t_0}, \text{ and } n_{t_0}, E_{t_0}, \text{or } M_{t_0}\right), \tag{2.3}$$

where a is the orbit semi-major axis, e is the eccentricity, i is the inclination, Ω is the right ascension of the ascending node, ω is the argument of perigee, n is the mean

motion, E is the eccentric anomaly, and M is the mean anomaly. A number of methods have been developed for preliminary orbit determination based on the observation type, including those developed by Gauss, Laplace, Herrick and Gibbs, and Gibbs [Escobal, 1976].

The second phase of orbit determination consists of collecting more observations (tracking measurements) to the spacecraft and fitting these data to an orbit by some systematic mathematical means, usually by the method of least-squares, the result being (differential) corrections to the preliminary orbit's parameters [Roy, 1982]. This problem can be defined by expanding equations (2.1) to take into account perturbing accelerations:

$$\ddot{\mathbf{r}} = -\frac{GM}{r^3}\mathbf{r} + \mathbf{P}, \tag{2.4}$$

where $\ddot{\mathbf{r}}$, GM and $\mathbf{r}$ are as defined in equations (2.1), and $\mathbf{P}$ represents the vectorial sum of the perturbing accelerations acting on the spacecraft. The primary perturbing accelerations consist of accelerations due to the non-sphericity of the earth and the inhomogeneity of the earth's mass density; other celestial bodies (particularly the sun, moon, and other planets); solid earth and ocean tides; atmospheric drag; direct and indirect solar radiation pressure; relativistic effects; and maneuvering thrusters [Seeber, 1993]. The magnitudes of these accelerations are functions of a number of parameters, most importantly spacecraft altitude.

With advances in electronic computing, this latter phase of orbit determination is no longer separated from the former [Seeber, 1993].

2.1.2. Solution to the Orbit Determination Problem

Following Tapley [1989], equations (2.4) can be expressed as a system of *n* non-linear first-order differential equations

$$\dot{\mathbf{X}} = \mathbf{F}(\mathbf{X}, t) \qquad \mathbf{X}(t_0) = \mathbf{X_0}, \tag{2.5}$$

where the state vector **X** has been augmented to include spacecraft position, velocity, and a set of time-invariant model constants. **F**(t) is the force vector and $\mathbf{X_0}$ is the known state at some initial epoch. The observations to the spacecraft can be represented by the non-linear equations

$$\mathbf{Y_i} = \mathbf{G}(\mathbf{X_i}, t_i) + \boldsymbol{\varepsilon}_i \qquad (i = 1, ..., p), \tag{2.6}$$

where a set of *p* observations $\mathbf{Y_i}$ are made at epochs $t_1, ..., t_p$, $\mathbf{G}(\mathbf{X_i}, t_i)$ represents the true observations, and $\boldsymbol{\varepsilon}_i$ represents random measurement errors. Equations (2.5) can be solved as

$$\mathbf{X}(t_i) = \Theta(\mathbf{X_0}, t_0, t_i). \tag{2.7}$$

The solution can be performed by analytical or numerical integration; but with present-day computing power, the latter is more prevalent. Numerical integration requires an orbit determination method and a numerical integration algorithm [Seeber, 1993]. The orbit determination method refers to the formulation of the equations of motion, such as Cowell's method and Encke's method [Roy, 1982]. Equation (2.5) follows Cowell's method. The spacecraft state for a particular epoch is then calculated using a numerical

integration technique, such as the Euler method, multi-step methods, Runge-Kutta methods, or collocation methods [Beutler, 1998].

When a solution is obtained, then

$$\mathbf{Y_i} = \mathbf{G}\left(\Theta_i\left(\mathbf{X_0}, t_0, t_i\right), t_i\right) + \boldsymbol{\varepsilon}_\mathbf{i} = \widetilde{\mathbf{G}}_\mathbf{i}\left(\mathbf{X_0}, t_0, t_i\right) + \boldsymbol{\varepsilon}_\mathbf{i}, \quad i = 1, \ldots, \ell \tag{2.8}$$

$$\text{or } \mathbf{Y} = \widetilde{\mathbf{G}}\left(\mathbf{X_0}, t_0\right) + \boldsymbol{\varepsilon}. \tag{2.9}$$

Equations (2.9) represent a system of $p \times \ell = m$ non-linear equations in terms of n unknown components of the state and m unknown components of the observation error. The intractable problem of adjusting these equations is circumvented by linearising the observation model prior to adjustment with a truncated Taylor's series expansion. A "best" estimate of the state can then be found, usually in the minimum sum of the squares of the observation residuals sense via a least-squares batch estimation process (adjustment). A more computationally efficient approach is to process each epoch of observations individually in a sequential estimation algorithm (*e.g.*, sequential least-squares filter or Kalman filter) rather than with a least-squares batch processor.

2.2. SPACEBORNE GPS PRECISE ORBIT DETERMINATION

The application of a SGPS receiver aboard a LEO for the goal of orbit determination began in civilian astronautics with the launch of Landsat 4 in 1982 [Birmingham *et al.*, 1983]. Since this time, there has been steady growth in LEO-based GPS activity (see, *e.g.*, Bisnath [1999]). This progression is due primarily to the characteristics of the GPS LEO tracking measurements, the details of which are discussed in the next section.

Before tackling this issue and describing SGPS POD strategies – a very good assessment of which is given in Yunck [1996], it is worthwhile defining what is meant by SGPS POD. Rather than meaning orbit determination in the classical sense as described in the introduction of the previous section, POD represents a precise and accurate quantitative description of the LEO path at some past time period. This can be realised in such forms as Special Product 3 (SP3) files containing discrete, time-stamped position or position and velocity records of the LEO, which can be interpolated by defined methods to any time of interest within that orbital arc. Estimation of the trajectory outside of the period of GPS observations would quickly degrade the precision and accuracy of the LEO state.

2.2.1. Variations Between Conventional and GPS Satellite Tracking Measurements

GPS provides a number of advantages over conventional tracking measurements. The GPS observing geometry provides three-dimensional information from range measurements, as opposed to just range, range-rate, or angular measurements. That is, the preliminary orbit determination problem is solved with the production of the SGPS receiver navigation solution. Another appealing aspect of GPS use aboard a LEO is its continuous data collection given sufficient power to sustain receiver operations and computer storage capacity to record measurements. Conventional techniques are limited to those data collection periods when the spacecraft is in line-of-sight of tracking stations, and, in the case of laser ranging, when atmospheric conditions permit measuring. The high costs involved with the operation of conventional tracking stations and their land-

based nature limits their use and hence reduces data collection quantity and distribution. SGPS removes the need for these expensive tracking stations and in the case of differential processing only requires additional data from relatively inexpensive terrestrial GPS reference stations.

Differential processing refers to the processing of simultaneously collected GPS data (specifically precise carrier phase observables) from a network of terrestrial reference receivers, and from the LEO receiver. This greatly attenuates the major observing errors of GPS satellite ephemerides and mis-synchronization of GPS satellite and GPS receiver clocks. The result is accurate, terrestrial reference station-to-LEO receiver vector estimates that are a prerequisite for the GPS-based precise orbit determination strategies described in the following sections. Note that although differential carrier phase GPS measurements are typically more accurate than those of radar, laser measurements are the most accurate [Unwin, 1995].

2.2.2. Dynamic Precise Orbit Determination Strategy

The dynamic strategy has been described in section 2.1. Again briefly, mathematical models of the forces acting on the LEO and mathematical models of the LEO's physical properties (altogether usually referred to as dynamic models) are used to compute a model description of the LEO's acceleration over time via the constraints of Newton's second law of motion. Double integration of this model using a nominal spacecraft state vector produces a nominal trajectory – thus developing the equations of motion of the LEO. A model trajectory is then estimated by selecting the LEO state that best fits (*e.g.*,

in a least-squares sense) the pre-processed (undifferenced or differenced) GPS tracking measurements.

An example of the most accurate SGPS dynamic orbit solution compared to satellite laser ranging (SLR)/Doppler Orbitography and Radiopositioning Integrated by Satellite (DORIS) orbits is that for the ~1300 km altitude TOPEX/Poseidon satellite. Using similar dynamic OD processing and dynamic models for both GPS and SLR/DORIS solutions, results of approximately 3 cm, 10 cm, and 9 cm (r.m.s.) for the radial, along track, and cross track orbit components, respectively, were obtained [Schutz *et al.*, 1994]. Ten day arcs comprising double-differenced, ionosphere-free carrier phase and P-code observables were used without the degrading effects of Anti-Spoofing (AS). AS refers to the encryption of the P-code by the U.S. military.

This OD strategy also allows for the simultaneous estimation of other parameters to improve the fit between the nominal trajectory and the tracking data, while still preserving available measurement strength by means of the dynamic models. These parameters can be classified as perturbing force and geometric parameters (*e.g.*, gravity coefficients and terrestrial observing station coordinates), and empirical parameters (*e.g.*, once- or twice-per-orbit revolution accelerations) [Yunck, 1996]. Over a long data arc (e.g., 6 hours), the effect of noisy instantaneous tracking measurements on the solution are reduced, given that the dynamic models are adequate. However, errors in these models will result in steadily growing systematic errors in the LEO state for longer data arc lengths. For example, the need for empirical parameter estimation indicates weakness in the dynamic models, which generally increases with decreasing LEO altitude, and increasing LEO dynamics complexity.

Other tracking system measurements, such as those from SLR and DORIS are restricted to a near fully dynamic OD strategy because of their discontinuous tracking and only one dimensional observability [Melbourne *et al.*, 1994].

2.2.3. Kinematic Precise Orbit Determination Strategy

In the kinematic or non-dynamic strategy, the trajectory smoothing caused by dynamic constraints in the estimation process is removed. The rationale for this is that, particularly at lower altitudes, the actual path of the LEO may be closer to the accurate GPS position estimates than the trajectory determined via the precise dynamics. This strategy can be applied by estimating in a Kalman filter formulation, along with the spacecraft state, a process noise vector representing three force corrections at each measurement epoch. Increasing the process noise can reduce almost completely the effects of the dynamic models. Simulated results for the ~700 km altitude Earth Observing System (EOS) satellite indicate that a radial precision approaching 3 cm r.m.s. could be achieved with this approach given a data arc of almost one day [Yunck, 1996].

The kinematic OD strategy is therefore actually based on an underlying dynamic formulation, however dynamic modelling errors are circumvented. The strategy relies almost entirely on the precision of the GPS observations and the strength of the observing geometry – that is, the relative location of the LEO and terrestrial receivers with respect to the GPS constellation, and the continuous GPS satellite tracking from the SGPS LEO receiver and the terrestrial GPS receiver array. Until recently, these measurement requirements represented severe problems due to receiver limitations [Melbourne *et al.*, 1994] and insufficient ground arrays [Yunck *et al.*, 1986].

2.2.4. Hybrid Dynamic and Kinematic Precise Orbit Determination Strategy

The previous two strategies each have counterbalancing disadvantages: various mis-modelling errors in dynamic OD, and GPS measurement noise or outages in kinematic OD. A hybrid dynamic and kinematic OD strategy would down-weight the errors caused by each strategy, but still utilise the strengths of each. One such strategy has been devised and is referred to as "reduced dynamic" precise orbit determination [Wu *et al.*, 1991]. Its basis is again the kinematic correction of the dynamic solution with continuous GPS data. By not completely removing the LEO dynamic and spacecraft models, a more accurate solution is possible because sensitivity to mis-modelling and GPS measurement error are both reduced – an equilibrium is reached. The weighting of the kinematic and dynamic data is performed again via the Kalman filter process noise. The process noise model contains two primary parameters: a time constant τ_i that defines the correlation in the dynamic model error over one update interval, and the dynamic model steady state variance σ_i^2. When $\tau_i \rightarrow \infty$ and $\sigma_i^2 \rightarrow 0$, the technique is reduced to the dynamic strategy, and when $\tau_i \rightarrow 0$ and $\sigma_i^2 \rightarrow \infty$, it approximates the kinematic strategy [Wu *et al.*, 1991].

Orbit determination results using the reduced dynamic technique for the TOPEX/Poseidon satellite have been consistent with results obtained with conventional dynamic techniques using GPS, and SLR and DORIS tracking data. Moreover, using refined dynamic models produces solutions that are even more similar, with differences of only a few centimetres (r.m.s.) in altitude [Melbourne *et al.*, 1994].

In the hybrid strategy, the proper weights of the process noise parameters must be chosen to give the most accurate orbit solution. These values can be derived from computer simulations, covariance analysis, or can be determined from real data. Once the correction parameter values are determined, this strategy provides equal or better accuracy compared to the other two strategies.

3. THE INITIAL UNB GEOMETRIC PRECISE ORBIT DETERMINATION STRATEGY

After studying the conventional orbit determination strategies of the time, it became apparent that a more direct approach might be possible, using the strong measurement capabilities of the GPS technology – accurate, global, continuous, and direct three-dimensional positioning. In this chapter, the development of the initial UNB geometric POD strategy is described. The term "initial" is used because major refinements to this approach were later made and are presented in Chapter 5. The use of the term "geometric" is explained in Section 3.1. The presentation of the initial strategy allows for the complete description of the logical progression of thoughts and development of the current technique. Also, the initial approach is still a completely viable option for POD. The chapter proceeds as follows: the thought process behind the development of the geometric strategy is first given; the related filter research that provides the basis for this work is reviewed and acknowledged; and the filter designed is provided, along with pertinent models and the least-squares solution to the over-determined problem.

3.1. Philosophical and Historical Foundations of the Geometric Strategy

Classical OD was designed to incorporate sparse, often imprecise measurement data that are not necessarily three-dimensional in nature. The advent of SGPS has allowed for the direct collection of continuous, accurate, direct, three-dimensional positions. Also, at low altitudes, *e.g.*, below approximately 1000 km, the hybrid strategy tends to reduce to the kinematic strategy [Wu *et al.*, 1991], in which the effects of the dynamic smoothing

of the GPS measurements by the inadequate dynamic models is removed. The kinematic strategy is required for LEOs that are in such described low orbits and also for LEOs that possess complex orbital motion, such as tethered vehicles or spacecraft of complex dimension and mass distribution (*e.g.*, a space station). Given these factors, a much less complex, direct and therefore very efficient approach became apparent: basically to use an augmented form of GPS relative positioning. This is to process simultaneous measurements from the LEO receiver and individual receivers at known locations from a terrestrial array to determine the position of the LEO with respect to the terrestrial receivers. This strategy was first proposed at the 1998 Canadian Aeronautics and Space Institute (CASI) Conference and first published in 1999 [Bisnath and Langley, 1999b]. The name "geometric" was used as the success of the strategy is based solely on the geometric strength of the GPS measurements. Also, the term "kinematic" (*i.e.*, non-dynamic) was already in use for another form of processing (Section 2.2.3).

Such a tracking strategy had been advocated in the early development of spacecraft tracking with GPS *(e.g.*, Yunck *et al.* [1986]); however, it was abandoned for dynamic strategies due to the depletion of data strength caused by the large number of parameters required to be estimated. At the time, precise GPS orbits were not available and therefore had to be estimated simultaneously with the LEO position in the solution. This would have required a large global array of terrestrial reference stations that was then unavailable. Given ideal circumstances, decimetre position component precisions were predicted in simulations [Yunck *et al.*, 1986]. If the GPS orbits were not simultaneously estimated, LEO position component precision would then be limited to the metre-level.

With the advent of global terrestrial receiver arrays such as the one maintained under the auspices of the International GPS Service (IGS), precise GPS orbits, a large global array of terrestrial GPS reference station data, and associated station coordinate and tropospheric zenith path delay estimates became available [Neilan *et al.*, 1997; Gendt, 1998]. A great deal of effort and expertise are involved in the generation of these data products, and the geometric strategy represents an opportunity to utilise these datasets as opposed to either re-estimating portions of them or ignoring them altogether. The idea of reducing the computational burden by utilising IGS precise GPS orbits in dynamic OD for example has been tested with only minor reductions in orbit accuracies by Davis *et al.* [1997].

The inputs to the geometric tracking strategy are precise GPS ephemerides, terrestrial array receiver measurements, receiver coordinates and tropospheric zenith path delay estimates, and dual-frequency pseudorange and carrier phase SGPS receiver data. The measurement data are not fit against a nominal trajectory determined by dynamic models and thus the development of such models is not required. The double-differenced, ionosphere-free pseudorange observable is used to determine noisy (*i.e.*, metre-level) absolute LEO position estimates. The double-differenced, ionosphere-free carrier phase observable differenced between adjacent epochs (triple-difference) is used to determine highly precise (*i.e.*, sub-centimetre-level) LEO position change estimates. The use of the dual-frequency observables allows for the removal of the vast majority of ionospheric effects, the error effects of GPS satellite and receiver clocks is eliminated with the double-differencing, and the phase ambiguity terms are removed by the third differencing (in time).

This measurement processing technique is a derivative of the processes described by Yunck and Wu [1986] for LEO orbit determination and Kleusberg [1986] for marine navigation, and is a generalised form of carrier-aided pseudorange smoothing developed by Hatch [1982]. At the crux of carrier and pseudorange combination is that averaged noisy pseudorange range measurements are used to estimate the ambiguity term in the precise carrier phase range measurements. The longer the pseudorange averaging, the better the carrier ambiguity estimate. In effect, the low noise carrier phase information is used to map the pseudorange information from all epochs to one epoch for averaging, and this is done for every observation.

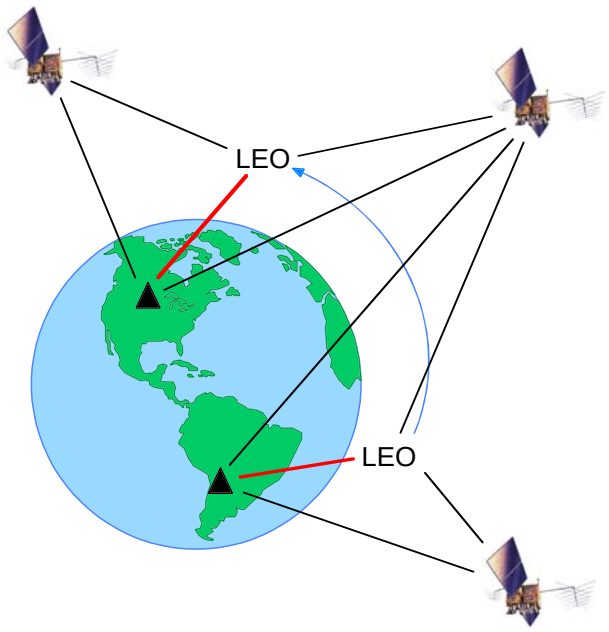

Figure 3.1: Frequently changing GPS satellite / LEO receiver / ground receiver pairing due to LEO orbital motion.

As can be appreciated from Figure 3.1 however, the averaging intervals are typically short in spaceborne applications due to the relatively fast motion of the LEO, ~7.5 km/s

for a satellite orbiting at between 500 and 1000 km, resulting in orbital periods of ~1.5 to 2 hours, necessitating frequent changing of GPS satellite-receiver pairs. This situation does not allow for the highest precision of the technique to be attained, as averaging intervals are only a few tens of minutes long. By performing the averaging in the *position* rather than the *range* domain, previous position *solutions* can be used in estimating present and future *solutions* regardless of changing spaceborne / terrestrial receiver vectors. Quiles-Blanco and Martin-Neira [1999] actually describe tests in which a Kalman filter realisation of this filter type provides superior performance to a standard carrier-smoothing algorithm.

To summarise, the flow charts of Figure 3.2 compare and contrast the fundamental constituents of the three existing tracking strategies described in Chapter 2 with the geometric strategy. As can be readily seen, the latter represents much less processing. Firstly, the generation of GPS satellite orbits (and therefore use of GPS satellite dynamic models) is not necessary – they are provided by the IGS. And secondly, the LEO dynamic models are not required; only precise, continuous SGPS measurements. A number of key questions arose during this theoretical development process: One, could GPS measurements alone produce near-decimetre-level orbits? Two, would the propagation of IGS product error too greatly contaminate the LEO position solutions? And three, would an SGPS receiver provide adequate precise, continuous data to drive the filter? These questions were partially addressed in the simulations of Chapter 4, but the underlying concern that dynamics are not available in this approach to bridge measurement gaps or increase solution precision would remain until actual data was processed.

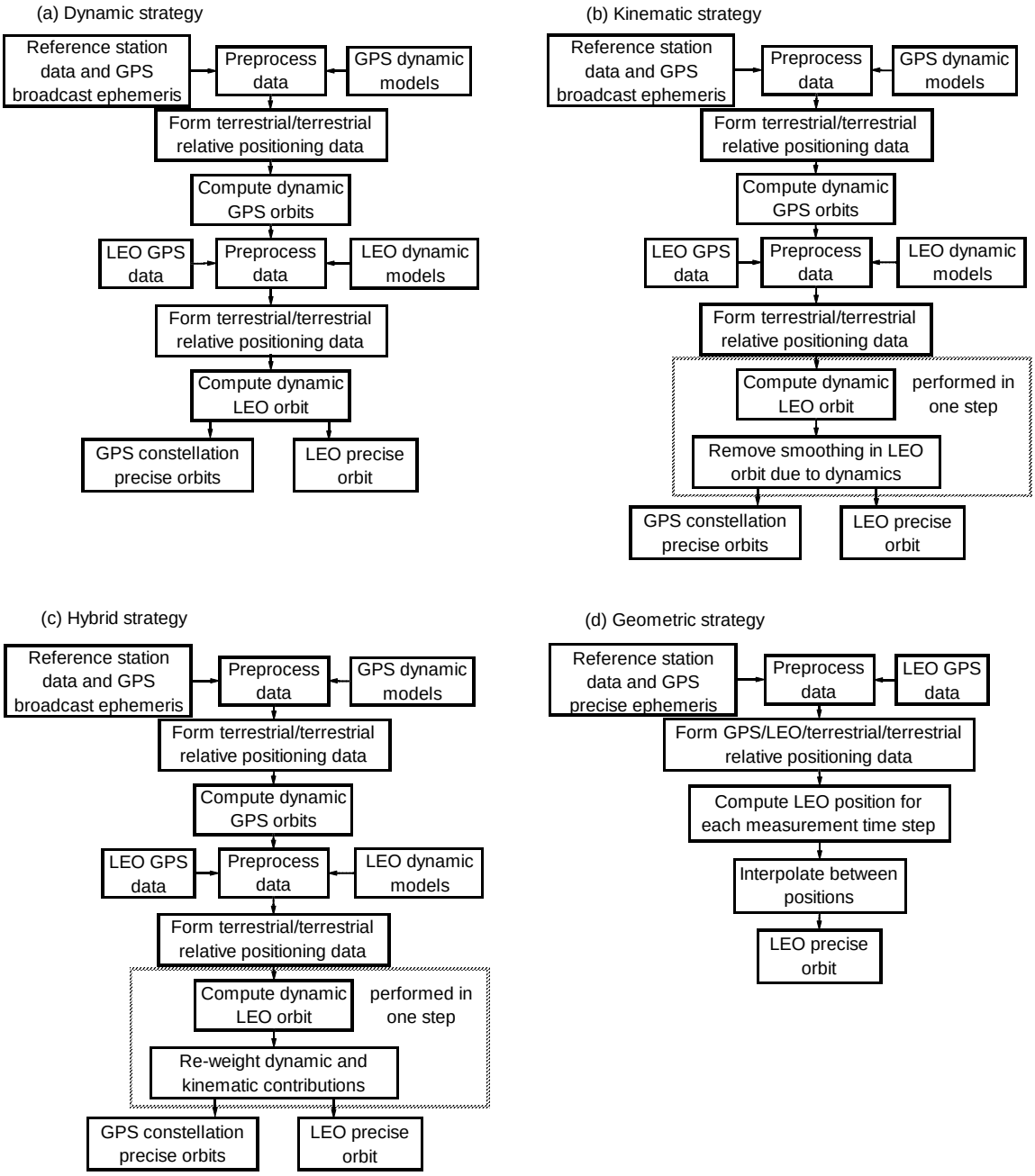

Figure 3.2. Flow charts of the fundamental constituents of the four GPS-based precise tracking strategies. (a) Dynamic strategy. (b) Kinematic strategy. (c) Hybrid strategy. (d) Geometric strategy.

3.2. GEOMETRIC STRATEGY FILTER MODELS AND SOLUTION

The derivation of the positioning filter is now presented. First, the combination of the pseudorange and carrier phase observables is given. This is followed by the derivation of the positioning model and the filter solution. Finally, an optimal least-squares smoother is derived.

3.2.1. Combination of the Pseudorange and Carrier-Phase Observables

The four measurement streams: L1 pseudorange, L1 phase, L2 pseudorange, and L2 phase can be combined to produce a single precise, unambiguous observable. The four observables can be represented by the following simplified measurement models:

$$P_{1t} = \rho_t + I_{1t} + e_{1_t}, \quad \{\sigma_P\} \tag{3.1}$$

$$\Phi_{1t} = \rho_t - I_{1t} + \lambda_1 N_1 + \varepsilon_{1_t}, \quad \{\sigma_\Phi\} \tag{3.2}$$

$$P_{2t} = \rho_t + I_{2t} + e_{2_t}, \quad \{\sigma_P\} \tag{3.3}$$

$$\Phi_{2t} = \rho_t - I_{2t} + \lambda_2 N_2 + \varepsilon_{2_t}, \quad \{\sigma_\Phi\} \tag{3.4}$$

where 1 and 2 represent L1 and L2 observable terms, t is the epoch of observation, ρ is the geometric range, I_1 and I_2 are the pseudorange delay or carrier-phase advance imparted by the ionosphere, λ is the carrier wavelength, N is the integer ambiguity, the e and ε terms represent the random noise on the pseudorange and carrier-phase observables, and the term in braces is the observation precision (1σ). Note that $\sigma_p / \sigma_\Phi \approx 100$.

The linear combination of these four observables removes the ionospheric term (ignoring higher-order terms) and hence is referred to as the "ionospheric-free" combination. I_1 and I_2 can be written as $I_1 = \alpha_1 I$ and $I_2 = \alpha_2 I$, where $\alpha_1 = f_2^2/\left(f_1^2 - f_2^2\right) \approx 1.546$ and $\alpha_2 = f_1^2/\left(f_1^2 - f_2^2\right) \approx 2.546$, where I is a quantity proportional to the line-of-sight ionospheric electron content and f_1 and f_2 are the L1 and L2 carrier frequencies, respectively. Noting that $\alpha_2 - \alpha_1 = 1$ and $\frac{\alpha_2}{\alpha_1} = \frac{f_1^2}{f_2^2}$, equations (3.1) through (3.4) can be combined to remove the ionospheric term with data noise magnification as dictated by the law of error propagation:

α_2 (3.1) – α_1 (3.3):

$$\widetilde{P}_t = \rho_t + \widetilde{e}_t, \quad \left\{\sqrt{\alpha_1^2 + \alpha_2^2}\,\sigma_p\right\} \tag{3.5}$$

where $\widetilde{e}_t = \alpha_2 e_{1t} - \alpha_1 e_{2t}$.

α_2 (3.2) – α_1 (3.4):

$$\widetilde{\Phi}_t = \rho_t + B + \widetilde{\varepsilon}_t, \quad \left\{\sqrt{\alpha_1^2 + \alpha_2^2}\,\sigma_\Phi\right\} \tag{3.6}$$

where $B = \alpha_2\lambda_1 N_1 - \alpha_1\lambda_2 N_2$, and $\widetilde{\varepsilon}_t = \alpha_2\varepsilon_{1t} - \alpha_1\varepsilon_{2t}$. (3.7)

The basic principle of the second linear combination is to estimate the GPS satellite-to-receiver carrier phase ambiguity bias (B) by averaging the difference between the carrier-phase ($\widetilde{\Phi}$) and pseudorange ($\widetilde{P}$) observables. That is, as long as the satellite-to-receiver bias remains constant (*i.e.*, no cycle-slips):

$$\hat{B} = \frac{1}{n}\sum_{t=1}^{n}\left[\tilde{\Phi}_t - \tilde{P}_t\right] \tag{3.8}$$

or

$$\hat{B} = B + \frac{1}{n}\sum_{t=1}^{n}\left[\tilde{\varepsilon}_t - \tilde{e}_t\right],\ \left\{\sqrt{\frac{\left(\alpha_1^2 + \alpha_2^2\right)\left(\sigma_\Phi^2 + \sigma_P^2\right)}{n}}\right\}. \tag{3.9}$$

And therefore, the best estimate of the range is

$$\hat{\rho}_t = \tilde{\Phi}_t - \hat{B} \tag{3.10}$$

or

$$\hat{\rho}_t = \rho_t + \tilde{\varepsilon}_t - \frac{1}{n}\sum_{t=1}^{n}\left[\tilde{\varepsilon}_t - \tilde{e}_t\right],\ \left\{\sqrt{\frac{\left(\alpha_1^2 + \alpha_2^2\right)\left[(n+1)\sigma_\Phi^2 + \sigma_p^2\right]}{n}}\right\}. \tag{3.11}$$

It must be noted that these two combinations are not optimum when producing a single data stream from the four initial streams. In the first combination, the common ionospheric term in the pseudorange and carrier phase equations are treated independently, and hence some data strength is lost. And in the second combination, the relative observable weighting is only optimal if $\sigma_\Phi << \sigma_P$, or else either the number of epochs averaged has to be limited or more appropriate weighting must be put into place. Small improvements can be obtained if these concerns are taken into account (see, *e.g.*, Wu and Melbourne [1993]).

3.2.2. Derivation of the Geometric Strategy Mathematical Model

As described, to avoid constantly changing GPS-satellite-to-receiver pairs, the carrier smoothing of the pseudoranges can be performed in the position domain. The more complete observation equations are now used to derive the required mathematical model. Continuing from (3.5) and (3.6)

$$\widetilde{P}_t = \rho_t + c\left[dT_t - dt_t\right] + T_t + \widetilde{e}_t \quad \text{and} \tag{3.12}$$

$$\widetilde{\Phi}_t = \rho_t + c\left[dT_t - dt_t\right] + T_t + B + \widetilde{\varepsilon}_t, \tag{3.13}$$

where the new terms are as follows: c is the nominal speed of light in a vacuum, dT_t and dt_t are the receiver and GPS satellite clock offsets, respectively, and T_t is the delay due to the troposphere. Again, the subscript t is the epoch of observation.

In the determination of the LEO receiver position, the tropospheric error does not apply (it however must be included in the terrestrial reference station receiver model), and the clock terms can be almost completely removed via double-differencing. Between epoch differencing of the double-differenced carrier phase (triple-difference) removes the bias term B.

$$\nabla\Delta\widetilde{P}_t = r_t + \widetilde{e}'_t \quad \text{and} \tag{3.14}$$

$$\nabla\Delta\widetilde{\Phi}_{t-1,t} = r_{t-1,t} + \widetilde{\varepsilon}'_{t-1,t} \tag{3.15}$$

where $\nabla\Delta\widetilde{P}_t$ is the double-differenced, ionosphere-free pseudorange observation, $\nabla\Delta\widetilde{\Phi}_{t-1,t}$ is the triple-differenced, ionosphere-free carrier phase observation, r_t is the

terrestrial receiver-to-LEO receiver geometric range, $r_{t-1,t}$ is the change in range of the LEO receiver with respect to the terrestrial receiver between epochs t-1 and t and $\tilde{e}'_t$ and $\tilde{\varepsilon}'_{t-1,t}$ are the associated processed pseudorange and carrier phase observation errors, respectively.

Finally, linearised and in matrix form, (3.14) and (3.15) represent the final mathematical model for the filter:

$$\begin{bmatrix} \nabla\Delta\mathbf{P}_t \\ \nabla\Delta\mathbf{\Phi}_{t-1,t} \end{bmatrix} = \begin{bmatrix} 0 & \mathbf{A}_t \\ -\mathbf{A}_{t-1} & \mathbf{A}_t \end{bmatrix} \begin{bmatrix} \delta\mathbf{x}_{t-1} \\ \delta\mathbf{x}_t \end{bmatrix} + \begin{bmatrix} \mathbf{e}_t \\ \boldsymbol{\varepsilon}_{t-1,t} \end{bmatrix}; \quad \mathbf{C_p}, \mathbf{C_\Phi}, \tag{3.16}$$

where $\nabla\Delta\mathbf{P}_t$ and $\nabla\Delta\mathbf{\Phi}_{t-1,t}$ are the vectors of double-differenced pseudorange and triple-differenced carrier phase observations (the ionosphere-free tilde notation has been left out), respectively, $\delta\mathbf{x}_{t-1}$ and $\delta\mathbf{x}_t$ are the corrections to the approximate LEO position coordinates at epochs t-1 and t, respectively, $\mathbf{A}_{t-1}$ and $\mathbf{A}_t$ are the measurement partials with respect to the two position coordinates, $\mathbf{e}_{t-1}$ and $\boldsymbol{\varepsilon}_t$ are the processed pseudorange and carrier phase vectors observation errors, and $\mathbf{C_p}$ and $\mathbf{C_\Phi}$ are the variance-covariance matrices of the processed pseudorange and carrier-phase observations, respectively. As can be seen, (3.16) is in the form $\ell = \mathbf{AX} + \mathbf{v}$, which can generate an optimal solution via the theory of least-squares.

3.2.3. Derivation of the Kinematic, Sequential, Least-Squares Positioning Filter from the Mathematical Model

From, *e.g.*, Wells [1997] the general linearised parametric least-squares adjustment can be represented by

$$\begin{bmatrix} \mathbf{C}_\ell^{-1} & \mathbf{I} & 0 \\ -\mathbf{I} & 0 & \mathbf{A} \\ 0 & \mathbf{A}^{\mathrm{T}} & 0 \end{bmatrix} \begin{bmatrix} \mathbf{r} \\ \mathbf{k} \\ \boldsymbol{\delta}\mathbf{x} \end{bmatrix} + \begin{bmatrix} 0 \\ \mathbf{w} \\ 0 \end{bmatrix} = 0\,, \tag{3.17}$$

where **w** is the misclosure vector, **δx** is the vector of corrections to the approximate parameters, **A** is the matrix of measurement partials with respect to the unknowns **δx**, k is the vector of Lagrange correlates, and $\mathbf{C}_\ell$ is the variance-covariance matrix of the observations. Through the use of matrix partioning this mathematical model can be altered to represent the observation model (3.16). That is, the addition of nuisance parameters $\boldsymbol{\delta}\mathbf{x} = \begin{bmatrix} \boldsymbol{\delta}\mathbf{x}_{t-1} \\ \boldsymbol{\delta}\mathbf{x}_t \end{bmatrix} \begin{matrix} \Leftarrow \text{"nuisance" parameters} \\ \Leftarrow \text{parameters of interest} \end{matrix}$ and consequently $\mathbf{A} = \begin{bmatrix} -\mathbf{A}_{t-1} & \mathbf{A}_t \end{bmatrix}$; the addition of observations $\ell = \begin{bmatrix} \ell_t \\ \ell_{t-1,t} \end{bmatrix} \begin{matrix} \Leftarrow \text{ new observations} \\ \Leftarrow \text{previous observations} \end{matrix}$ and consequently $\mathbf{A} = \begin{bmatrix} 0 & \mathbf{A}_t \\ -\mathbf{A}_{t-1} & \mathbf{A}_t \end{bmatrix}$; $\mathbf{w} = \begin{bmatrix} \mathbf{w}_{t-1} \\ \mathbf{w}_t \end{bmatrix}$: $\mathbf{r} = \begin{bmatrix} \mathbf{r}_{t-1} \\ \mathbf{r}_t \end{bmatrix}$; $\mathbf{C}_\ell^{-1} = \begin{bmatrix} \mathbf{C}_\mathbf{P}^{-1} & 0 \\ 0 & \mathbf{C}_\mathbf{\Phi}^{-1} \end{bmatrix}$; and $\mathbf{k} = \begin{bmatrix} \mathbf{k}_{t-1} \\ \mathbf{k}_t \end{bmatrix}$; and the incorporation of the previous estimate of the LEO position and associated covariance ($\mathbf{C}_{\hat{\mathbf{x}}}$). The result is

$$\begin{bmatrix} \mathbf{C}_\mathbf{P}^{-1} & 0 & -\mathbf{I} & 0 & 0 & 0 \\ 0 & \mathbf{C}_\mathbf{\Phi}^{-1} & 0 & -\mathbf{I} & 0 & 0 \\ -\mathbf{I} & 0 & 0 & 0 & 0 & \mathbf{A}_t \\ 0 & -\mathbf{I} & 0 & 0 & -\mathbf{A}_{t-1} & \mathbf{A}_t \\ 0 & 0 & 0 & -\mathbf{A}_{t-1}^{\mathrm{T}} & \mathbf{C}_{\hat{\mathbf{x}}_{t-1}}^{-1} & 0 \\ 0 & 0 & \mathbf{A}_t^{\mathrm{T}} & \mathbf{A}_t^{\mathrm{T}} & 0 & 0 \end{bmatrix} \begin{bmatrix} \mathbf{r}_1 \\ \mathbf{r}_2 \\ \mathbf{k}_1 \\ \mathbf{k}_2 \\ \boldsymbol{\delta}\mathbf{x}_{t-1} \\ \boldsymbol{\delta}\mathbf{x}_t \end{bmatrix} + \begin{bmatrix} 0 \\ 0 \\ \mathbf{w}_{t-1} \\ \mathbf{w}_t \\ 0 \\ 0 \end{bmatrix} = 0\,. \tag{3.18}$$

The solution of (3.18) is

$$\begin{bmatrix} \boldsymbol{\delta}\hat{\mathbf{x}}_{t-1} \\ \boldsymbol{\delta}\hat{\mathbf{x}}_{t} \end{bmatrix} = \begin{bmatrix} \mathbf{x}_{t-1}^{0} \\ \mathbf{x}_{t}^{0} \end{bmatrix}$$

$$+ \begin{bmatrix} \mathbf{A}_{t-1}^{T}\mathbf{C}_{\boldsymbol{\Phi}}^{-1}\mathbf{A}_{t-1} + \mathbf{C}_{\hat{\mathbf{x}}_{t-1}}^{-1} & -\mathbf{A}_{t-1}^{T}\mathbf{C}_{\boldsymbol{\Phi}}^{-1}\mathbf{A}_{t} \\ -\mathbf{A}_{t}\mathbf{C}_{\boldsymbol{\Phi}}^{-1}\mathbf{A}_{t-1} & \mathbf{A}_{t}^{T}\left(\mathbf{C}_{\mathbf{P}}^{-1} + \mathbf{C}_{\boldsymbol{\Phi}}^{-1}\right)\mathbf{A}_{t} \end{bmatrix}^{-1} \begin{bmatrix} -\mathbf{A}_{t-1}^{T}\mathbf{C}_{\boldsymbol{\Phi}}^{-1}\mathbf{w}_{t} \\ \mathbf{A}_{t}^{T}\mathbf{C}_{\mathbf{P}}^{-1}\mathbf{w}_{t-1} + \mathbf{A}_{t}\mathbf{C}_{\boldsymbol{\Phi}}^{-1}\mathbf{w}_{t} \end{bmatrix}. \tag{3.19}$$

We therefore have a kinematic, sequential, least-squares filter based solely on GPS measurement for LEO tracking. Note that this equation was previously presented in Kleusberg [1986].

As can be seen, the position estimate at the previous epoch t-1 is used to estimate the position at epoch t and so on for the moving LEO. This equation represents a kinematic, sequential, least-squares filter. This filter is a subset of the Kalman filter as shown in Appendix A. Simply put, from (3.19) the pseudorange measurement contributions are basically

$$\nabla\Delta P_{t} = A_{t}\delta x_{t} + e_{t}; \quad C_{\nabla\Delta P_{t}} \tag{3.20}$$

and can be extracted along with the carrier phase measurement contribution, which is essentially

$$\nabla\Delta\Phi_{t-1,t} = -A_{t-1}\delta x_{t-1} + A_{t}\delta x_{t} + \varepsilon_{t-1,t}; \quad C_{\nabla\Delta\Phi_{t-1,t}}. \tag{3.21}$$

The terms in (3.20) can be directly mapped to those of the Kalman filter measurement model, and with some rearrangement the terms in (3.21) can be effectively related to those of the Kalman dynamic model. That is, the kinematic, sequential, least-squares positioning filter behaves like a Kalman filter because the carrier phase measurements

represent its dynamic model – precise change in state information. This is illustrated in Figure 3.3.

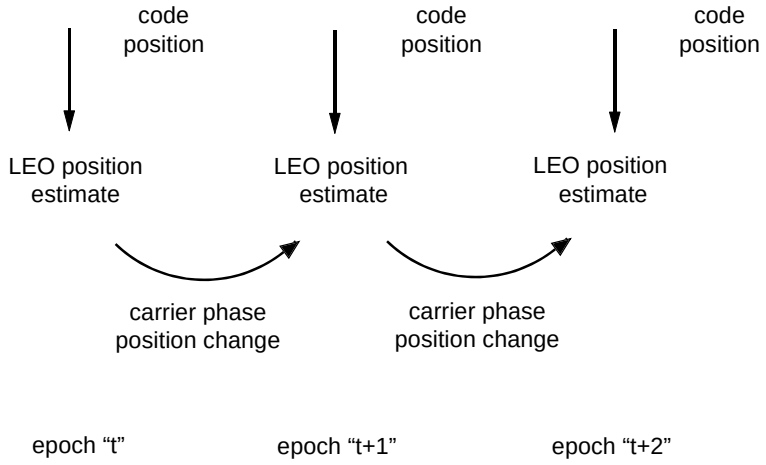

Figure 3.3: Combination of pseudorange and carrier phase observations in the kinematic, sequential, least-squares filter – parallels the Kalman filter [Bisnath and Langley, 1999a].

3.2.4. The Optimal Least-Squares Smoother for Parameter Covariance

Finally, since this tracking strategy is performed after-the-fact, data smoothing can be performed. That is, the data arc can be processed in the forward and reverse directions and the results can be optimally combined. The *best* parameter estimate for an epoch can be represented by, *e.g.*, Gelb [1974]

$$\hat{\mathbf{x}}_{\mathbf{s}t} = \mathbf{F}\hat{\mathbf{x}}_{\mathbf{f}t} + \mathbf{R}\hat{\mathbf{x}}_{\mathbf{r}t}, \tag{3.22}$$

where $\hat{\mathbf{x}}_{\mathbf{s}t}$, $\hat{\mathbf{x}}_{\mathbf{f}t}$ and $\hat{\mathbf{x}}_{\mathbf{r}t}$ are the optimal smoothed, forward filter, and reverse filter parameter estimates, respectively, and **F** and **R** are the weighting matrices to be determined. Given that the relationship between an estimate $\hat{\mathbf{x}}$ is

$$\hat{\mathbf{x}} = \mathbf{x} + \tilde{\mathbf{x}} \;\Rightarrow\; \hat{\mathbf{x}}_{\mathbf{s}} = \mathbf{x} + \tilde{\mathbf{x}}_{\mathbf{s}}, \quad \hat{\mathbf{x}}_{\mathbf{f}} = \mathbf{x} + \tilde{\mathbf{x}}_{\mathbf{f}}, \quad \hat{\mathbf{x}}_{\mathbf{r}} = \mathbf{x} + \tilde{\mathbf{x}}_{\mathbf{r}}. \tag{3.23}$$

(3.22) can be written as

$$\tilde{\mathbf{x}}_{\mathbf{s}t} = \left(\mathbf{F} + \mathbf{R} - \mathbf{I}\right)\mathbf{x}_{\mathbf{f}t} + \mathbf{F}\,\tilde{\mathbf{x}}_{\mathbf{f}t} + \mathbf{R}\,\tilde{\mathbf{x}}_{\mathbf{r}t}. \tag{3.24}$$

If we let **R** = **I** – **F**, as it must in this weighting scheme, then

$$\tilde{\mathbf{x}}_{\mathbf{s}t} = \mathbf{F}\,\tilde{\mathbf{x}}_{\mathbf{f}t} + \left(\mathbf{I} - \mathbf{F}\right)\tilde{\mathbf{x}}_{\mathbf{r}t}. \tag{3.25}$$

Since $\mathbf{P}_{\mathbf{s}} = \mathrm{E}\left\{\tilde{\mathbf{x}}_{\mathbf{s}t}\,\tilde{\mathbf{x}}_{\mathbf{s}t}^{\mathrm{T}}\right\}$, applying the law of error propagation to (3.25) results in

$$\mathbf{P}_{\mathbf{s}t} = \mathbf{F}\,\mathbf{P}_{\mathbf{f}}\mathbf{F}^{\mathrm{T}} + \left(\mathbf{I} - \mathbf{F}\right)\mathbf{P}_{\mathbf{r}t}\left(\mathbf{I} - \mathbf{F}\right)^{\mathrm{T}}, \tag{3.26}$$

or dropping the epoch notation, simply

$$\mathbf{P}_{\mathbf{s}} = \mathbf{F}\,\mathbf{P}_{\mathbf{f}}\mathbf{F}^{\mathrm{T}} + \left(\mathbf{I} - \mathbf{F}\right)\mathbf{P}_{\mathbf{r}}\left(\mathbf{I} - \mathbf{F}\right)^{\mathrm{T}}. \tag{3.27}$$

We can now chose the *best* weighting of the forward and reverse filter results by way of the least-squares criterion. Therefore, taking the partial derivative of (3.27) with respect to F and setting the result equal to zero $\Rightarrow \dfrac{\partial \mathbf{P}_{\mathbf{s}}}{\partial \mathbf{F}} = 0$ gives

$$\mathbf{F} = \mathbf{P}_{\mathbf{r}}\left(\mathbf{P}_{\mathbf{f}} + \mathbf{P}_{\mathbf{r}}\right)^{-1} \tag{3.28}$$

and

$$\mathbf{R} = \mathbf{I} - \mathbf{F} = \mathbf{P_f}\left(\mathbf{P_f} + \mathbf{P_r}\right)^{-1}. \tag{3.29}$$

Substituting (3.28) and (3.29) into (3.27) gives

$$\mathbf{P_s} = \mathbf{P_r}\left(\mathbf{P_f} + \mathbf{P_r}\right)^{-1}\mathbf{P_f}\left(\mathbf{P_f} + \mathbf{P_r}\right)^{-1}\mathbf{P_r} + \mathbf{P_f}\left(\mathbf{P_f} + \mathbf{P_r}\right)^{-1}\mathbf{P_r}\left(\mathbf{P_f} + \mathbf{P_r}\right)^{-1}\mathbf{P_f}, \tag{3.30}$$

which after some manipulation (multiplying through and cancelling) results in

$$\mathbf{P_s} = \left(\mathbf{P_f}^{-1} + \mathbf{P_r}^{-1}\right) \tag{3.31}$$

or

$$\mathbf{P_s}^{-1}{}_t = \mathbf{P_f}^{-1}{}_t + \mathbf{P_r}^{-1}{}_t. \tag{3.32}$$

Therefore, the result for the parameter covariance is

$$\mathbf{C}_{\mathbf{s}_t} = \mathbf{C}_{\mathbf{f}_t} + \mathbf{C}_{\mathbf{r}_t}, \tag{3.33}$$

where $\mathbf{C}_{\mathbf{s}_t}$ is the smoothed parameter covariance, $\mathbf{C}_{\mathbf{f}_t}$ is the forward filter parameter covariance, and $\mathbf{C}_{\mathbf{r}_t}$ is the reverse filter parameter covariance. This is a fixed-interval smoother and as can be seen from (3.33) and Figure 3.4, the smoothed parameter covariance is less than or equal to the results from either filter.

3.3. SUMMARY

The philosophical and historical foundations for the initial geometric strategy have been presented. The filter models, both mathematical and stochastic were developed and explained, as was the kinematic, sequential least-squares solution. The next chapter uses these definitions to assess the usefulness of the strategy for POD by use of simulations.

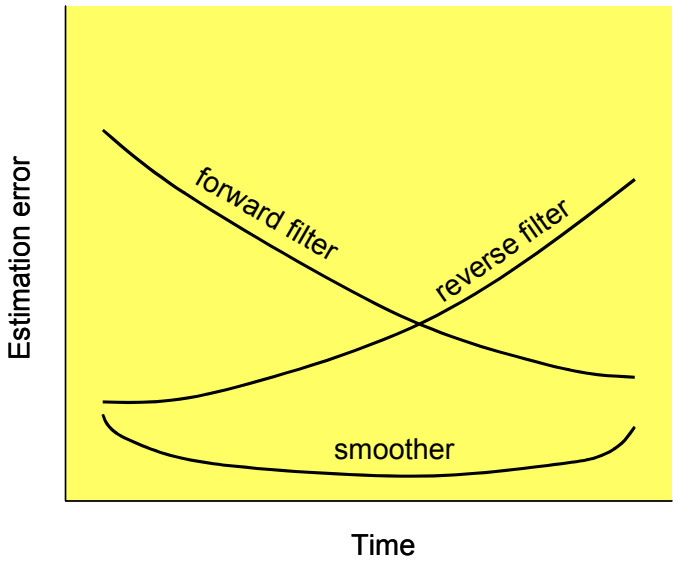

Figure 3.4: Sketch of estimation error functions for forward filter, reverse filter, and fixed-interval smoother.

4. GEOMETRIC STRATEGY PROOF OF CONCEPT STUDY

In order to proceed with the development of the initial geometric POD strategy, since such an approach had not been attempted in the literature, it was deemed necessary to perform some form of simulation to confirm if the geometric technique would indeed provide precisions on the order of a few decimetres; otherwise the strategy would not be a viable alternative to existing approaches. The research carried out for this task produced a number of papers and presentations including Bisnath and Langley [1999a] and Bisnath and Langley [1999b].

The proof of concept consisted of two components: the major component was an assessment of the filter viability via an error propagation study, and the minor component was a solution interpolation study. The filter study propagates the expected noise levels in the system (*i.e.*, SGPS measurements and infrastructure) through the least-squares functional model as is done, for example, in surveying theory pre-analysis. Given the stochastics and geometry of the problem, the expected precision of the solution can be estimated. The interpolation study inputs varying time-spaced discrete LEO coordinates into a standard interpolator algorithm to determine if such discrete data can accurately represent a LEO orbit. By successfully addressing these two concerns, justification is provided that the geometric strategy is feasible, and therefore the dissertation work is worth pursuing.

4.1. FILTER ERROR PROPAGATION STUDY

The filter error propagation study consisted of first developing the propagation models based on the geometric filter and available information on the precision of the measurements. The models were then implemented in software for analysis and simulated data were created for processing. The orbit scenario used was that for the proposed BOLAS LEO mission, which will be described. The results and analysis then follow.

4.1.1. Filter Error Propagation Study Methodology

To determine how well this processing strategy would work, *i.e.*, with what precision could the position of the LEO receiver be determined, the covariance matrix for the estimated position unknowns was computed. Beginning with the set of linear or linearised observation equations of the form

$$\ell = \mathbf{A}\mathbf{x}\,, \tag{4.1}$$

where ℓ is the vector of measurements, $\mathbf{x}$ is the vector of unknowns, and $\mathbf{A}$ is the matrix of measurement partials (design matrix). Such observation equations can be represented in the form

$$\ell = \mathbf{A}\hat{\mathbf{x}} + \mathbf{r}; \qquad \mathbf{P}_\ell = \sigma_o^2 \mathbf{C}_\ell^{-1}, \tag{4.2}$$

where $\hat{\mathbf{x}}$ is the estimated vector of unknowns, $\mathbf{r}$ is the vector of residuals which completes the system, $\mathbf{P}_\ell$ is the (generally diagonal) weight matrix, σ_o^2 is the *a priori* variance factor, and $\mathbf{C}_\ell$ is the (generally diagonal) matrix of measurement precisions

(measurement covariance matrix). For this application, the system is over-determined, that is number(ℓ) > number($\mathbf{x}$). The "best" solution to this equation in terms of minimising the magnitudes of the residuals is the weighted least-squares estimator

$$\hat{\mathbf{x}} = \left(\mathbf{A}^{\mathrm{T}}\mathbf{P}_{\ell}\mathbf{A}\right)^{-1}\mathbf{A}^{\mathrm{T}}\mathbf{P}_{\ell}\ell, \qquad \mathbf{P}_{\ell} = \sigma_{\mathrm{o}}^{2}\mathbf{C}_{\ell}^{-1}. \tag{4.3}$$

The covariance matrix for the estimated unknowns is

$$\mathbf{C}_{\hat{\mathbf{x}}} = \left(\mathbf{A}^{\mathrm{T}}\mathbf{C}_{\ell}^{-1}\mathbf{A}\right)^{-1}. \tag{4.4}$$

Therefore, only the mathematical model and the stochastic model are needed for this estimate and no actual measurements.

This estimate only contains direct measurement errors propagated through the geometry of the observing strategy. Other indirect sources of error are not included in this estimate. These two types of errors have been referred to as internal and external errors, respectively (*e.g.*, Strang and Borre [1997]). For the processing at hand, the internal errors are the pseudorange and carrier phase measurement noise, and the external errors arise from tropospheric zenith delay residuals, and GPS satellite and terrestrial reference receiver position uncertainties. Pseudorange and carrier phase multipath were not considered; however, much of the negative effect of such errors would be averaged out in the filtering. $\mathbf{C}_{\hat{\mathbf{x}}}$ can be augmented to include the effects of these external errors and hence provide a larger, but *more realistic* covariance for the estimated parameters

$$\mathbf{C}'_{\hat{\mathbf{x}}} = \left(\mathbf{A}^{\mathrm{T}}\mathbf{C}_{\ell}^{-1}\mathbf{A}\right)^{-1} + \left(\mathbf{A}^{\mathrm{T}}\mathbf{C}_{\ell}^{-1}\mathbf{A}\right)^{-1}\mathbf{A}^{\mathrm{T}}\mathbf{C}_{\ell}^{-1}\mathbf{B}\mathbf{C}_{\mathbf{B}}\mathbf{B}^{\mathrm{T}}\mathbf{C}_{\ell}^{-1}\mathbf{A}\left(\mathbf{A}^{\mathrm{T}}\mathbf{C}_{\ell}^{-1}\mathbf{A}\right)^{-1}, \tag{4.5}$$

where $\mathbf{C}'_{\hat{\mathbf{x}}}$ is the more realistic covariance for the estimated parameters, **B** is the design matrix containing the measurement partials with respect to external error terms, and $\mathbf{C_B}$ is the covariance matrix of the external error terms. This pivotal derivation and the specific derivations for the total LEO position error covariance that are the centre of this proof of concept study are given in Appendix B.

This expanded covariance procedure has been described by, *e.g.*, Blaha [1974] and Strang and Borre [1997] for propagating control monument variances through geodetic network least-squares adjustments. Bierman [1977] adapts the procedure for the square root information filter and refers to its use as consider covariance analysis based on *considering* the effects of other error sources.

Therefore by deriving the **B** matrix and constructing the $\mathbf{C_B}$ covariance matrix based on the given data, the precision with which the LEO receiver position can be determined for a given mission scenario can be estimated.

4.1.2. Filter Error Propagation Software

In order to test the proposed tracking strategy, GPS constellation, terrestrial receiver array and LEO positions were needed for use in design and covariance matrix construction. Software created primarily to predict the visibility between an arbitrary satellite and the GPS satellite constellation [Gerrits and Langley, 1998] was used to produce these data. The software, entitled GGSIM (Gps Geometry SIMulator), is written in FORTRAN 77 with Matlab visualisations. The main inputs (via a command file) are the satellite and GPS constellation two line element files. Other parameter inputs include

start and end epoch, and estimation time step. The Keplerian elements along with the orbital perturbation due to the J_2 spherical harmonic term of the earth's gravitational potential are used to compute the celestial Cartesian coordinates of all the involved satellites. Vector calculus is then used to compute LEO-to-GPS tracking intervals given the constraints of the size and shape of the earth and the field-of-view and orientation of the LEO GPS antenna. The outputs include GPS satellite visibility times and elevation angle, azimuth and range information. The results were verified with the Satellite Tool Kit (STK) Version 4.0 commercial satellite tracking software package.

GGSIM was modified for the purpose of this precision study. The major changes are that the celestial Cartesian coordinates for the visible GPS satellites and for the LEO are output, and terrestrial receiver-to-GPS constellation tracking was added to output the visible GPS satellites and the terrestrial receiver coordinates. The flow chart of the software to output common GPS satellite and LEO antenna time-stamped positions is given in Figure 4.1. As can be seen, basically the LEO coordinates are computed and the GPS satellite coordinates are computed for the epoch of interest. Then the visibility is determined based on the constraints defined above. The procedure is repeated for each GPS satellite and for all epochs of interest. The LEO, GPS and terrestrial coordinates are written to files for further processing.

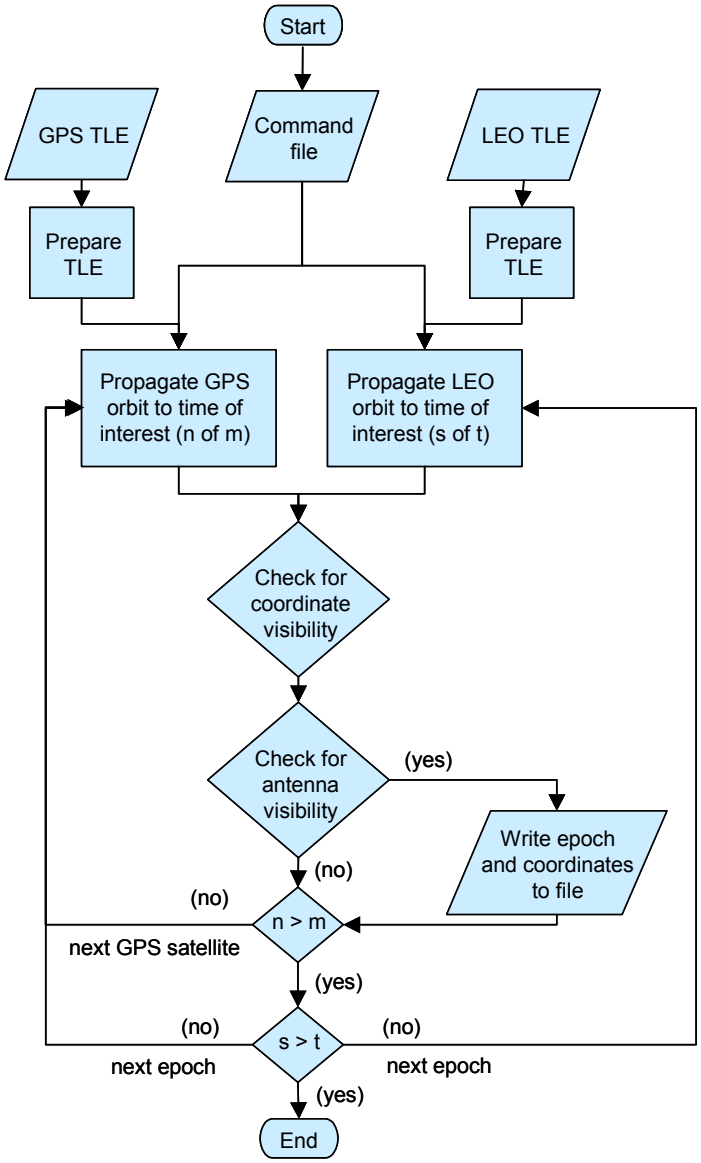

Figure 4.1: Program GGSIM flowchart of operation.

The program LEOCOVEST (Low Earth Orbiter COVariance ESTimator) was created to process time-stamped GPS, LEO and terrestrial reference receiver celestial Cartesian coordinates derived from the GGSIM program and input noise values with the described kinematic, sequential, least-squares filter/smoother. The result is a time series of the covariance of the estimated LEO position in radial, along-track and cross-track components. This time series can be analysed in terms of the input error sources. The

program was created with Matlab code. Flowcharts of the operation of the program are given in Figures 4.2 and 4.3.

In the generalised Figure 4.2, the input parameters and the GGSIM output are first used in relative dilution of precision (RDOP) calculations. RDOP is a measure of relative GPS positioning geometric strength (between terrestrial reference receiver and SGPS receiver) and is therefore a measure of the relative measurement precision. The pseudorange RDOP is computed with respect to each terrestrial reference receiver. From these time series, values are chosen in terms of a three-epoch moving average to identify the best reference station to use for relative LEO position for each epoch of the solution.

Again, the initial LEO position covariance as well as the design and observation covariance matrices for all additional epochs are computed for use in the forward filter as described in Appendix B. The same procedure, but backwards, is carried-out for the reverse filter. Finally, the two filter results are combined as specified in section 3.2.4 to produce a smoothed set of results. At each step of the processing, results are plotted on the computer screen and written to file.

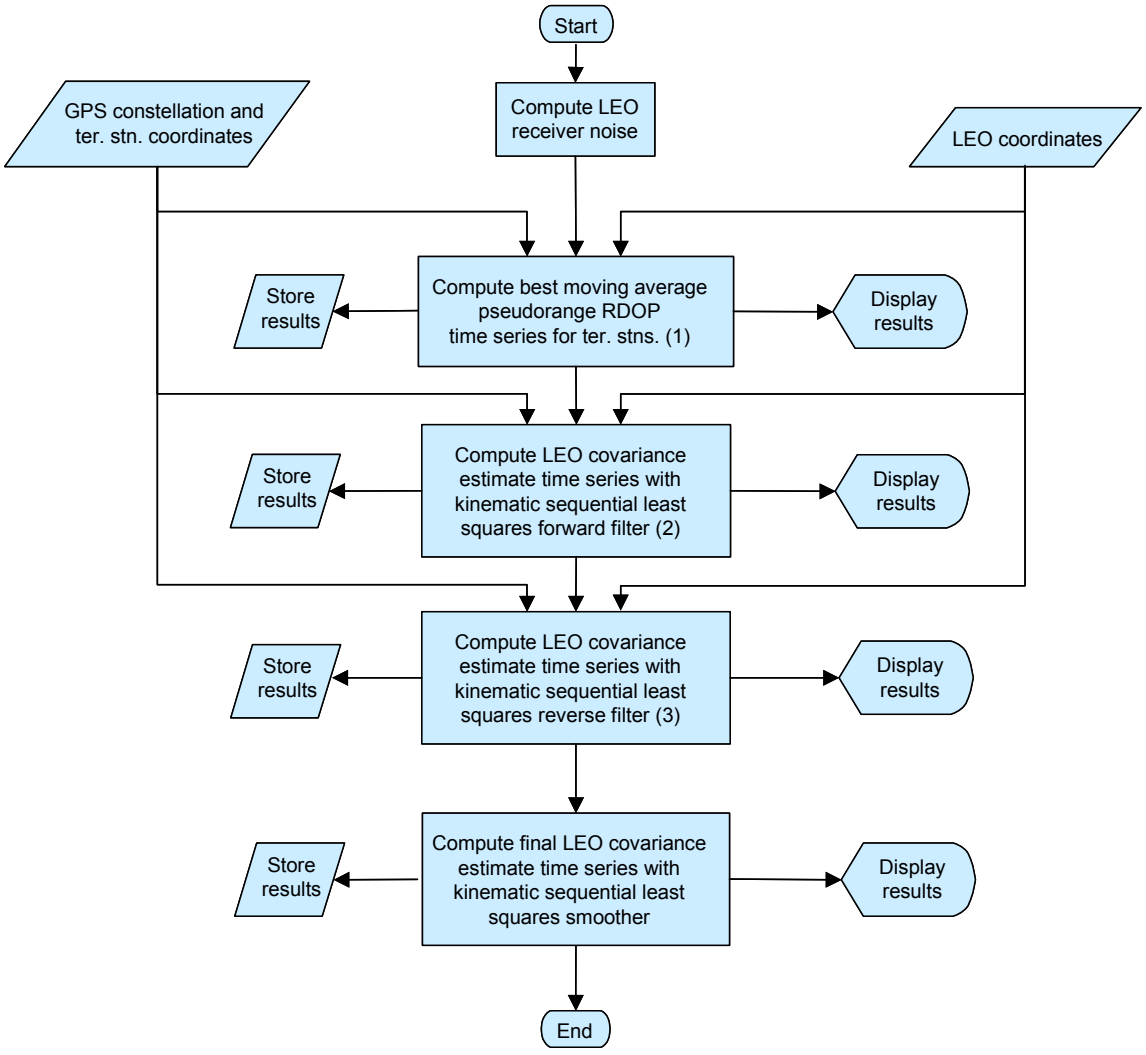

Figure 4.2: Flowchart of the overall operation of program LEOCOVEST.

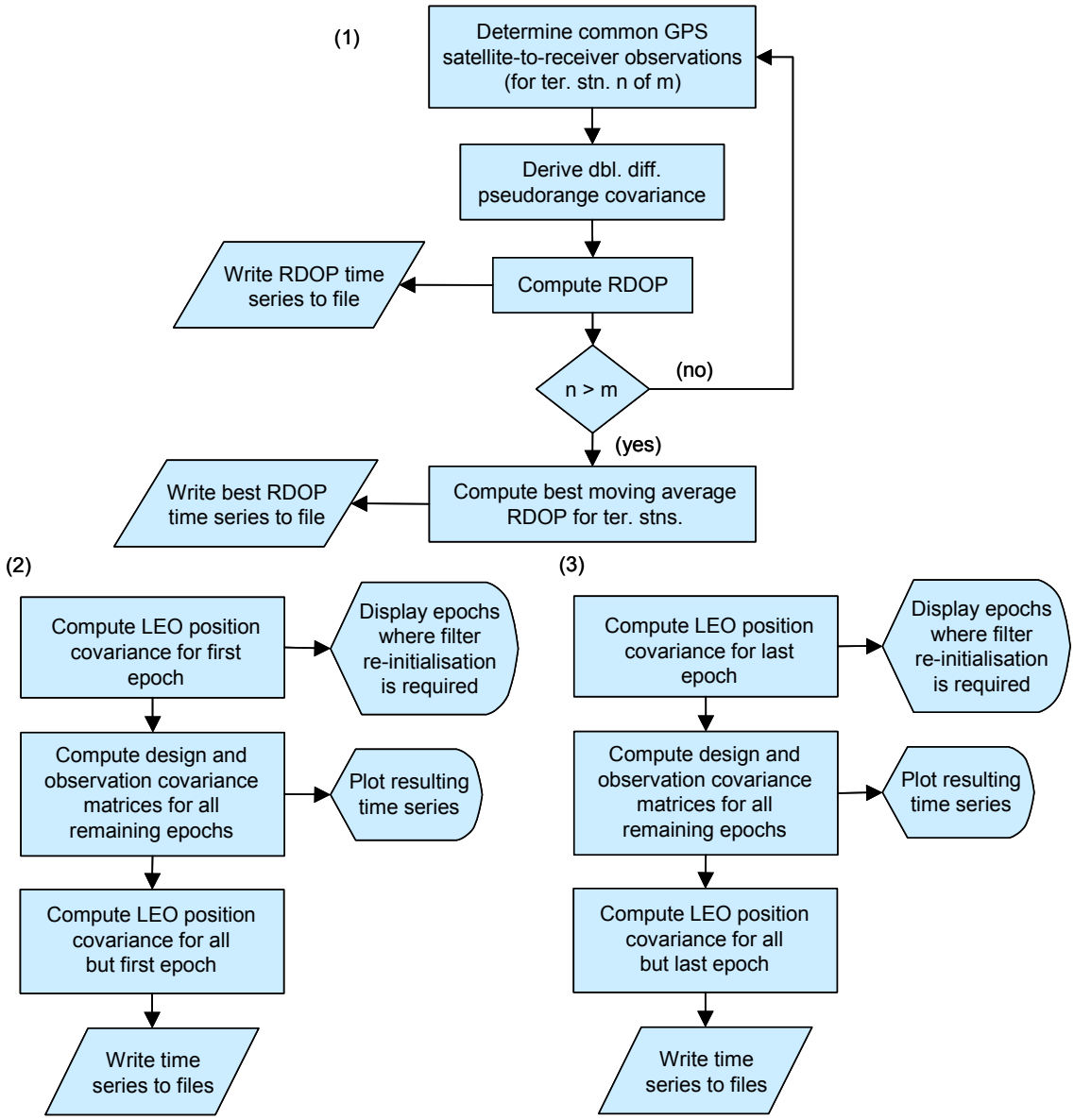

Figure 4.3: Flowchart of the detailed operation of the main components of program LEOCOVEST. (1) Selection of double-difference measurements. (2) Forward filter covariance computation. (3) Reverse filter covariance computation.

4.1.3. BOLAS Mission Scenario and Data Simulation

The baseline orbit and GPS receiver used for this analysis were from the proposed tethered Canadian Bistatic Observations with Low Altitude Satellites (BOLAS) ionospheric science mission [James, 1997] and the Allen Osborne Associates, Inc. TurboStar SGPS receiver [Kunze, 1997], respectively. BOLAS required near-decimetre *a posteriori* satellite positions. The nominal BOLAS orbital parameters are given in Table 4.1. To accommodate the use of GPS on each subsatellite, it was proposed that a 4π steradian phased antenna array be developed. In this study, the effect of using both a 2π steradian zenith-pointing antenna and a 4π steradian antenna (covering both zenith and nadir hemispheres) were analysed.

Orbital parameter	Value
Perigee	350 km
Apogee	780 km
Period	90 minutes
Inclination	103°
Perigee drift rate	-2.794°/day
Right ascension drift rate	1.657°/day

Table 4.1: Orbital parameters for the proposed BOLAS spacecraft.

The assumed input noise parameters for the study are given in Table 4.2. The carrier phase and pseudorange noise values were provided by the manufacturer. The pseudorange noise is based on a five minute integration time and the presence of Anti-Spoofing (AS). The remaining parameters are defined according to the International GPS Service (IGS) documentation [Neilan *et al.*, 1997; Gendt, 1998]. Note that the tropospheric error for the ground stations was mapped to the line of sight via the cosecant of the elevation angle. This is a sufficiently accurate mapping function for these

preliminary studies. All signals arriving at the LEO are assumed to be free of tropospheric effects. The effects of ionospheric refraction are assumed completely removed by means of the ionosphere-free, dual-frequency observable combination. The effect of signal multipath was not considered, but would degrade the solution if the SGPS antenna were located in a high multipath environment.

Parameter	Std. dev. (cm)
L1 pseudorange	2.2*
L2 pseudorange (AS on)	15.8*
L1 carrier phase	0.02
L2 carrier phase (AS on)	0.3
GPS precise ephemerides	5.0
Ground station coordinates	1.0
Tropospheric zenith path delay	1.0

Table 4.2: Input noise parameters for the error propagation study. *300 second integration period.

The BOLAS ground track for the first five hours of one arc is shown in Figure 4.4. Scenarios with 24, 32, and 40 globally distributed IGS ground stations were used, with ground station GPS satellite tracking elevation mask angles of 10º.

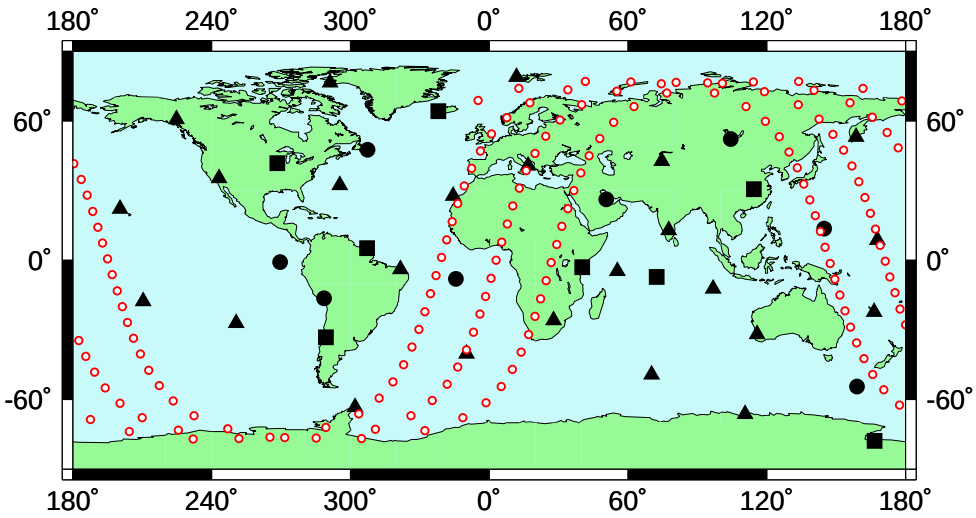

Figure 4.4: Example of a tracking scenario showing BOLAS ground track for a 5 hour arc. First 24 stations (▲). Additional 8 stations (■). And final 8 stations (●).

4.1.4. Filter Error Propagation Study Results and Analysis

In order to observe the performance and characteristics of the geometric strategy, the error propagation study was focused on a number of processing parameters including: data combination; number of ground stations; data arc length; and GPS-to-LEO signal cut-off altitude.

The first type of analysis was the observation of forward filter convergence. As can be seen in Figure 4.5, approximately 25 minutes of data was all that was required for filter convergence. The convergence occurred smoothly without spikes due to changing LEO-terrestrial receiver combinations. The positioning component noise settled at the one to two decimetre-level. This behaviour was a very encouraging sign that the geometric strategy would be successful.

Figure 4.6 represents a near-optimal situation, in which the most benefit was gained from the double-differenced pseudorange and carrier phase observables filtered and smoothed over 24 hours, using 32 ground stations, with a LEO elevation mask of zero degrees. As the terrestrial receiver / LEO / GPS constellation geometry changed, few centimetre variations in the solution standard deviations were observed, but the overall average of these values were less than ten centimetres for each position component. These results, although optimistic represent the approximate precision of the geometric strategy. And given that decimetre-level orbits are the state-of-the-art, these simulation results represented strong evidence that the technique should be developed.

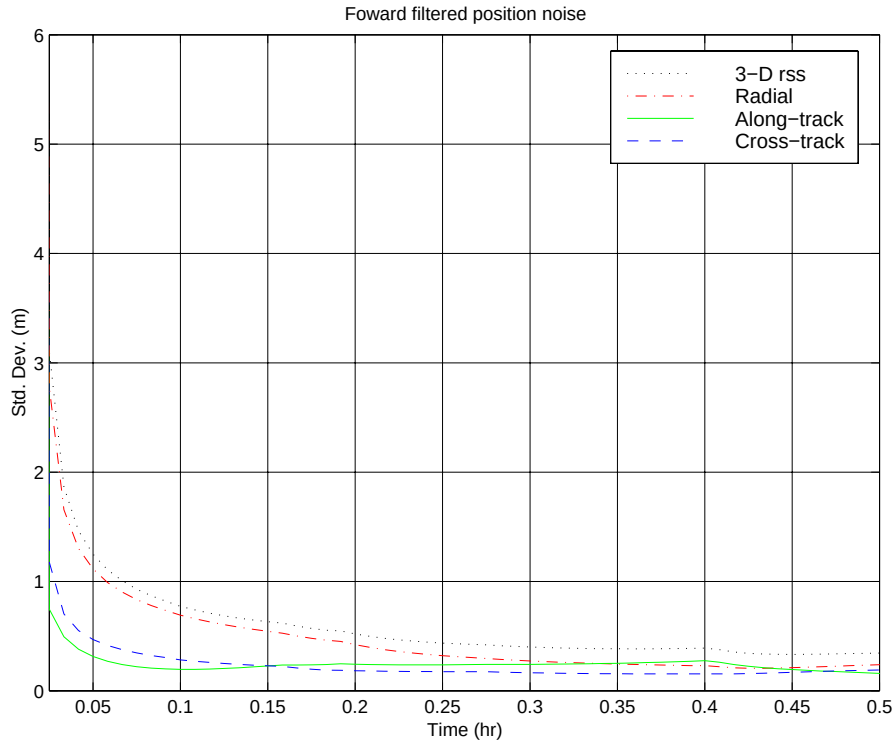

Figure 4.5: Forward filter convergence.

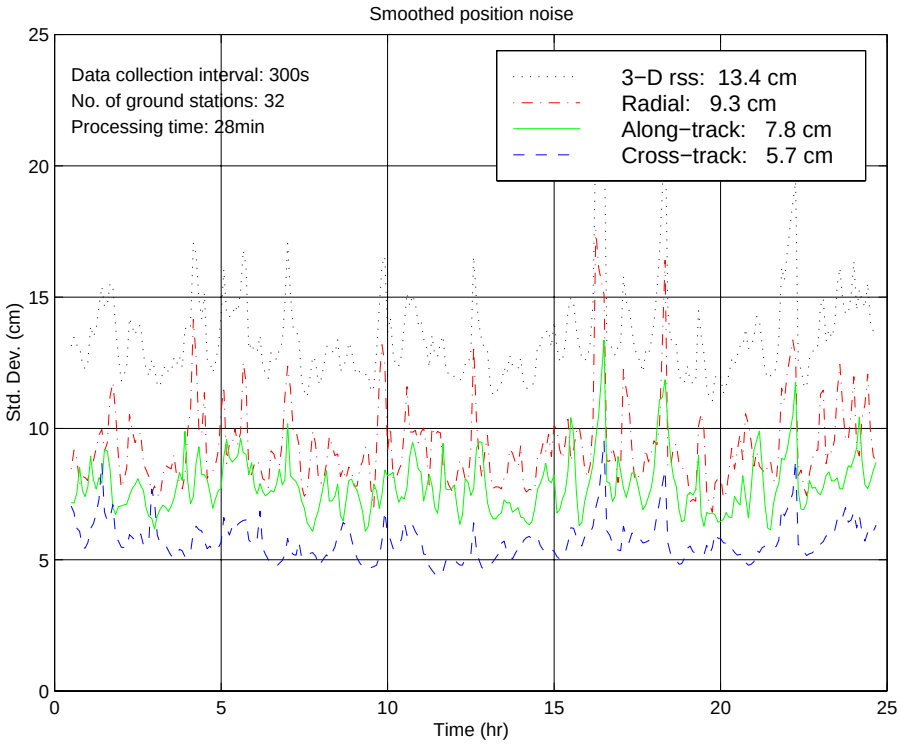

Figure 4.6: Smoothed results for near-optimal processing scenario. (Std. dev. for each component over 24 hours given in legend.)

To further understand the sensitivity of the geometric strategy to various processing parameters, a few of these parameters were varied and the resulting effects on LEO position covariances observed. Unless otherwise specified, the defaults for the processing parameters were: single-differencing; 32 ground stations; 6 hour data arc length, with 30 minutes removed from the data arc tails after processing; 300 second measurement integration period; no GPS-to-LEO signal cut-off altitude; and AS active.

Figure 4.7 shows the effects of estimating (the bold lines) or not estimating (the thin lines) the receiver clock. That is, single-differenced pseudoranges and double-differenced carrier phases versus double-differenced pseudoranges and triple-differenced carrier phases, respectively. The use of double-differenced observations resulted in a mean radial component error that was approximately 1 cm larger than the along-track error and more than 3 cm larger than the cross-track error. Representing the behaviour of the LEO receiver clock with a simple white noise model, the single-differenced solution provided marginally more precise results.

The number of ground stations used for the processing was next investigated. Given that for the simulation, only one terrestrial reference station was used in the processing at any one epoch, the improvement by adding ground stations was expected to be minimal. And as can be seen from Figure 4.8, this is the case. The improvement from 24 stations to 40 stations came primarily in a half centimetre reduction in the radial component position error. The largest error value also does not change significantly with varying the number of reference stations.

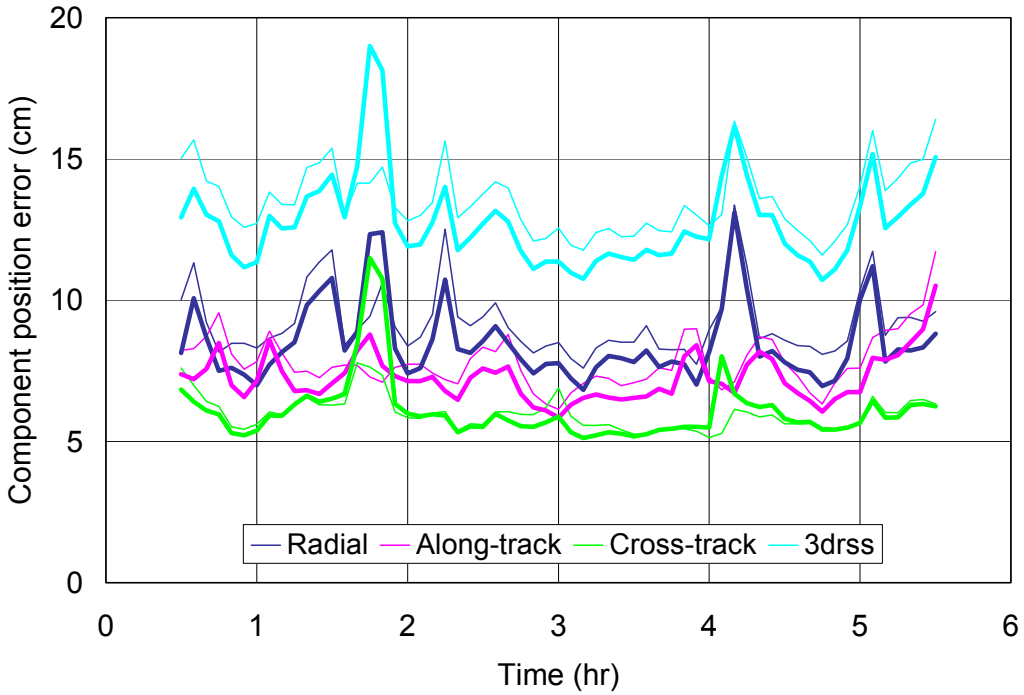

Figure 4.7: Effect of estimating (bold lines) and not estimating (thin lines) LEO receiver clock on component position error.

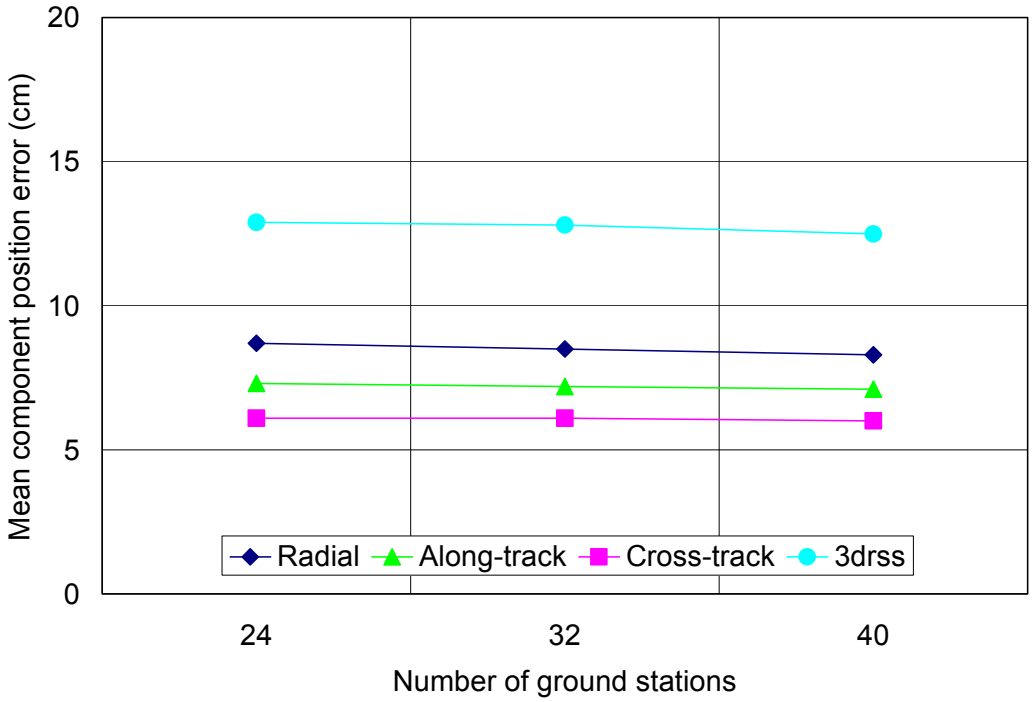

Figure 4.8: The effect of varying the number of ground stations on mean component position error.

Another processing parameter that does not have a significant effect on the position precision was the length of the data arc used in the processing. The mean position error presented in Figure 4.9 can be explained by the fact that the filter converges very quickly, and reaches a very reliable steady state.

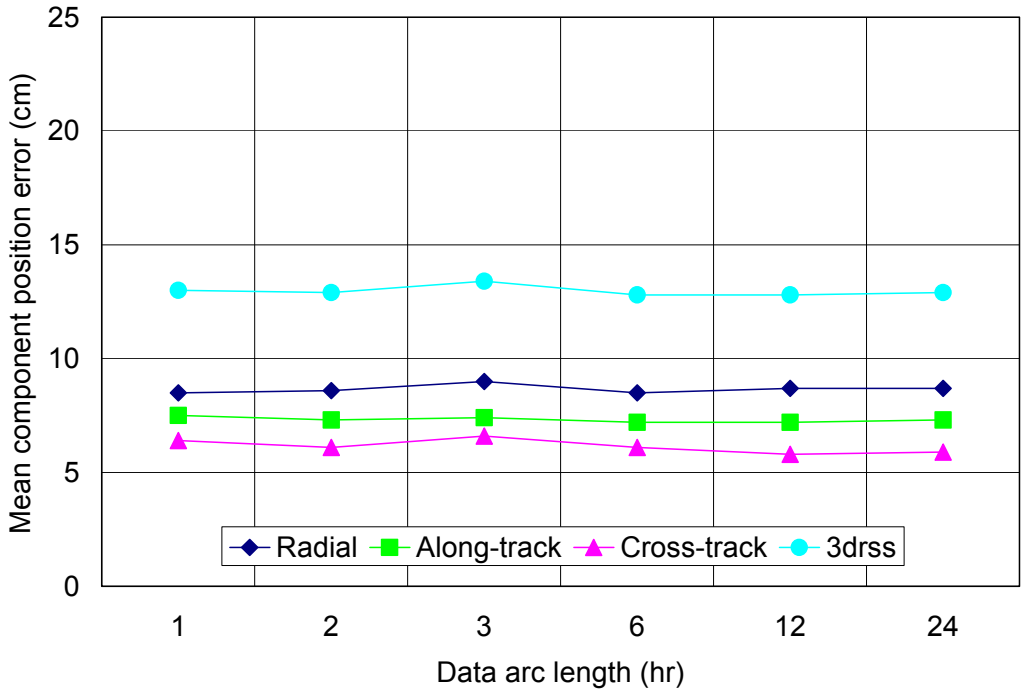

Figure 4.9: The effect of varying the data arc length on mean component position error.

As mentioned, the BOLAS mission called for the use of a 4π steradian LEO GPS antenna. Such an antenna would obviously improve the results of this purely geometric approach. However, the use of dual-frequency GPS signals that pass in and out of portions of the earth's atmosphere would increase the noise in those measurements. Therefore, either these types of signals must not be used in processing, or they must be subjected to further corrections based on existing physical models for tropospheric and ionospheric noise. In terms of the former method, an altitude cut-off term was created.

That is, line-of-sight vectors from GPS satellites to the LEO were not used for processing below a certain altitude threshold – the altitude cut-off.

Figure 4.10 compares the 2π results with a number of 4π results. For BOLAS, orbiting at relatively low proposed altitudes, the effects of introducing a 4π steradian antenna with a 1000 km cut-off altitude was negligible compared to the zenith-hemisphere 2π steradian field-of-view antenna. However, when the cut-off was reduced to 350 km (the approximate altitude of peak ionospheric electron density) the resulting mean total displacement position noise decreased from 12.8 cm to 10.7 cm. Further reduction in the altitude cut-off to 50 and 0 km produced few millimetre improvements, indicating that the increased low elevation angle data provided by the longer GPS satellite data arcs did not improve the precision of the position solution.

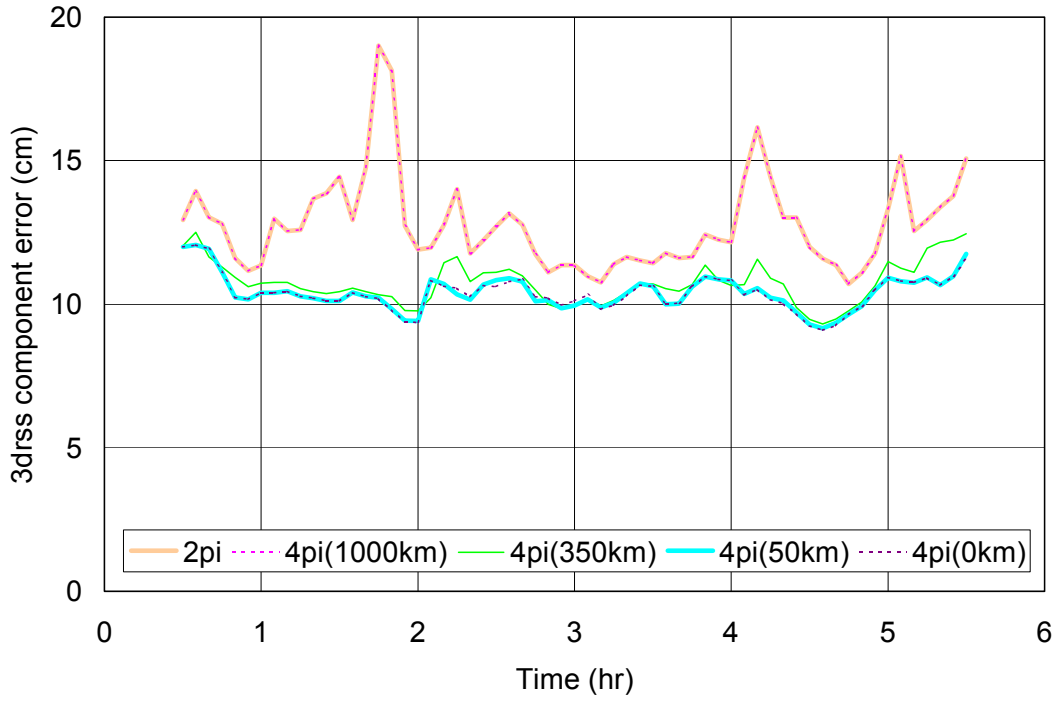

Figure 4.10: The effect of using a 4π steradian LEO GPS antenna on 3drss component error.

4.2. INTERPOLATION STUDY

In order to utilise discrete GPS-based position estimates in LEO mission applications, positions need to be accurately interpolated or approximated to epochs in between these estimates to epochs of interest to users of the orbit information. Since satellite orbits are smoothly varying for the most part, with the excepting of thrusters firings, *etc*., interpolation should produce suitable results. A basic study of the use of interpolation was carried out.

4.2.1. Interpolation Study Methodology and Datasets

Investigating the use of data interpolation, three parameters were of interest: the order of the interpolator, the spacing of the nodes of known functional values (in the case of the geometric tracking strategy, position estimates spaced in time as dictated by the measurement integration period), and the accuracy to which the interpolation is to be carried out. Of course, the type of interpolator has a significant effect on the results of the interpolator. For this study, a 15^{th} order Lagrange interpolator was used. The Lagrange interpolator was chosen as it is a standard for interpolating satellite orbits, such as those of GPS [Remondi, 1989]. Varying the interpolator by one or two orders had little effect considering the relatively smooth nature of satellite trajectories.

A 24 hour, one second dataset of the ERS2 satellite precise earth-centred, earth-fixed position estimates was used as a "truth" source [Gerrits, 2000]. ERS2 orbits at a nominal altitude of only 785 km and therefore is significantly perturbed by the earth's gravity field. The estimates were computed at the Delft University of Technology with satellite laser ranging (SLR) measurements, using the GEODYN II software package with all

orbit perturbations activated. Subsets of this data set were selected (depending on the node spacing), and processed with the interpolator. The results were then differenced with the original data set to determine the accuracy of the interpolation process.

4.2.2. Interpolation Study Results and Analysis

The results for interpolation node spacing of 0 seconds to 180 seconds can be seen in Figure 4.11. The results with spacing up to 300 seconds goes off the scale of the figure. The results have been represented in terms of the 99.73 percentile (3σ) interpolation error. That is, 0.27 percent of the errors are greater than or equal to the 3σ value. If the node interval is 90 seconds or less, basically no error is introduced in the LEO position solution due to interpolation. However, if an interval of 120 seconds is used, a small interpolator bias of approximately 10 mm is introduced, particularly to the Cartesian Y position component. Using a longer node interval would produce errors at a level equal to or greater than the resulting position noise from the above processing. The use of more sophisticated interpolation or approximation procedures might improve these results.

The conclusion, therefore is that for the ERS2 satellite and satellites with similar orbits as long as the state estimation interval is not too large, *e.g.*, > 90 seconds, there should be no ill effects in orbit accuracy due to interpolation for this altitude LEO.

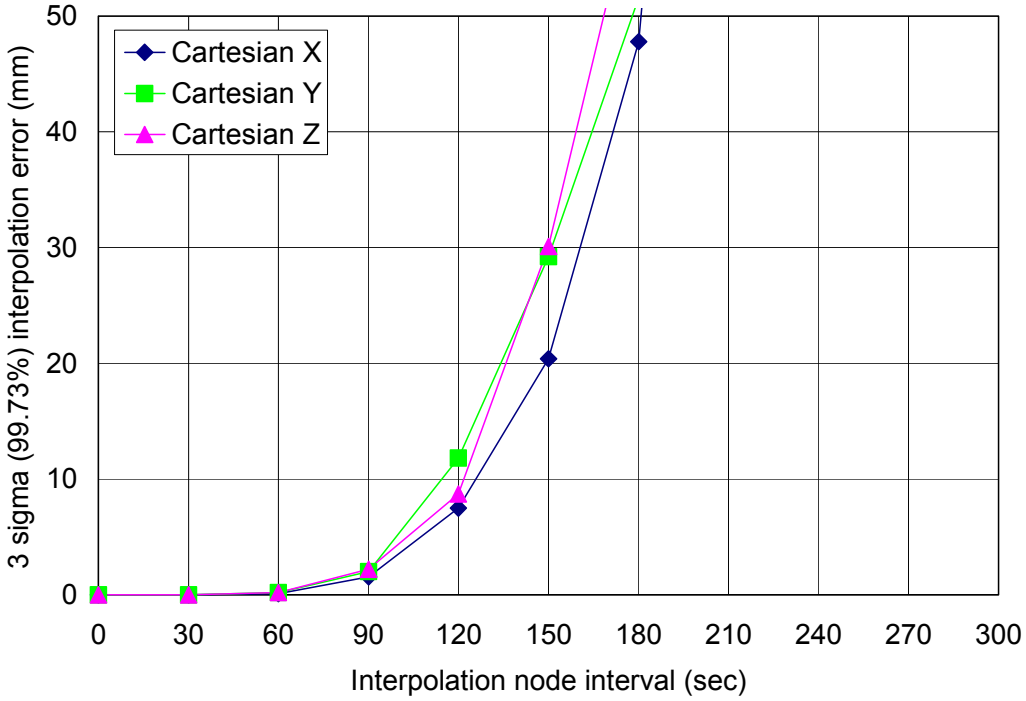

Figure 4.11: The effect of interpolation node interval on interpolation accuracy, for tests using ERS2 data.

4.3. SUMMARY

In this chapter, the initial geometric strategy was tested by means of covariance analyses in order to assess the level of orbit determination precision capable by means of the approach. The filter error propagation methodology was described, the filter error propagation software developed to carry out the analysis was presented, and the test case: the BOLAS mission scenario, was described along with its associated simulation data. Results from the simulations showed that near-decimetre level precision in each position component was possible with the geometric strategy. This level of precision was attainable under a typical SGPS data collection scenario, with the radial component solution being a few centimetres weaker.

An interpolation study was also carried out to determine the usefulness of the discrete geometric solution. Results indicate that for a LEO, interpolation between two minute nodes produces only mm level errors.

Due to changes in GPS operation, the geometric strategy was revised. The revision is presented in the next chapter.

5. THE REVISED UNB GEOMETRIC PRECISE ORBIT DETERMINATION STRATEGY

Change in the actual GPS operation by the U.S. Department of Defense profoundly altered the way in which the algorithms presented in Chapter 4 were subsequently implemented. This change, the shutting off of the intentional GPS satellite clock degradation referred to as Selective Availability (SA), and its result is described in the next section. This is followed by the presentation of the two premises of the finalised geometric strategy. Given the significant research (as will be described in detail later) into what is often referred to as precise point positioning (PPP), the relationship between the independently developed UNB strategy – termed phase-connected, point positioning and generic PPP is explained. The updated observation and solution equations are then given with descriptions of the error modelling undertaken. The chapter ends with a description of the processing code developed and used.

5.1. THE REMOVAL OF SELECTIVE AVAILABILITY (SA)

Selective Availability was the intentional dithering of the atomic clocks used by GPS satellites in the generation of transmitted signals – this in turn degraded GPS position solutions. SA was introduced by the U.S. military to protect against the exploitation of GPS by anti-U.S. and anti-allied forces, by degrading the stand-alone or real-time point positioning capabilities of a GPS receiver. With the advancement of localized GPS signal jamming techniques by the U.S. military, growing civilian use of the system, and possibly for political reasons (the proposed development of Galileo – a European version of GPS and an obvious competitor), the U.S. government de-activated SA on 2 May 2000

[OSTP, 2003]. The removal of SA had a profound affect on GPS performance. In the position domain, for stand-alone point positioning, Figure 5.1 illustrates the radical improvement.

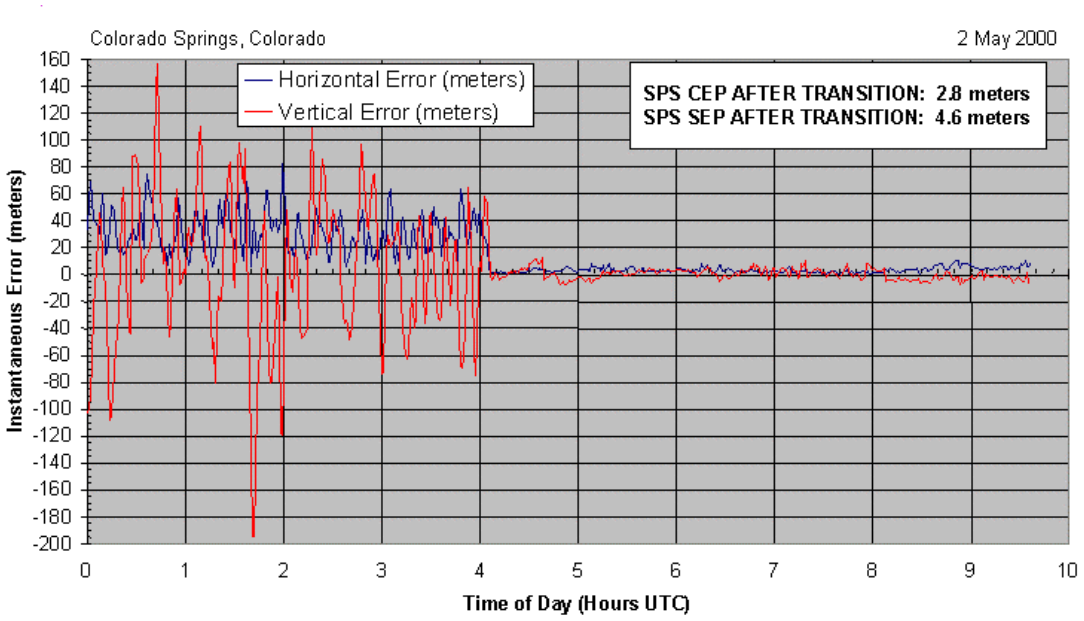

Figure 5.1: GPS point positioning accuracy transition through SA removal [IGEB].

For the algorithms and approach developed and evaluated in the simulations of chapter four, the removal of SA meant that a straightforward mathematical interpolation of GPS clock offset values over periods of minutes could now be accomplished without significant accuracy loss, and therefore double differencing of the pseudorange and carrier phase observables to cancel the GPS satellite clock error (and receiver clock error) were no longer necessary. This had two results: one, less observable differencing meant increased observable precision as error is no longer propagated through the differencing operator; and two, of much greater consequence to the processing strategy, the removal

of the need for double-differencing meant that the terrestrial reference receiver network was no longer necessary.

5.2. Philosophical Foundations of the Revised Geometric Strategy – Phase-Connected, Point Positioning

As introduced in the previous section, the removal of SA resulted in a shift from the *relative positioning* simulation software to the *stand-alone positioning* processing software. The change in positioning mode coupled with the fundamental dynamics-free nature of the simulation processing engine, resulted in the solidifying of the two foundations on which the revised geometric strategy filter is based. This form of filtering was given the intuitive name "phase-connected, point positioning".

5.2.1. Single-Receiver Positioning Due to Autonomy from Reference Receivers

GPS was originally designed to operate as a stand-alone system – that is, a receiver was all the equipment that a user required. GPS satellite orbit and clock information is transmitted to the user receiver, which in turn is responsible for all signal demodulation (GPS ranging and satellite navigation messages) and receiver state estimation. This process was modified (or augmented) with differential, and wide area differential operation. As stated, with the removal of SA, the GPS satellite clock parameters can be well estimated, rather than eliminated through between-receiver differencing. Phase-connected, point positioning reverts back to stand-alone positioning, in the sense that only a single receiver is necessary. However, this is the case because precise GPS

satellite orbit and clock parameters are being determined by some global array of monitoring receivers and subsequently ingested into the estimation process. Fundamentally what is being done is the receiver position / clock solution is being "hung" off the precise GPS constellation orbits and clocks. And therefore the reference frame and time scale of the latter will also apply to the receiver estimates.

For the processing presented in this dissertation, the IGS orbit and clock products were used, as they were readily available and represent a filtered average of a half dozen or more solutions from scientific organisations around the globe. With the IGS final 15 minute orbit and clock product and final 5 minute clock product, parameters were estimated with a Lagrange interpolator and supplied to the processor. Figure 5.2 illustrates the complete processing flow for the revised geometric POD strategy. The GPS code and phase data; and the precise ephemerides and clock offsets are scanned, edited and reformatted by the data preprocessor. The main processor performs the least-squares filtering / smoothing and outputs position and position covariance. If required, the solution can be interpolated to provide platform trajectory.

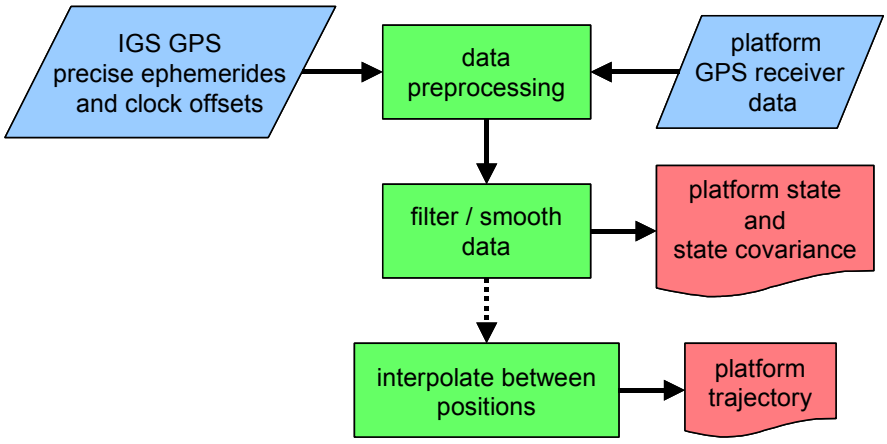

Figure 5.2: Geometric orbit determination strategy processing flow.

5.2.2. Receiver Platform Independence Due to Autonomy from Dynamical Information

In Chapter 3, the dynamics-free nature of the processing filter was described, as was the fact that this characteristic was the driving force for researching and utilising this particular filter. Again, by using the adjacent-in-time difference of the carrier phase measurements in a state-space formalism, the change in receiver position can be precisely observed, while not requiring any dynamic information about the platform the receiver is aboard. Therefore a completely kinematic solution is produced. Of course this also means that dynamic models available are not utilised, but this situation is tolerated as two aims of the research were to determine the accuracy of such non-dynamic solutions versus dynamic ones, and to develop a POD strategy not reliant on dynamic models that may not be of high enough fidelity to produce the desired results.

Figure 5.3 illustrates the phase-connected, point positioning filter operation. This is an advancement of Figure 3.3, and better describes the recursive behaviour of the filter. Code estimates are used to initialise the filter. Code and carrier measurements from the original epoch are used, in combination with code and carrier measurements from the next epoch, to re-estimate the state at the original and next epoch. The new state covariance is the connective information in the process, as it is used to initialise the next estimation epoch. If not enough code or phase measurements are present at any point of the filtering, the estimation process breaks down and the filter must be re-initialised with the next available code solution.

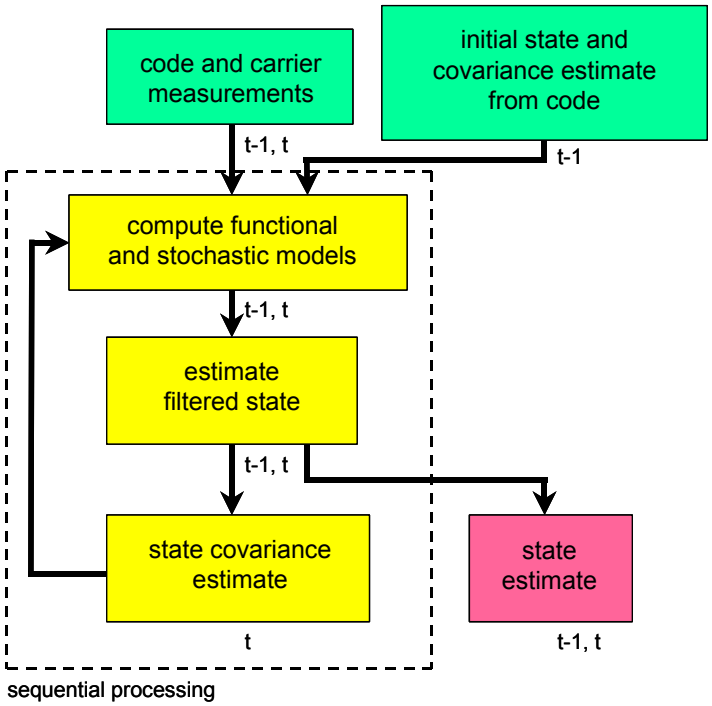

Figure 5.3: Combination of pseudorange and carrier phase observations in the kinematic, sequential least-squares filter.

5.3. Relationship Between Phase-Connected, Point Positioning and Precise Point positioning

GPS Precise Point Positioning (PPP) is a term apparently coined by Natural Resources Canada (NRCan) [Héroux and Kouba, 1995], and referred to undifferenced pseudorange stand-alone (or point) positioning, in which precise GPS constellation orbits and clock offsets are used, and receiver position, clock offset, tropospheric delay, along with a number of other error sources (to be described in section 5.4) are estimated or modelled. Lachapelle *et al.* [1994], Gao [1994] and others performed similar code-based research around the same time. The first account in the literature processing of pseudorange and carrier phase measurements from a single receiver to obtain precise positions was by Zumberge *et al.* [1997]. Since this time, precise point positioning has become a very

active research area, and much work has been done in both post-processed and real-time scenarios, including that by Muellerschoen *et al.* [2000], Kouba and Héroux [2001], and Gao *et al.* [2003].

The precise point positioning and phase-connected, point positioning architectures are similar. Both use all available pseudorange and carrier phase measurements, rely on precise GPS satellite orbits and clocks, and require the estimation of a number of parameters, some of which are ignorable in differential processing. This last point will be explained in the next section. Both techniques are initialised by the pseudorange measurements, which are gradually down-weighted as compared to the phase measurements as more data are processed by the filter. The major differences between the two approaches are: one, PPP utilises undifferenced phase measurements and therefore must somehow estimate the real-valued (float) phase ambiguities, whereas phase-connected, point positioning differences the phase measurements in time, slightly increasing the phase observable noise, but removing the ambiguity terms so long as cycle slips do not occur; and two, unlike phase-connected, point positioning which uses the time differenced phase positioning to provide kinematic information, PPP approaches require either a transition matrix if a Kalman filter formulation is used, as with the JPL approach [Muellerschoen *et al.*, 2000], or the use of process noise in a least-squares filter formulation, as with the NRCan approach [Kouba and Héroux, 2001].

5.4. PHASE-CONNECTED, POINT POSITIONING FILTER DESIGN, MODELS AND SOLUTION

With the fundamental change to GPS data processing made possible by the removal of SA and for real data processing rather than simulator results, the revised and expanded modelling undertaken is now presented.

5.4.1. Basic Modelling Requirements For Phase-Connected, Point Positioning

The revised filter was constructed in much the same way as the original simulator filter described in section 3.2 – the main difference being the removal of the double-difference operator on the code and phase observables. Therefore, following the derivations of section 3.2, the filter design, solution, and optimal smoothed solution are presented.

The filter design is reduced to:

$$\begin{bmatrix} \mathbf{P}_t \\ \mathbf{\Phi}_{t-1,t} \end{bmatrix} = \begin{bmatrix} 0 & \mathbf{A}_t \\ -\mathbf{A}_{t-1} & \mathbf{A}_t \end{bmatrix} \begin{bmatrix} \delta\mathbf{x}_{t-1} \\ \delta\mathbf{x}_t \end{bmatrix} + \begin{bmatrix} \mathbf{e}_t \\ \boldsymbol{\varepsilon}_{t-1,t} \end{bmatrix}; \quad \mathbf{C_p}, \mathbf{C_\Phi}, \tag{5.1}$$

where (following equation 3.16) $\mathbf{P}_t$ and $\mathbf{\Phi}_{t-1,t}$ are the vectors of undifferenced, ionosphere-free pseudorange and time-differenced carrier phase observations, respectively, $\delta\mathbf{x}_{t-1}$ and $\delta\mathbf{x}_t$ are the corrections to the approximate LEO position coordinates and receiver clock at epochs t-1 and t, respectively, $\mathbf{A}_{t-1}$ and $\mathbf{A}_t$ are the measurement partials with respect to the position coordinates, $\mathbf{e}_{t-1}$ and $\boldsymbol{\varepsilon}_t$ are the processed pseudorange and time-differenced carrier phase observation error vectors, and $\mathbf{C_p}$ and $\mathbf{C_\Phi}$ are the variance-covariance

matrices of the processed pseudorange and time-differenced carrier phase observations, respectively. The lack of terrestrial reference stations and double-differencing operator significantly reduces the matrix construction task.

The sequential, least-squares solution for this set of equations is the same as that in equation 3.19:

$$\begin{bmatrix} \boldsymbol{\delta}\hat{\mathbf{x}}_{t-1} \\ \boldsymbol{\delta}\hat{\mathbf{x}}_{t} \end{bmatrix} = \begin{bmatrix} \mathbf{x}^{0}_{t-1} \\ \mathbf{x}^{0}_{t} \end{bmatrix}$$

$$+ \begin{bmatrix} \mathbf{A}_{t-1}^{T}\mathbf{C}_{\boldsymbol{\Phi}}^{-1}\mathbf{A}_{t-1} + \mathbf{C}_{\hat{\mathbf{x}}_{t-1}}^{-1} & -\mathbf{A}_{t-1}^{T}\mathbf{C}_{\boldsymbol{\Phi}}^{-1}\mathbf{A}_{t} \\ -\mathbf{A}_{t}\mathbf{C}_{\boldsymbol{\Phi}}^{-1}\mathbf{A}_{t-1} & \mathbf{A}_{t}^{T}\left(\mathbf{C}_{\mathbf{P}}^{-1} + \mathbf{C}_{\boldsymbol{\Phi}}^{-1}\right)\mathbf{A}_{t} \end{bmatrix}^{-1} \begin{bmatrix} -\mathbf{A}_{t-1}^{T}\mathbf{C}_{\boldsymbol{\Phi}}^{-1}\mathbf{w}_{t} \\ \mathbf{A}_{t}^{T}\mathbf{C}_{\mathbf{P}}^{-1}\mathbf{w}_{t-1} + \mathbf{A}_{t}\mathbf{C}_{\boldsymbol{\Phi}}^{-1}\mathbf{w}_{t} \end{bmatrix}. \tag{5.2}$$

And the smoothed solution represents the same weighted combination of forward and backward filter runs:

$$\hat{\mathbf{x}}_{\mathbf{s}t} = \mathbf{F}\hat{\mathbf{x}}_{\mathbf{f}t} + \mathbf{R}\hat{\mathbf{x}}_{\mathbf{r}t}, \tag{5.3}$$

where (as with equation 3.22) $\hat{\mathbf{x}}_{\mathbf{s}t}$, $\hat{\mathbf{x}}_{\mathbf{f}t}$ and $\hat{\mathbf{x}}_{\mathbf{r}t}$ are the optimal smoothed, forward filter, and reverse filter parameter estimates, respectively, and **F** and **R** are the weighting matrices to be determined (as discussed in Section 3.2.4).

When dealing with real rather than simulated GPS data, a number of other basic modelling requirements must be met. The first of these is dealing with carrier phase cycle slips caused by the receiver's inability to maintain phase lock on a carrier signal. This may occur for a variety of reasons, such as signal blockage, scintillation, multipath, *etc*. The approach developed for dealing with cycle slips followed the algorithms

developed by Blewitt [1990] and are a revised version (for undifferenced rather than double-differenced observables) of the algorithms presented in Bisnath [2000] and Bisnath *et al.* [2001]. The technique automatically detects, determines, and repairs cycle-slips in dual-frequency, kinematic (and static) GPS data. Given that the time-differenced phase observable is used in the current application, only the detection feature of the technique is necessary. The technique relies on the detection of cycle slips via two geometry-free linear combinations of the dual-frequency GPS measurements, namely the geometry-free phase:

$$\begin{aligned}&\lambda_1\phi_1 - \lambda_2\phi_2 \\ &= \left(d_{ion2} - d_{ion1}\right) + \left(\lambda_1 N_1 - \lambda_2 N_2\right) + \left(m_1 - m_2\right) + \left(\varepsilon_1 - \varepsilon_2\right),\end{aligned} \tag{5.4}$$

and the widelane phase minus narrowlane pseudorange:

$$\begin{aligned}&\lambda_4\left(\phi_1 - \phi_2\right) - \lambda_5\left(\frac{P_1}{\lambda_1} + \frac{P_2}{\lambda_2}\right) \\ &= \lambda_4\left(N_1 - N_2\right) + \lambda_4\left(\frac{m_1}{\lambda_1} - \frac{m_2}{\lambda_2}\right) - \lambda_5\left(\frac{M_1}{\lambda_1} + \frac{M_2}{\lambda_2}\right) + \lambda_4\left(\frac{\varepsilon_1}{\lambda_1} - \frac{\varepsilon_2}{\lambda_2}\right) - \lambda_5\left(\frac{e_1}{\lambda_1} + \frac{e_2}{\lambda_2}\right),\end{aligned} \tag{5.5}$$

where P_i is the measured pseudorange (in distance units), respectively; λ_i is the carrier wavelength; ϕ_i is the measured carrier phase (in cycles); N_i is the number of cycles by which the initial phases are undetermined; d_{ioni} is the delay due to the ionosphere; m_i and M_i represent the effect of multipath on the carrier phases and the pseudoranges, respectively; and ε_i and e_i represent the effect of receiver noise on the carrier phases and the pseudoranges, respectively, and $\lambda_4 = \left(\lambda_1^{-1} - \lambda_2^{-1}\right)^{-1}$ and $\lambda_5 = \left(\lambda_1^{-1} + \lambda_2^{-1}\right)^{-1}$. Slips are detected for each combination via a number of geometric tests and statistical tests based

on the noise of the observables, the results of which when combined represent a high-resolution, yet straightforward method for detecting cycle slips. Phase measurements containing slips are removed from further computations by the pre-processor.

In terms of stochastic modelling, the main concern was the input values for the code and phase measurement precisions that would provide for a realistic ratio between the two observable types. For example, these values for the CHAMP satellite data processing (to be discussed in Chapter 6) were 75 cm for the ionosphere-free pseudorange and 2.0 cm for the time-differenced, ionosphere-free carrier phase, and were determined based on BlackJack SGPS receiver specifications and data processing experience. The choice of observable noise levels did not have any significant influence on the filter so long as good quality, continuous phase measurements are used, resulting in the bulk of the solution being provided by the precise change-in-phase data. To increase the realism of these noise values, the carrier phase weights were made a function of GPS satellite elevation angle. Tests indicated that the function cosecant of elevation angle produced improved positioning results at the centimetre-level for static, terrestrial GPS baselines of tens of kilometres in length [Collins and Langley, 1999] and also for spaceborne data processing [Bock *et al*., 2001]. The cosecant weighting function was tested with CHAMP satellite spaceborne data and produced no significant improvement in positioning. This result can be explained by the lack of low elevation angle (*i.e.*, < 10-15 degrees) data used in the processing with which to down-weight.

Another stochastic modelling possibility for the GPS data is the de-weighting of multipath-corrupted pseudorange measurements. This can potentially be performed by first constructing the so-called pseudo-multipath observable which represents code and

phase multipath and noise [Braasch, 1994]. This observable is created by: 1) subtracting the L1 carrier phase from the L1 pseudorange; 2) removing the ionospheric delay term by estimating the dual-frequency biased ionospheric delay from the L1 and L2 carrier phases; and 3) removing the bulk of the ambiguity terms by subtracting the mean of all of the observable values from the observable values. This results in:

$$pm_1 \approx M_1 - m_1 + dTRK_1 - dtrk_1 + E_1 - e_1 , \tag{5.6}$$

where pm_1 is the so-called pseudo-multipath, M_1 and m_1 represent the effect of multipath on the pseudoranges and the carrier phases, respectively; $dTRK_1$ and $dtrk_1$ represent the effect of dynamics-induced tracking error on the pseudoranges and the carrier phases, respectively (see, *e.g.*, Braasch [1994]); and E_1 and e_1 represent the effect of receiver noise on the pseudoranges and the carrier phases, respectively. This observable can be readily constructed for static and kinematic data alike, but cannot be used to actually estimate pseudorange multipath due to the small (few centimetre to decimetre-level) residual phase ambiguity term left from step 3 above. However, it may be possible to de-weight pseudorange observations which correspond to an above average pseudo-multipath value. This was attempted in Bisnath and Langley [2001b], with modest success. More research is needed in this area to make it effective, so the procedure has not been applied in the LEO processor, but will be referred to in the potential future research section of this dissertation.

5.4.2. Additional Modelling Requirements For Phase-Connected, Point Positioning

A number of additional potential position-determination-contaminating phenomena must be taken into account in point positioning that would otherwise be cancelled in relative positioning. An excellent review of these correction models is given in Kouba and Héroux [2001].

The GPS satellite antenna phase centre offset was taken into account. This is the separation vector between the satellite centre of mass, to which precise ephemerides refer, and the transmitting antenna phase centre, to which the measured ranges refer. The offsets used for Block II and IIA satellites are 0.279, 0, 1.023 m, for the X (towards the Sun), Y (completes right-handed coordinate system) and Z (towards the earth) components, respectively, and zero for Block IIR satellites [see, *e.g.*, Kouba and Héroux, 2001]. Since point positioning relies on the accuracy of GPS satellite coordinates for reference frame stability in determining receiver coordinates, any transmitter antenna offset would map into receiver position. A standard transformation (see, *e.g.*, Santos [1995]) is required to model the offset and this was applied in the orbit determination software.

Another potential metre-level point positioning error source is the relativity term observed in range measurements due to the ellipticity of the GPS satellite orbits, also referred to as periodic relativity. This term is modelled by observing the satellite position and velocity in the following equation (after, *e.g.*, ICD [1993]):

$$T_{rel} = -2\vec{X}_S \cdot \vec{V}_S / c^2, \tag{5.7}$$

where $\vec{X}_S$ and $\vec{V}_S$ are the GPS satellite position and velocity vectors, respectively, and c is the speed of light.

Carrier phase wind-up [Wu *et al*., 1993] can cause decimetre-level phase range error in point positioning. This is the phenomenon whereby the rotation of a transverse wave's transmitter or receiver increases or decreases the phase of the signal resulting in an altered (biased) range measurement. The complex relationship between the transmitting GPS satellite's constantly changing orientation with respect to the receiving antenna's orientation must be modelled (see, e.g., Kouba and Héroux [2001]). Receiver antenna related wind-up is common to all measured carrier signals and maps directly into the receiver clock offset term [Wu *et al*., 1993]. Fortunately with the time differencing of the phase observable in phase-connected, point positioning, the effective time-differenced wind-up effect is at the sub-millimetre-level.

This effect is illustrated in Figure 5.4. In (a) the observed wind-up for GPS PRN29 observed at 5 minute intervals at the Algonquin Park (ALGO) reference receiver on 31 March 2002 is estimated by NRCan [Collins, 2002]. The associated time-differenced wind-up was computed and is given in (b). The magnitudes of the wind-up are very small and give an indication that even for a fast-moving LEO with an orbital period 12 to 16 times faster than a static terrestrial station, these time-differenced magnitudes are at the sub-millimetre to millimetre level. Further proof can be seen in Chapter 6, where time-differenced, ionosphere-free carrier phase residuals contain no noticeable biases, drifts, or significantly large magnitudes.

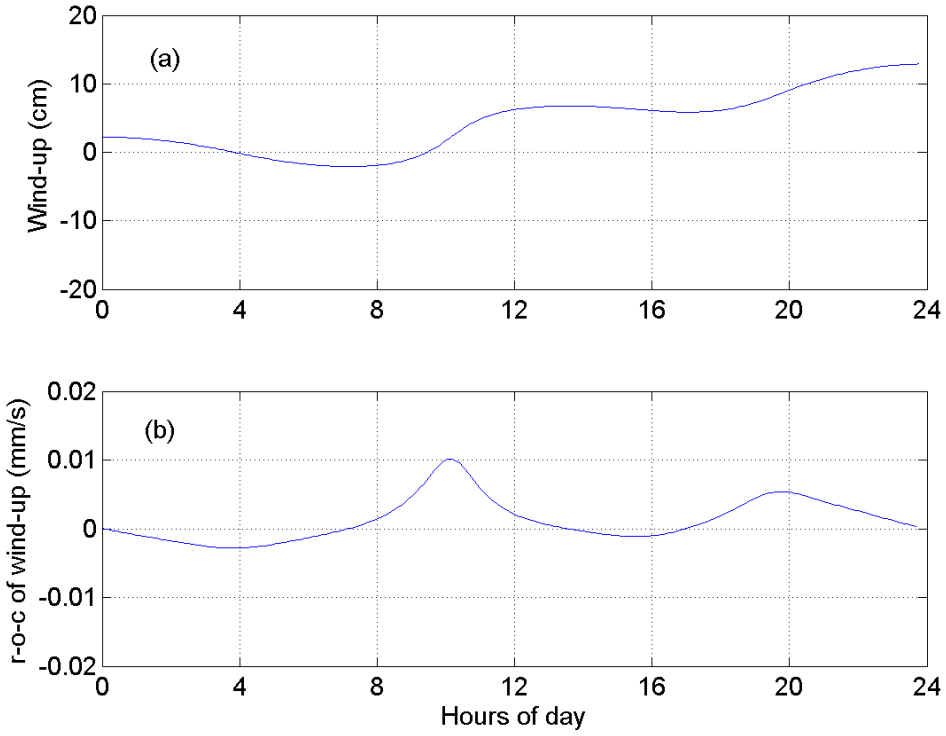

Figure 5.4: Phase wind-up and rate-of-change of wind-up for PRN29 observed at station ALGO on 31 March 2002 (after Collins [2002]).

A number of non-LEO data processing modelling terms are also required for the processing of terrestrial receiver measurements. They are briefly mentioned here for completeness and given that some terrestrial data were processed for testing and evaluation purposes. The tropospheric delay plays a significant role in point positioning estimation and for related testing conducted in Chapter 6 the UNB3 tropospheric delay prediction model [Collins, 1999] was used, as it is accurate and requires no meteorological input. The solid earth-tide model available in DIPOP was used to model the displacement effects caused by the sun, moon and other planets on the visco-elastic earth. The effect of ocean loading, also modelled in DIPOP, was not implemented in the processing software due to its small effect at the test terrestrial stations.

5.5. REALISATION OF GEOMETRIC STRATEGY IN PROCESSING SOFTWARE

The computer code created for the processing of GPS data was based on UNB DIfferential PrOcessing Package (DIPOP) code [Kleusberg *et al*., 1993]. DIPOP was designed for static, high-precision, long-baseline processing, and its architecture involves a pre-processor program and a main processor program, all coded in FORTRAN 77. The geometric POD strategy uses the DIPOP programs as a foundation, closely following some modules, while completely diverging from others.

The major programs used or created in the entire data processing and analysis procedure are shown in Figure 5.5. The pre-processor edits and reformats the measurement and GPS ephemeris and clock information, and the main processor, which contains the phase-connected, point position filter / smoother estimates LEO positions. These two programs form the core of the developed software and are the subject of the next two subsections.

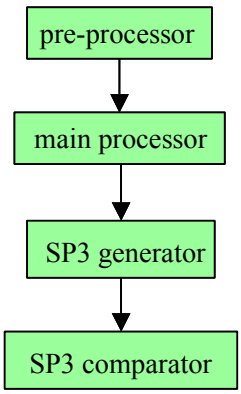

Figure 5.5: Flowchart of data processing and analysis procedure.

The solution coordinates file is then converted to SP3 format with the SP3 generator program. Since the main processor generates LEO GPS antenna phase centre coordinates

and SP3 coordinates are generally related to spacecraft centre of mass, the antenna phase centre to centre of mass offset vector is applied after transformation from the LEO spacecraft coordinate system to the ECEF coordinate system. These rotations represent LEO attitude and are typically presented in quaternion form as supplied by satellite attitude sensor processed output. DLR (Montenbruck [2002]) provided a routine to convert quaternions to vector displacements for SP3 file generation.

Finally, the capability was created to compare the UNB computed LEO SP3 files against orbits generated by other research groups using different processing strategies. The SP3 comparator was developed by the European Space Agency (ESA) [Boomkamp, 2001]. The program relies on Lagrange interpolation of each orbit's discrete coordinates to a temporally common set of coordinates. The coordinate subset is then differenced and various statistics computed.

5.5.1. Data Pre-Processor: PREGO

The original PREGO (short for PREprocess GPS Observations) program is the DIPOP pre-processor. PREGO was expanded in the dissertation to include kinematic data, specifically kinematic RINEX files. Figure 5.6 illustrates the flow of data pre-processing in PREGO. The version of PREGO developed for LEO processing utilises an ASCII command (input) file to control processing runs. This file contains, among other items, the input observation file name, the desired data arc and sampling interval, and output observation and summary file names. Once the command file has been read, the appropriate RINEX observation file is scanned into memory. The observations are then screened for outliers and partial records. This is followed by cycle slip detection for

which an output cycle slip file is created for main processor use. The ionosphere-free pseudoranges are then computed. During the entire pre-processing run, selected processing parameters and output are collected. These arrays are then written to a summary file. Finally, the UNB formatted observation array is written to file.

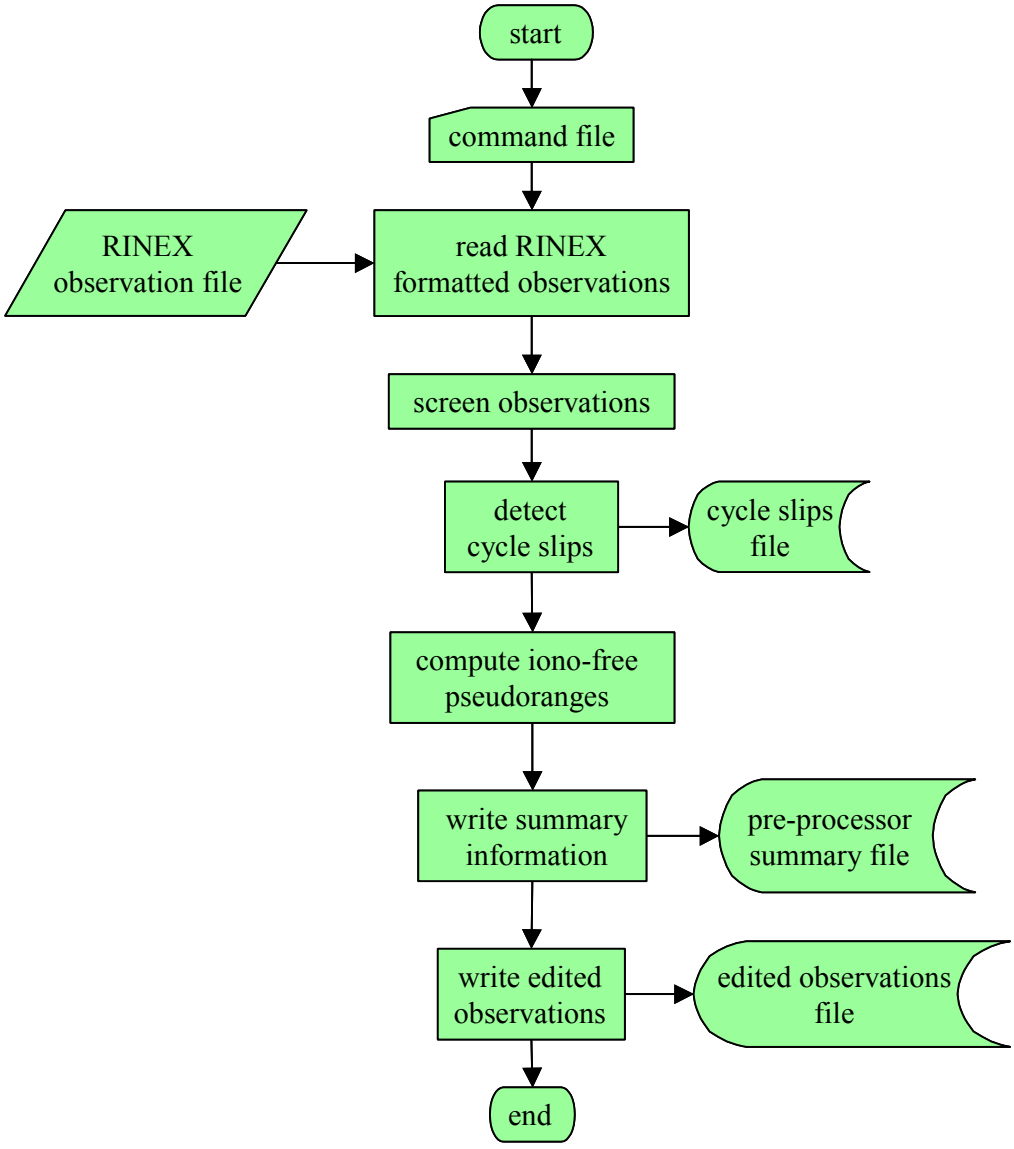

Figure 5.6: Flowchart of PREGO – GPS data pre-processor.

5.5.2. Data Main Processor: KMPROC

KMPROC (short for Kinematic Main PROCessor) is based loosely on MPROC from DIPOP. The observation and ephemeris file formats have been kept, as well as some of the processing structure. Figure 5.7 illustrates the KMPROC processing flow. As with the pre-processor, the main processor is command file-driven. This ASCII file contains input and output file names, as well as a number of processing parameters: elevation mask angle; application of solid earth tide; and GPS satellite arc editing. The first step is to scan the UNB-formatted observation file and the SP3-formatted GPS satellite orbit and clock files into memory. From these data files an initial pseudorange-based point position solution trajectory is computed. With this trajectory an optional elevation mask filter can be applied as well as tropospheric delay predictions, and an improved pseudorange-based solution can be computed. (Note that the two-stage pseudorange solution is a result of the step-by-step development of the software.) After the optional application of solid earth tide corrections (which are only required for ground-based receivers) the pseudorange trajectory and associated solution residuals are written to files. (Again, these corrections are applied in a sequential manner due to the step-by-step writing of the software.)

The pseudorange solution provides a basis for the phase-connected, point positioning solution, which is next computed. (The two-stage process is again a product of the software evolution.) The phase-connected, point positioning solution is optionally corrected for earth tides and is written to file along with the associated residuals. The

observation arrays are then reversed and the backward filter solution and residuals computed and written to files. Finally, the forward and backward filter solutions are combined in a weighted average to produce the smoothed trajectory, which is also written to file.

Given the importance of the phase-connected, point positioning filter implementation, it is now explained in detail. Figure 5.8 illustrates the flow of this subroutine, which represents the forward and backward filter solution processes in the Figure 5.7 KMPROC flowchart. The filter solution trajectory is first initialised with the pseudorange solution. The process then proceeds epoch-by-epoch, first checking for and applying cycle slip information from PREGO and selecting observables from the present and past epochs. All deterministic parameters, such as the relativity corrections and GPS satellite orbit and clock corrections are then computed. Finally, the least-squares solution for the LEO antenna position and receiver clock offset is iterated (due to the Taylor series expansion of the non-linear mathematical model) until solution convergence is achieved.

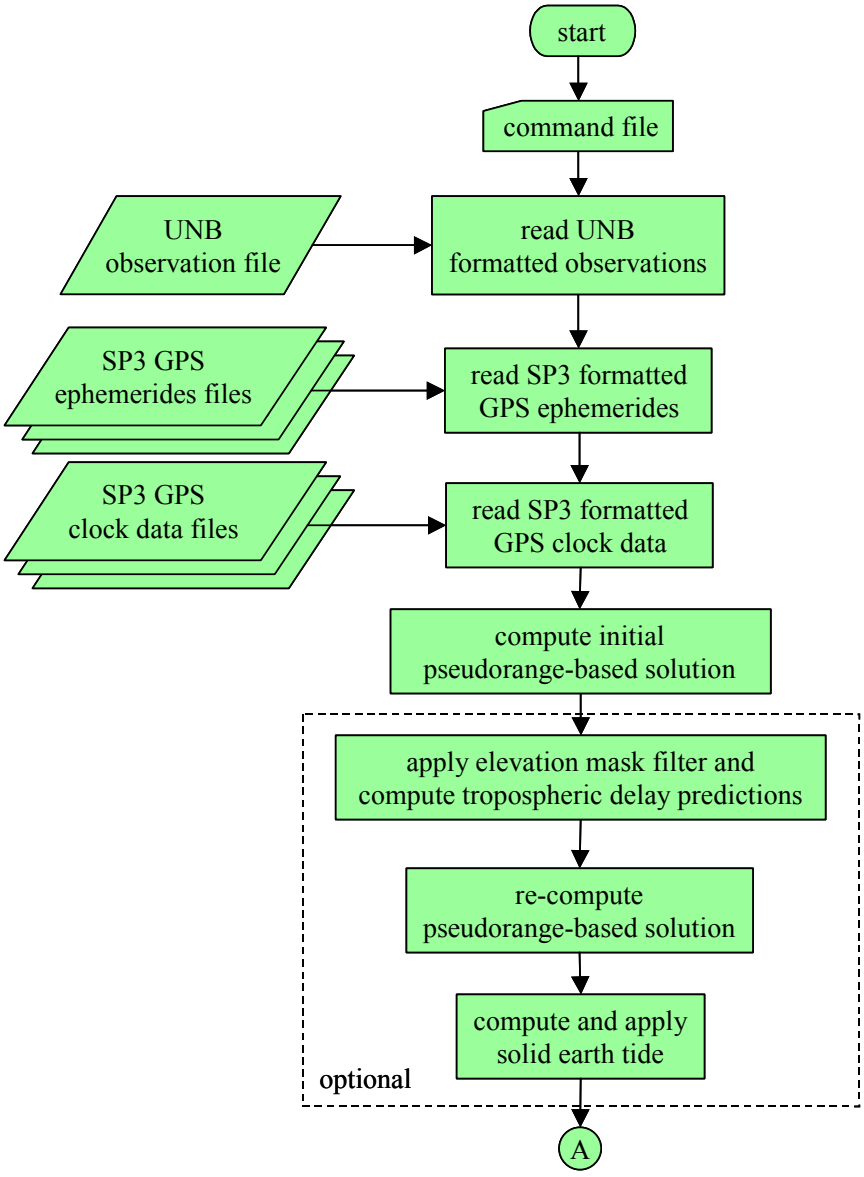
start
command file
UNB
observation file
read UNB
formatted observations
SP3 GPS
ephemerides files
read SP3 formatted
GPS ephemerides
SP3 GPS
clock data files
read SP3 formatted
GPS clock data
compute initial
pseudorange-based solution
apply elevation mask filter and
compute tropospheric delay predictions
re-compute
pseudorange-based solution
compute and apply
solid earth tide
optional
A

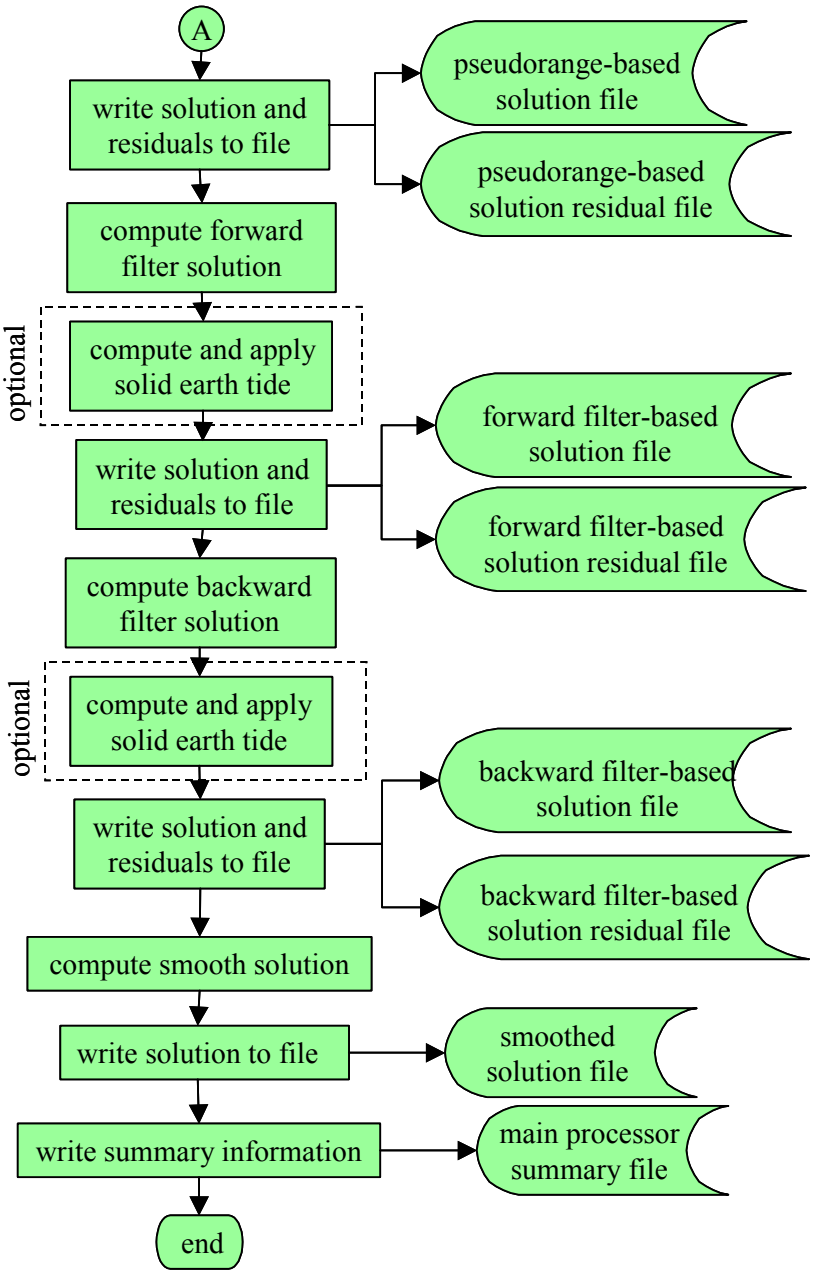

Figure 5.7: Flowchart of KMPROC – GPS data main processor.

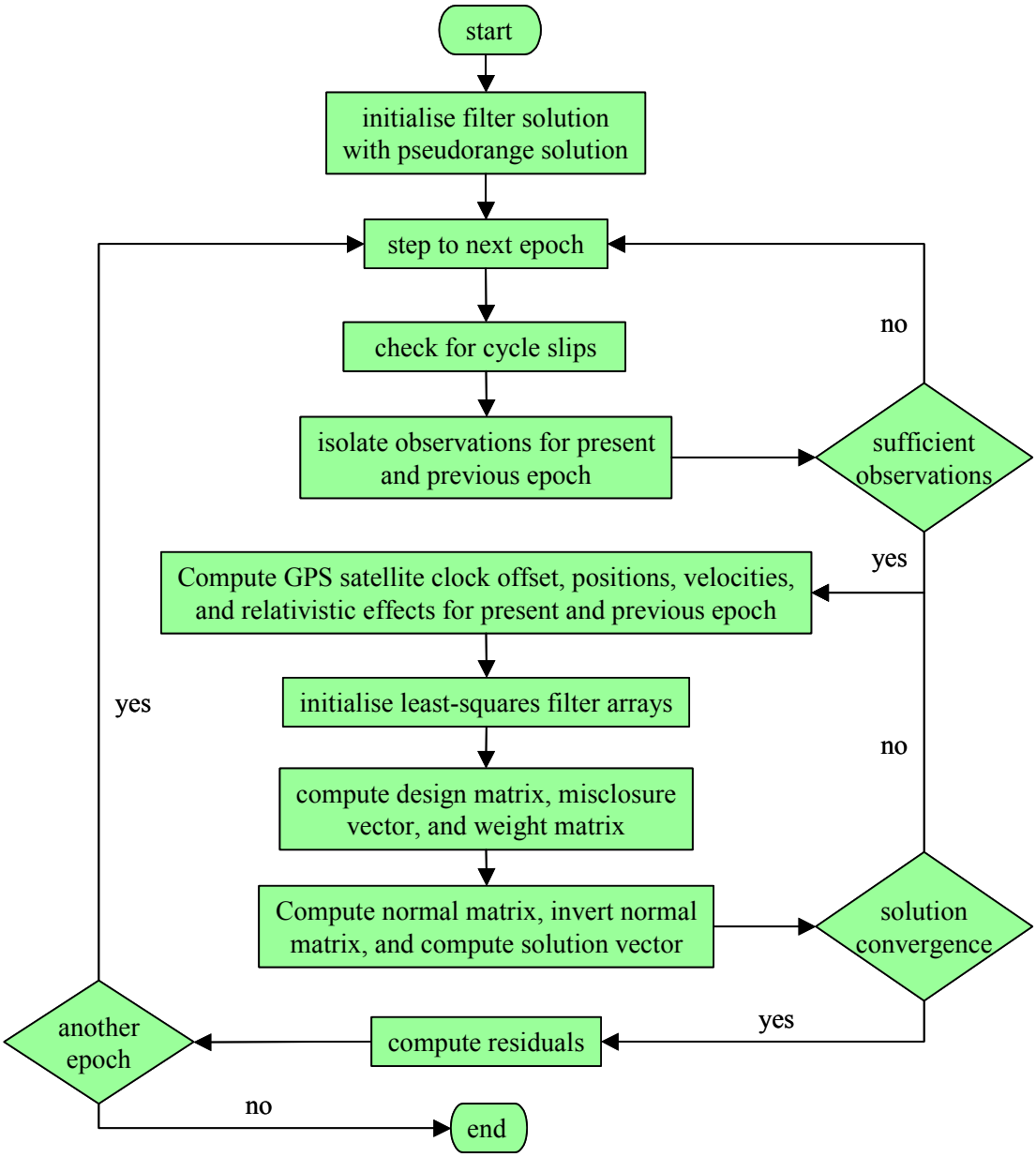

Figure 5.8: Flowchart of the FORTRAN "filt" subroutine – GPS phase-connected, point positioning filter containing kinematic, sequential least-squares filter.

5.6. SUMMARY

In this chapter the geometric strategy was revised due to the removal of SA. The technique evolved from a transmitter / receiver double-differenced approach to a transmitter / receiver undifferenced point positioning one. The term developed to define the positioning mode is phase-connected, point position, since the time-differenced phase observable is used to remove the integer ambiguity terms. The revised filter design models and solutions were presented, as well as descriptions of the processing software modules created to apply the developed algorithms.

The next chapter will present results and analysis from a number of different data sources using the developed software.

6. GEOMETRIC STRATEGY PROCESSING RESULTS AND ANALYSIS

The software development and processing of test data sets were carried out simultaneously. As additional modelling aspects were undertaken and subroutines added to the software, continual testing was performed on static and kinematic data sets to gauge the influence and correctness of the modifications. Section 6.1 summarises some of the static results as well as some other initial results on various platforms including a LEO. Section 6.2 reviews the work performed for the IGS LEO Orbit Campaign of 2001, including problems encountered, results and analysis of our UNB results, and the overall results presented by all of the campaign participants. The chapter concludes with the most important result set of this dissertation from more recent LEO GPS data, which more appropriately brings into focus the strengths of the processing approach.

6.1. INITIAL DATA PROCESSING

In order to validate the viability and performance of the processing strategy, a number of tests were conducted using the latest version of the developed software at the time. This software was brought to realisation in the form of a pre-processor and a main processor as described in Chapter 5. Even though the FORTRAN 77 code was not designed to be optimal in terms of processing speed, the presented results were generated in minutes on a 1.5 MHz Pentium 5 laptop computer. Where applicable, mention will be made of additional processing or modelling that, with future development, will improve the accuracy of the results. Note that most of these results have been presented earlier by Bisnath and Langley [2001a, 2002a, 2002b, 2003] and Bisnath *et al.* [2002].

To illustrate the platform-independent nature of the technique, three widely varying types of data are presented: terrestrial, airborne, and spaceborne. The only common (and required) characteristic of these datasets is that they were collected with geodetic-grade receivers – that is, the receivers were capable of measuring high-quality pseudorange and carrier phase dual-frequency observables. The only other data used in the processing were the requisite IGS precise GPS constellation orbit and high-rate GPS constellation clock offset products.

6.1.1. Static, Terrestrial Calibration Tests

The objective of the testing with static terrestrial data was to investigate the repeatability of position computations with the technique and to test the performance of the technique against positioning results derived from the highest quality geodetic techniques.

The data used for this testing were collected over a one day period on 5 February 2001 at NRCan station Algonquin (IGS station identifier ALGO) in Algonquin Park, Ontario, Canada (latitude 46°N, longitude 78°W). Note that the data set was chosen at random. The NRCan edited for outliers TurboRogue BenchMark receiver output contains measurements with a 30 second sampling interval and a 10° elevation mask angle.

Although LEO data are the prime concern in this research, as described in Chapter 5 the UNB3 tropospheric prediction model was used for this terrestrial data to compensate for tropospheric delay, and therefore un-estimated residual tropospheric delay could cause up to few-centimetre errors in the position domain. The receiver position and clock

were estimated at the data sampling interval and this produced a satellite clock modelling error – a few centimetres (about 0.1 ns) at the most, arising from the interpolation of the available 300 second interval IGS satellite clocks product.

The first aspect of the processing that was analysed, since this technique relies solely on GPS observations, was the geometric strength of the measurements used. Figure 6.1 shows the number of satellites tracked and the position dilution of precision (PDOP). As can be seen, there are always at least 5 satellites being tracked in this data set and on occasion up to 10. The average number for the processed data is 7.3. The PDOP typically remains between 1.5 and 3, but a few spikes exist where the PDOP reaches approximately 4.5 and 6. The average PDOP is 2.2. Given that there is a 10° elevation mask angle, these values are reasonable and represent geometrically strong measurements. However, given again the complete reliance on measurements, low elevation angle data, *e.g.*, down to 5°, would have aided in improved accuracy position results.

The results of the processing are presented in Figure 6.2. The error values are computed by differencing the estimated position from the benchmark International Earth Rotation and Reference Systems Service (IERS), epoch-of-date, International Terrestrial Reference Frame 1997 (ITRF97) coordinates, which are known to the one cm level [Neilan *et al*, 1997]. The ITRF97 coordinates were used, since ITRF97 GPS satellite orbits were used in the estimation. As can be seen, the error in each component reaches a maximum of ± 50 cm. The error fluctuates the most in the vertical component. This is

expected, given that the residual tropospheric delay was not estimated, and the inherent limitation brought about by the GPS constellation geometry.

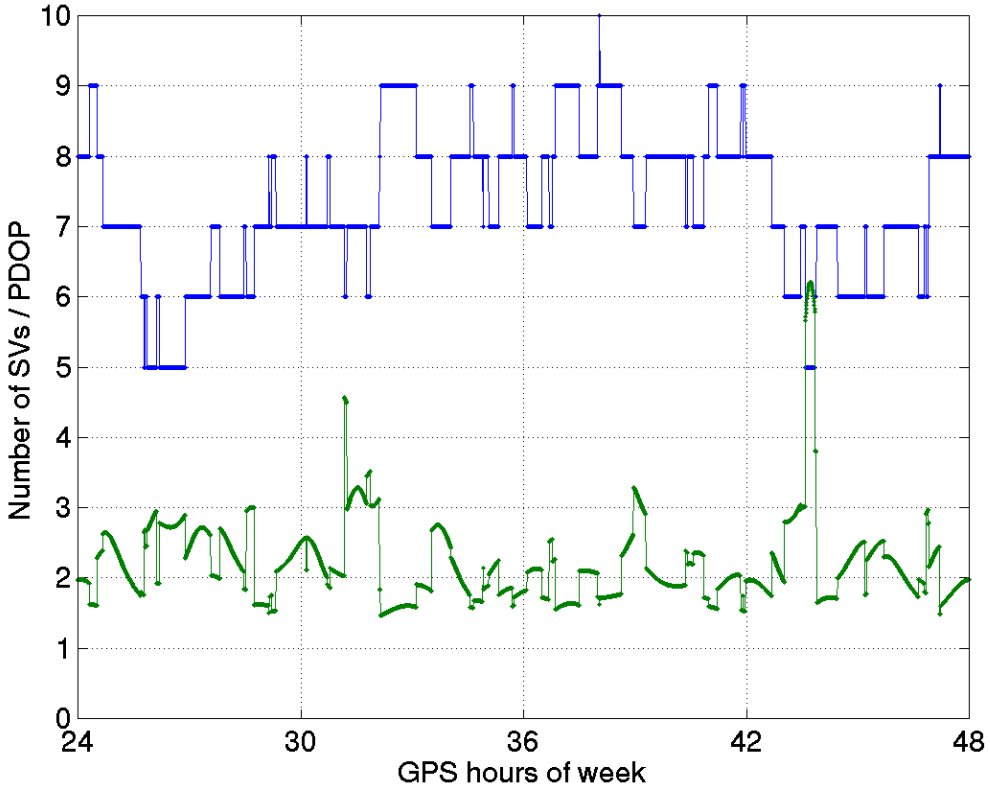

Figure 6.1: Number of space vehicles (SVs) and the position dilution of precision (PDOP) for static, terrestrial dataset.

Summary statistics for this data set are given in Table 6.1. The r.m.s. of the smoothed solution is 15 cm in each horizontal component, while the vertical component is 20 cm. The smoothed total displacement r.m.s. is just under 30 cm. Also of note are the few-centimetre biases that exist in the horizontal components. Given that such correction terms as the residual tropospheric delay, sub-daily earth rotation variations, ocean loading, and antenna phase centre variation have not been applied, and that the GPS satellite orbits and clocks were interpolated to 30 seconds, these results compare favourably with other published single-receiver processing results, *e.g.*, Héroux *et al.*

[2001], which show high accuracies. This is said, since such other published techniques include dynamic information to constrain the solution space – in the case of the mentioned reference, process noise values indicating stationary position. The geometric strategy places no *a priori* covariance constraint on the receiver antenna coordinates.

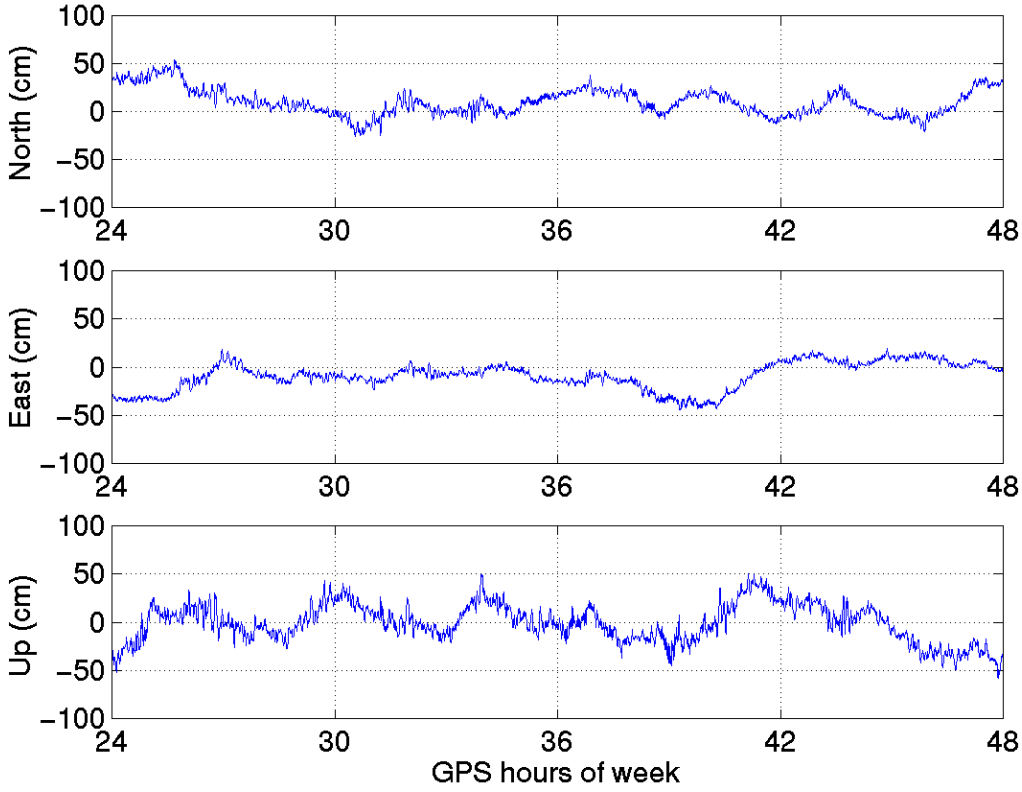

Figure 6.2: Component errors in smoothed position estimates for static, terrestrial dataset.

Component	bias	std.	r.m.s.
North	4.4	13.9	14.5
East	-4.3	14.2	14.8
Up	0.6	19.8	19.8
3-D	6.2	28.0	28.7

Table 6.1: Summary statistics (cm) of component errors in smoothed position estimates for static, terrestrial data set.

The forward filter residuals, along with the associated GPS satellite elevation angles, are shown in Figure 6.3. The large initial ionosphere-free, time-differenced phase values are due to filter initialisation. The ionosphere-free pseudorange r.m.s. is 66 cm with peak-to-peak variations of 10 m, and the phase observable r.m.s. is 2 cm with peak-to-peak variations of 15 cm, aside from the initialisation period. These values appear to be reasonable for the particular linear combinations of the pseudorange and carrier phase combinations they represent.

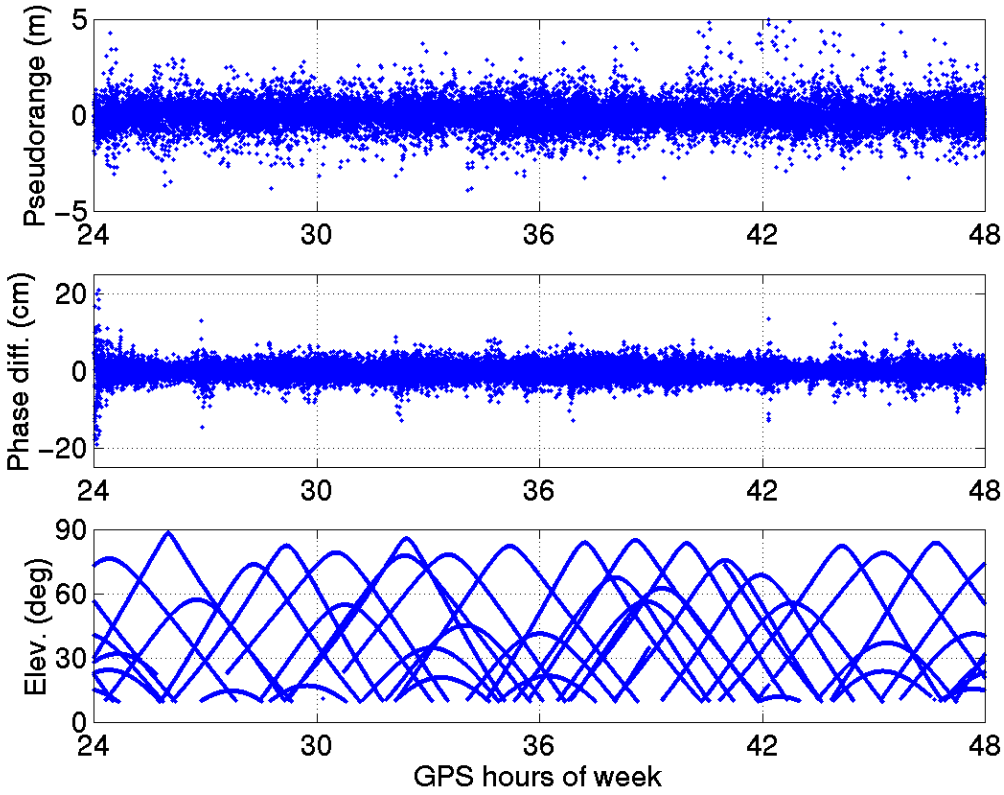

Figure 6.3: Forward filter observable residuals and associated satellite elevation angles for static, terrestrial data set.

6.1.2. Various Other Tests

The next test illustrates the performance of the processing technique for a receiver on a kinematic platform – a small airplane in level flight in the vicinity of Sendai Airport, in Japan on 5 December 2000. Figure 6.4 depicts the complete trajectory for the approximately 2 hour flight. The cross pattern of the flight path meant that the aircraft reached a maximum horizontal distance of over 50 km from the cross-over area (Sendai Airport), at which is located a reference receiver that was used for conventional kinematic, relative carrier phase processing. The conventional solution was obtained with commercial software, using automatic processing parameter settings.

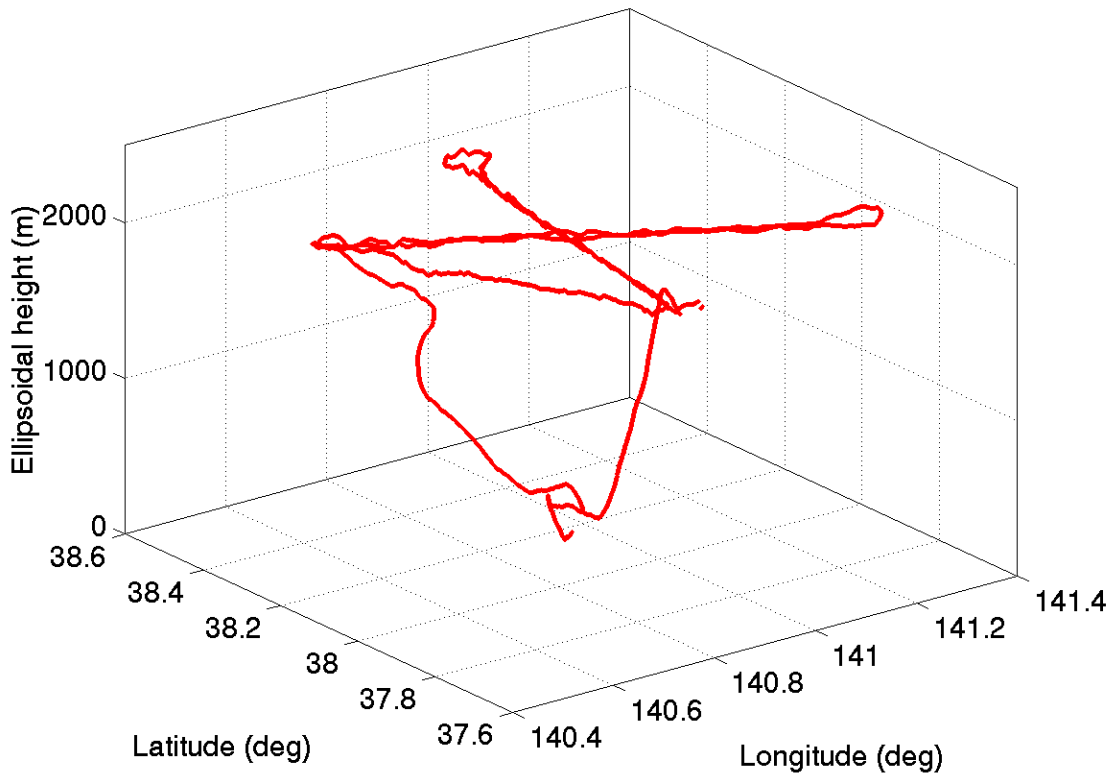

Figure 6.4: Airborne data set trajectory.

Measurement interruption is a casualty of such level, straight flight with banking turns. As can be seen in Figure 6.5, the number of tracked satellites is reduced to five or four when the aircraft banks. The actual number can be lower, but the epochs when fewer than four SVs are being tracked are not displayed in Figure 6.5. The average number of tracked SVs is 6.7. The associated spikes in the PDOP are more acute in this case, since not only are the number of SVs reduced, but their sky distribution is far from optimum. Hence, even though the mean PDOP is a respectable 2.4, there are PDOP spikes over 4 during nearly every turn the aircraft makes. This had a significant effect on both the reference double-differenced solution produced by commercial GPS software and the single-receiver solution.

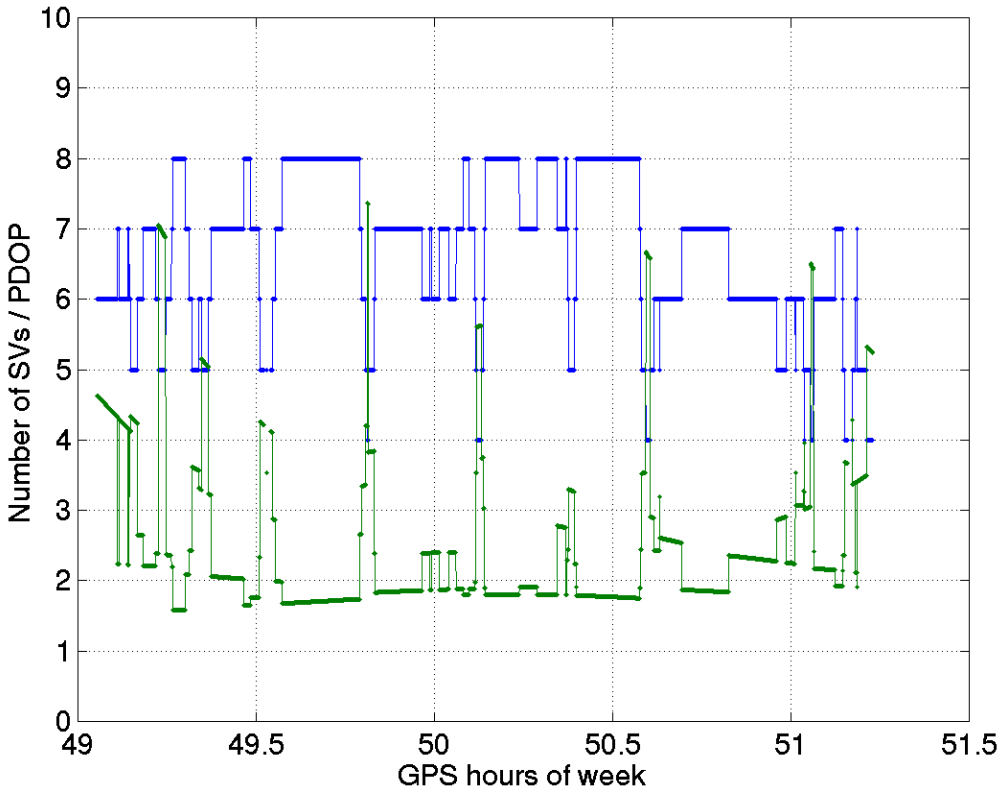

Figure 6.5: Number of SVs and PDOP for airborne data set.

Figure 6.6 shows the differences between the two solutions for one straight-line section of the flight. Table 6.2 contains the summary statistics of the component differences between the two solutions for this period. The horizontal components show 50 cm and 70 cm biases in the north and east components, respectively, with standard deviations of 5 cm or less. The up component has a near-one metre drift, causing a 30 cm standard deviation, but very little bias. One possible explanation for the biases and drift can be the use of incorrect double-differenced ambiguities in the commercial software solution. This seems to be a strong possibility for a number of reasons. Firstly, incorrect ambiguities can produce such offsets and drifts [Ackermann, 1993]. Secondly, offsets and drifts were observed between the used commercial solution and another commercial result. And thirdly, such large biases have not been observed with *any* other data set processed with our technique. These results present another possible use for this technique – the avoidance of incorrectly determined phase ambiguities for long baseline kinematic data sets. As a further test of the geometric strategy, it would be useful to process uninterrupted code and phase data from an aircraft.

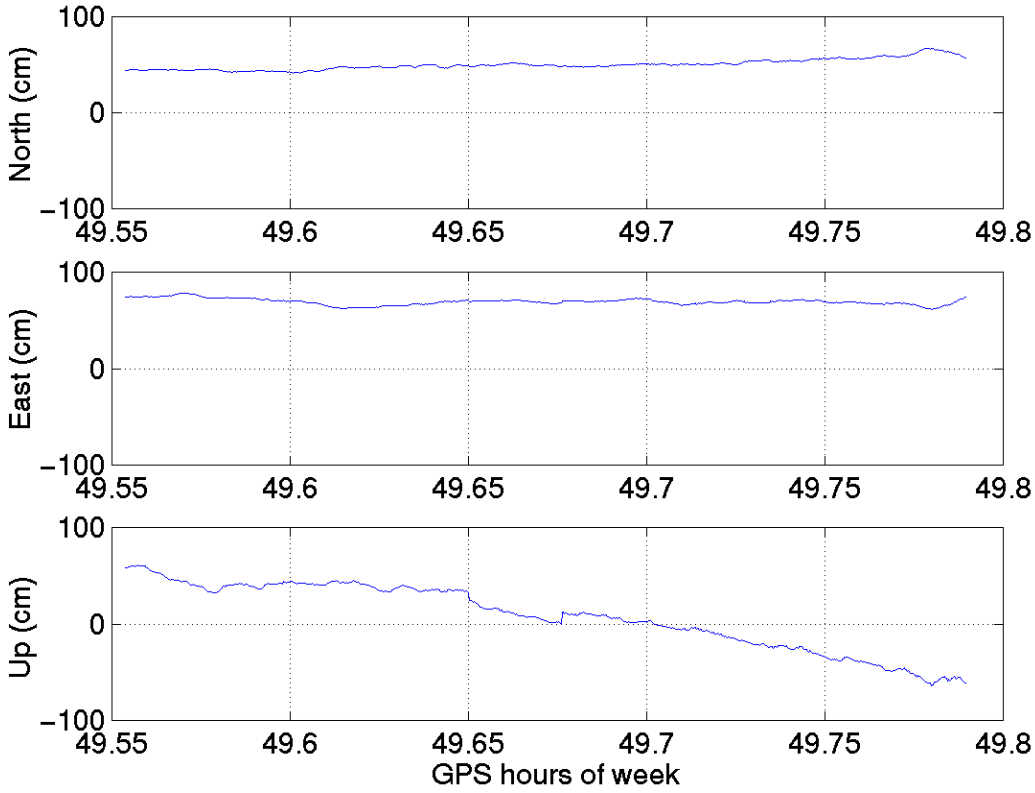

Figure 6.6: Component differences in smoothed position estimates for airborne data set.

This subsection ends with an early LEO dataset. Spaceborne data is unique for a number of reasons. The very high velocity of the platform carrying the receiver and its high altitude in the atmosphere means that the tracked GPS satellites change constantly; there is no tropospheric delay on the received signals; high-fidelity dynamic models are typically required for accurate position and orbit determination (especially for LEOs); and given precise orbits, this data type is an excellent benchmark for mobile receiver positioning.

Component	bias	std.	r.m.s.
North	50.3	5.7	50.1
East	69.1	3.0	69.3
Up	7.4	33.4	34.8
3-D	85.8	34.0	92.3

Table 6.2: Summary statistics (cm) of component differences in smoothed position estimates for airborne data set.

The spaceborne data set processed consists of three hours of CHAMP [CHAMP, 2001] data from 4 June 2001. This LEO orbits at a nominal altitude of 450 km, with a nominal period of 90 minutes, and provides dual-frequency pseudorange and carrier phase data from a Jet Propulsion Laboratory BlackJack receiver. Figure 6.7 shows a segment of the ground track of the near-polar orbiting spacecraft.

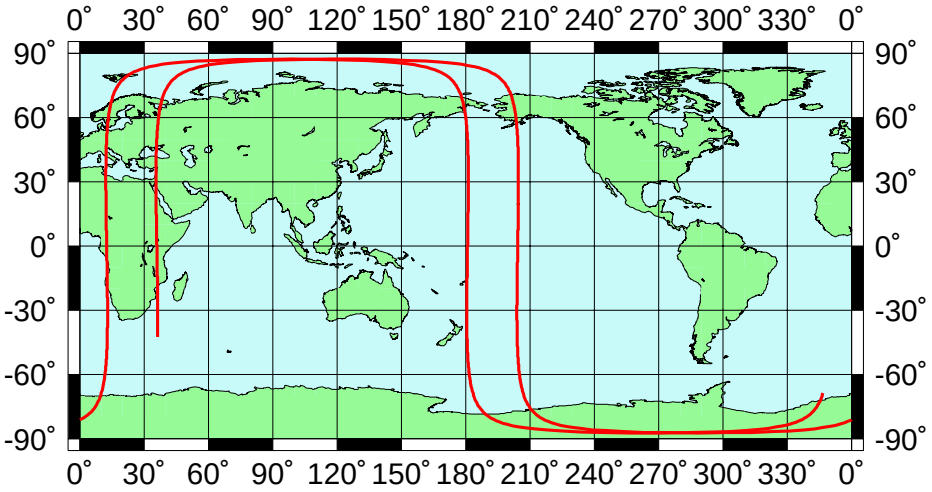

Figure 6.7: Ground track of CHAMP data set.

The data provided by the CHAMP Data Center is unedited (for blunders and outliers) and provided at 10 second intervals. No elevation mask angle appears be have been applied, as angles as low as -10° were computed. These very low elevation angle measurements also have very low signal-to-noise (SNR) values (in BlackJack SNR

units). It was found that using these measurements produced large phase residuals, and an SNR rather than an elevation angle cutoff was applied in our data pre-processing to attempt to remedy the situation. This will be expanded upon in section 6.2.2. The cutoff used in this processing was 10 units.

The purpose of processing these test data was to investigate the geometric strength of the spaceborne measurements and to assess the practicality and performance of the technique against high-quality CHAMP orbits. Figure 6.8 shows that the geometric strength of the available observations is significantly lower than that for the terrestrial data set analysed, even though a relatively good (in terms of data availability) data arc was selected. This occurs, even though the spaceborne BlackJack receiver can track up to 8 GPS satellites and much of the time is tracking the maximum number. The average number of tracked satellites is 6.6. However, the distribution of these tracked satellites causes significant measurement strength degradation. The mean PDOP is 3.1, or almost 50% larger than that for the terrestrial data set processed. This circumstance will be further discussed later in this section.

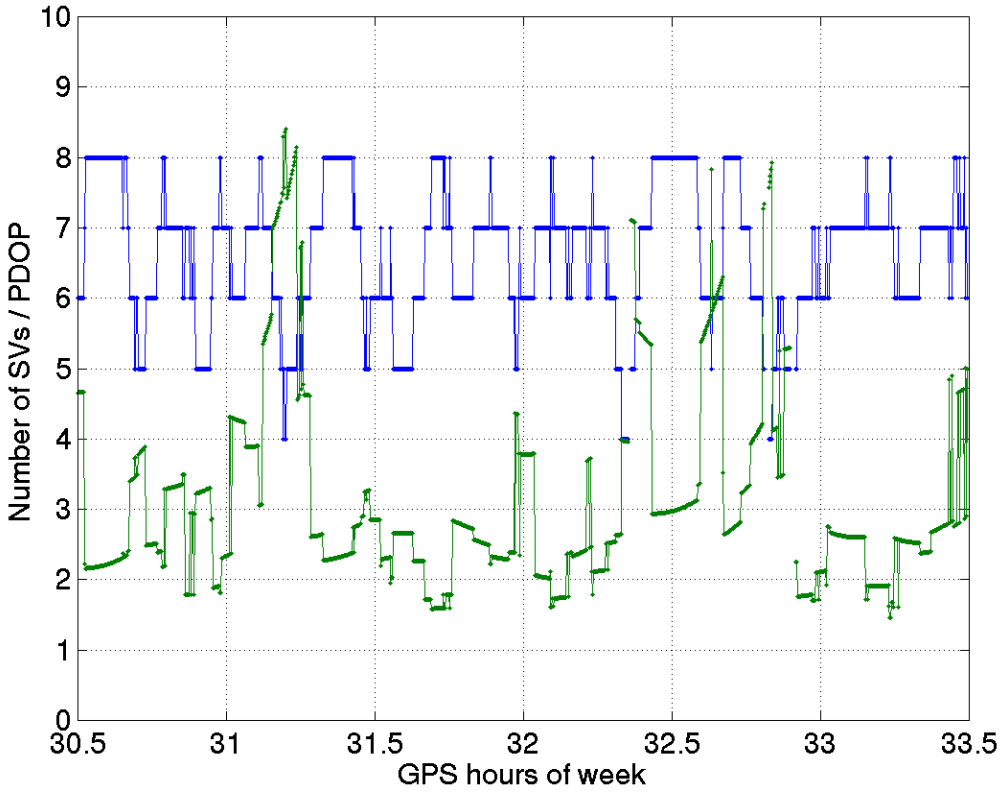

Figure 6.8: Number of SVs and PDOP for the CHAMP data set.

Figure 6.9 shows the total displacement difference of our pseudorange-only and smoothed pseudorange / carrier-phase solution and that of the GeoForschungsZen-trum-determined dynamic orbit. Only 3-D differences are provided, since the spacecraft attitude information was not used. Note that there are a few small gaps due to the lack of sufficient observations after data pre-processing. Even though the PDOP is relatively high for this data set, the determined pseudorange-only solution is quite accurate as indicated in Table 6.3. The 3-D r.m.s. is about 2 m, which is equivalent to 1.2 m in each axis assuming equal uncertainty in each axis. The approximate smoothed solution r.m.s. is about 20 cm. This difference statistic is judged to be good, considering that the position accuracy of the dynamic orbit is only somewhat better than 20 cm [Koenig,

2001]. That is, the phase-connected point positioning results have an r.m.s. similar to that of the benchmark solution.

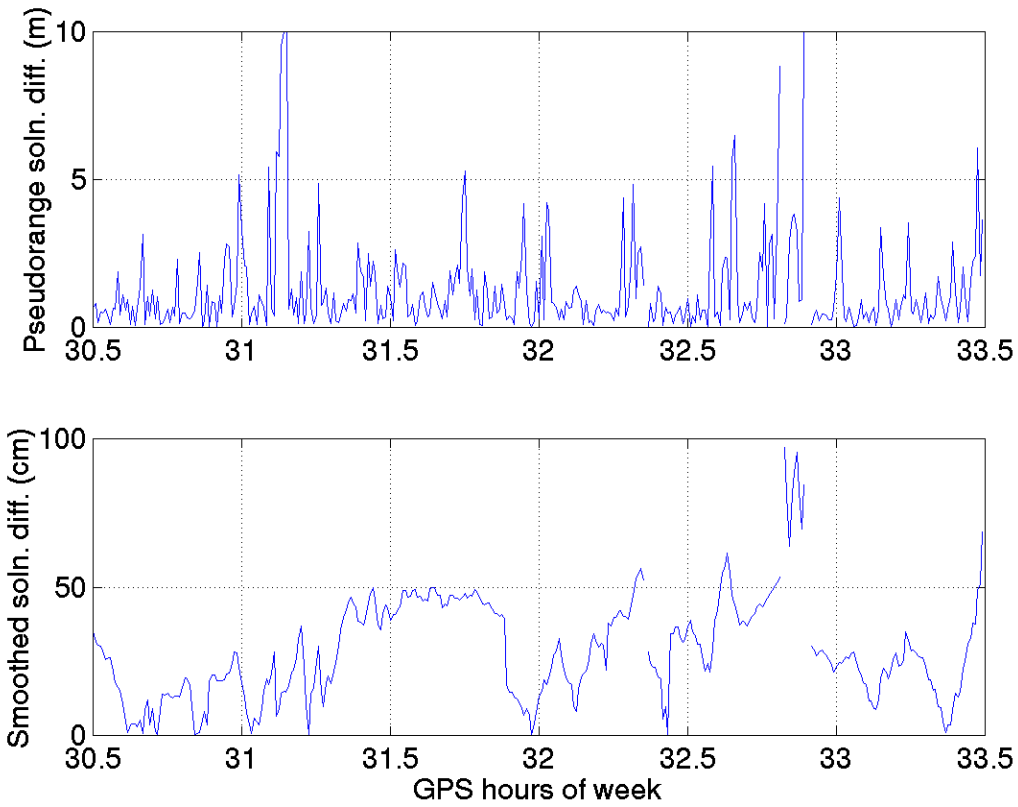

Figure 6.9: Total displacement errors in position estimates for CHAMP data set.

Sol'n.	Component	bias	std.	r.m.s.
Pseudorange	3-D	125	162	205
	~1-D	72	93	118
Smoothed	3-D	28.7	17.1	33.5
	~1-D	16.5	9.8	19.3

Table 6.3: Summary statistics (cm) of component differences in pseudorange-only and smoothed position estimates for CHAMP data set.

Figure 6.10 depicts the forward filter observable residuals and associated GPS satellite elevation angles. Again the data gaps can be clearly seen. The ionosphere-free pseudorange r.m.s. is 90 cm and the ionosphere-free, time-differenced phase r.m.s. is 3

cm. These results compare reasonably well with those from the terrestrial data set, indicating high-quality observations fitting well with the mathematical and stochastic models.

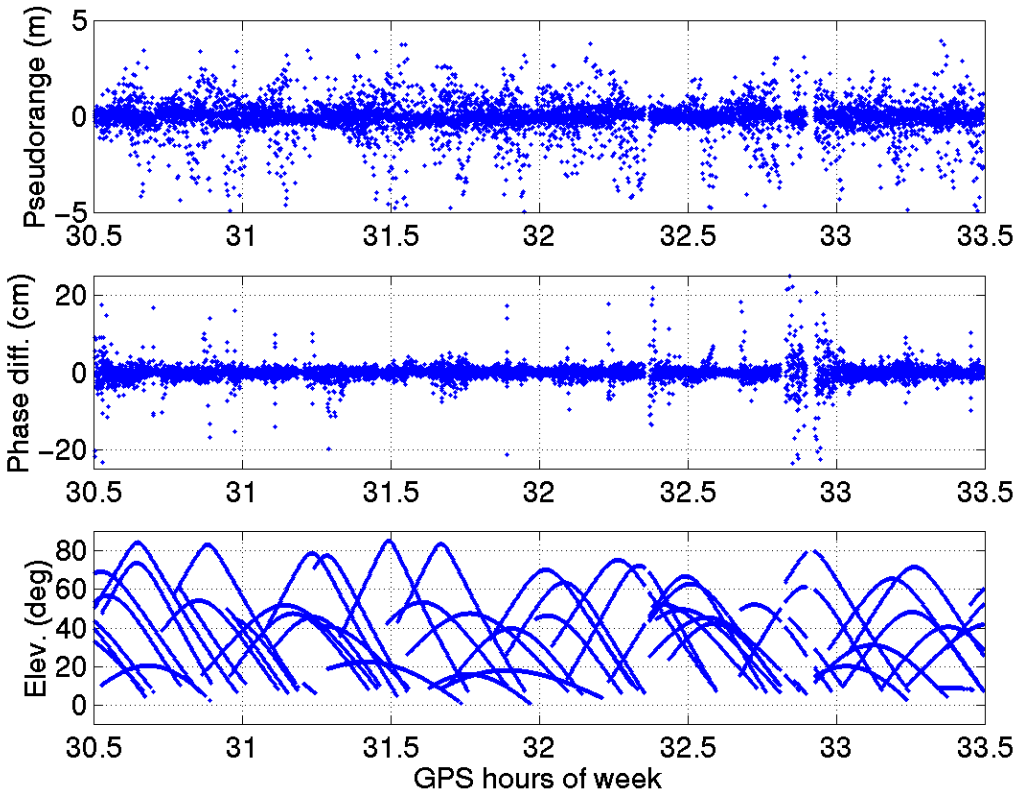

Figure 6.10: Forward filter observable residuals and associated satellite elevation angles for CHAMP data set.

A property of great interest is the GPS tracking which can be seen in the elevation angle subplot. The very low elevation angle tracking performed by the receiver causes the late tracking of newly rising SVs due to the eight SV hardware limit. Given that a portion of these very low elevation angle measurements are outliers, it would be of great benefit for a GPS-only processing technique, if the low noise, higher elevation angle measurements were collected. This would not only provide more low noise

measurements, but more measurements overall, potentially removing most if not all position solution gaps.

6.2. IGS LEO ORBIT COMPARISON CAMPAIGN

The IGS recognised in 1998 that there existed an emerging need of many diverse organisations for precise orbits for LEOs carrying quality GPS receivers. To stimulate research and collaboration the "Working Group on Low-Earth Orbiters" was created [IGS, 2001]. One of the major activities of the Group was to place a call for LEO orbit determination proposals as part of a LEO orbit campaign. UNB submitted a proposal which was accepted and this allowed us to participate in the "CHAMP Orbit Comparison Campaign" of 2001 [ESOC, 2001] as an Associate Analysis Center (AAC). The main objectives of the campaign were to: offer external reference orbits for all ACCs to compare and contrast, so any remaining systematic errors could be identified; determine the status of CHAMP orbit precision levels; provide a venue to discuss IGS LEO data exchange formats; and allow for analysis of combination solution methods for LEO satellites. Eleven days of CHAMP measurement data were selected (20 May to 30 May 2001) to be processed by eleven ACCs from North America and Europe.

6.2.1. The CHAMP Satellite Mission

CHAMP (CHAllenging Minisatellite Payload), initially described in section 6.1.2, is a German small satellite mission designed for geoscientific and atmospheric research being managed by GeoForschungsZentrum (GFZ) [CHAMP, 2001]. The satellite was launched in July 2000. The CHAMP satellite's payload includes a magnetometer, accelerometer,

star sensor, GPS receiver, laser retro-reflector, and ion drift meter. The satellite orbits in a near-polar (87° inclination), low altitude (454 km at launch) orbit. The main scientific goals for the LEO are highly precise gravity field, magnetic field, and radio occultation measurements over a five year period.

Figures 6.11 and 6.12 depict the locations of the instruments. The JPL SGPS receiver is shown in Figure 6.13. A cleanroom photograph of the POD and occultation GPS antennas is shown in Figure 6.14.

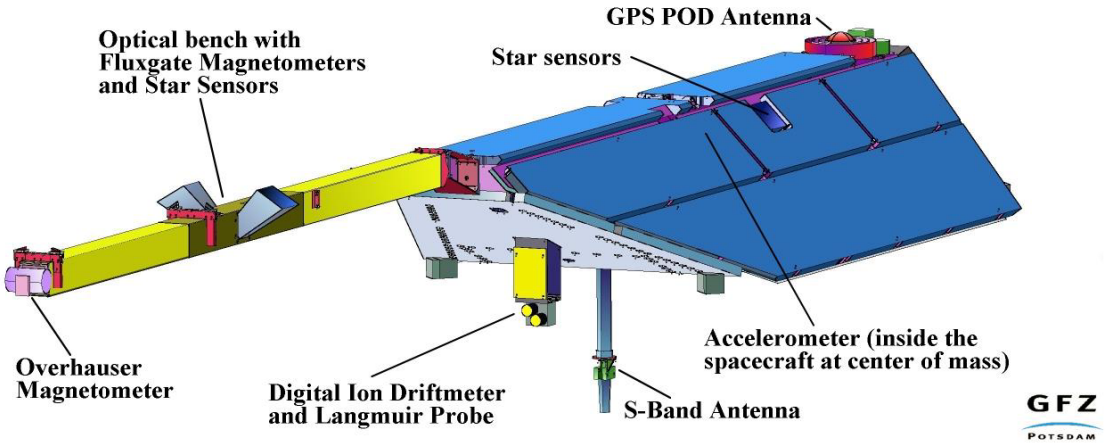

Figure 6.11: Front view of CHAMP satellite and instrument locations [CHAMP, 2001].

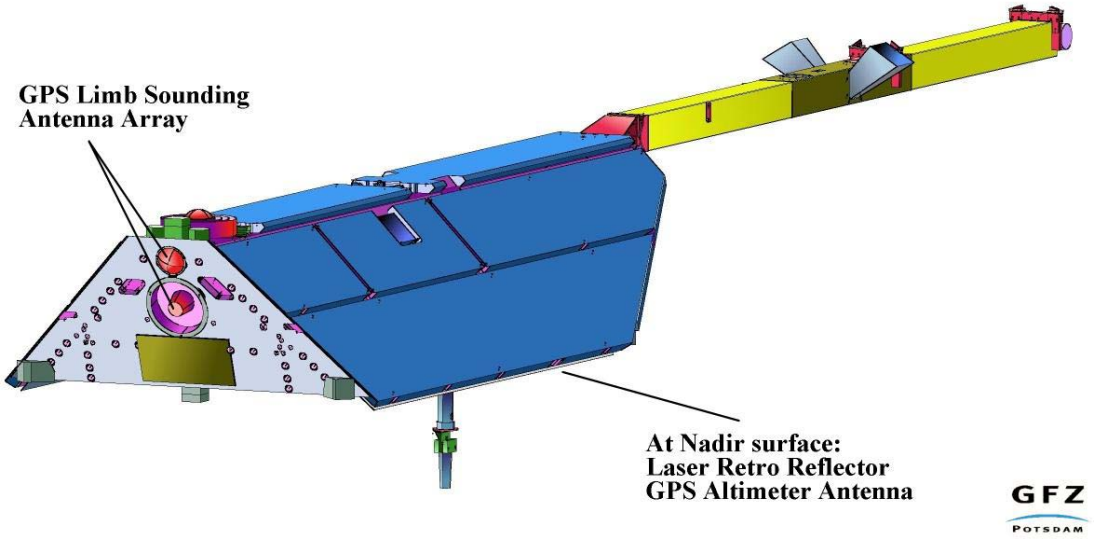

Figure 6.12: Rear view of CHAMP satellite and instrument locations [CHAMP, 2001].

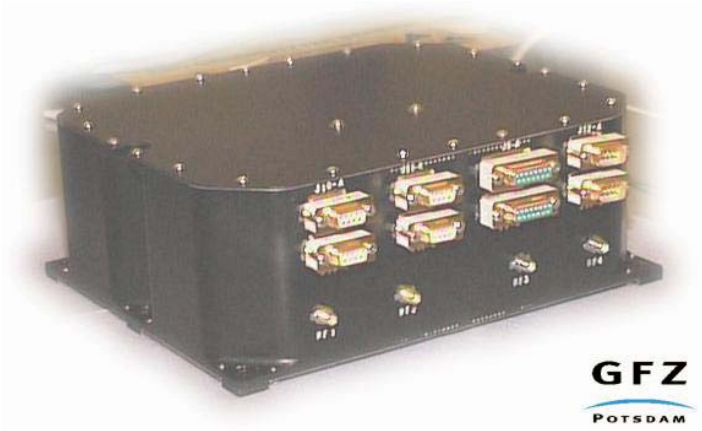

Figure 6.13: CHAMP satellite JPL BlackJack dual-frequency GPS receiver [CHAMP, 2001].

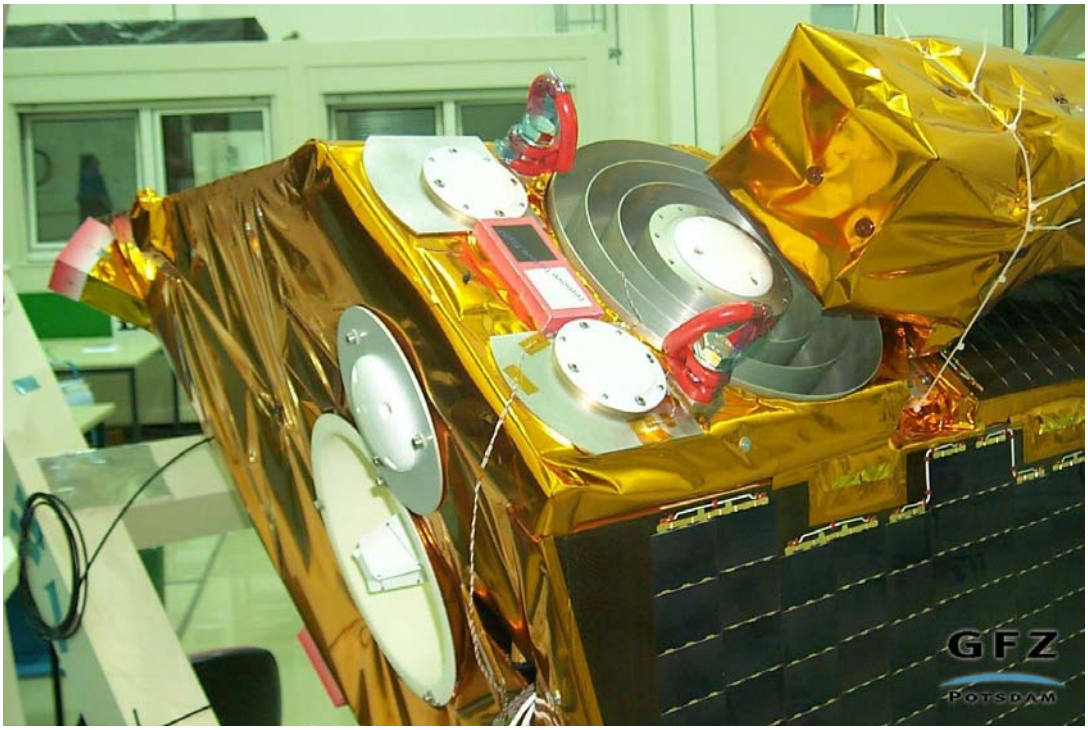

Figure 6.14: CHAMP satellite photograph of, among other instruments, POD and occultation antennas [CHAMP, 2001].

6.2.2. Preprocessing of CHAMP data anomalies

It was found that the geometric CHAMP orbit solutions are very sensitive to data editing performed in the preprocessor [Bisnath and Langley, 2002a and 2003]. Data editing consisted of applying a signal-to-noise filter and a rate-of-change of widelane-phase minus narrowlane-pseudorange linear combination filter. The former removes low strength signals at the measurement input stage, while the latter eliminates measurements that deviate from the norm before the initial estimation process. This preprocessing strategy therefore cleans the data in the measurement domain, without need for post-estimation residual analysis, as is the case for the University of Berne kinematic POD processing [Bock *et al*., 2003], or need for a reference CHAMP orbit to constrain the definition of typical measurement behaviour, as is the case for the kinematic POD

processing of the Technical University of Munich [Švehla and Rothacher, 2003] and Ohio State University [Grejner-Brzezinska *et al*., 2002].

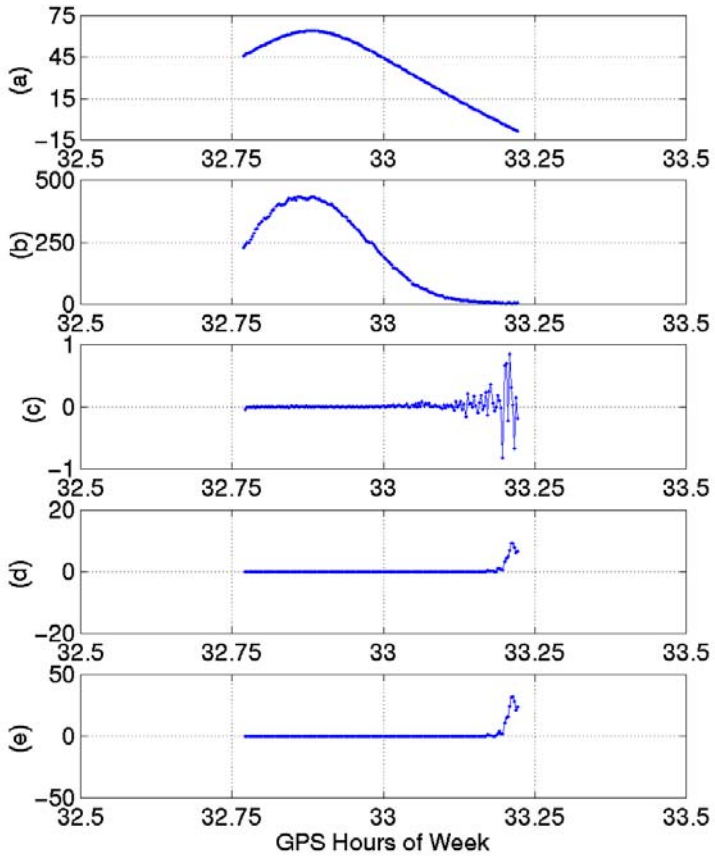

Figure 6.15: Poor behaviour of measurements at low signal-to-noise values. **a**) Elevation angle (degrees); **b**) L1 phase signal-to-noise (GPS receiver units); **c**) L1 P-code - L2 P-code rate-of-change (m/s); **d**) L1 phase - L2 phase rate-of-change (m/s); **e**) widelane phase - narrowlane pseudorange rate-of-change (m/s). GPS PRN08, day of year 148, 2001.

Figure 6.15 illustrates an example of data editing. The GPS satellite was tracked to almost -15°, causing the signal-to-noise values to approach zero BlackJack units, and the rates-of-change of the geometry-free linear combinations to deviate significantly from

zero. The receiver satellite-tracking algorithm is responsible for this situation, producing large numbers of low elevation angle satellites tracked in the CHAMP anti-velocity direction. Measurements accumulated from these weak signals are deleted, resulting in intermittent poor data availability as can be seen in Figure 6.16. Before editing, the number of SVs was 8 and the PDOP was 1.7. Given that the azimuth of 180° represents the CHAMP velocity direction, most of the SVs are in the aft-quadrant. After removal of the low SNR measurements which degrade the position solution, the number of SVs reduced to 5 and the PDOP increased to 4.0.

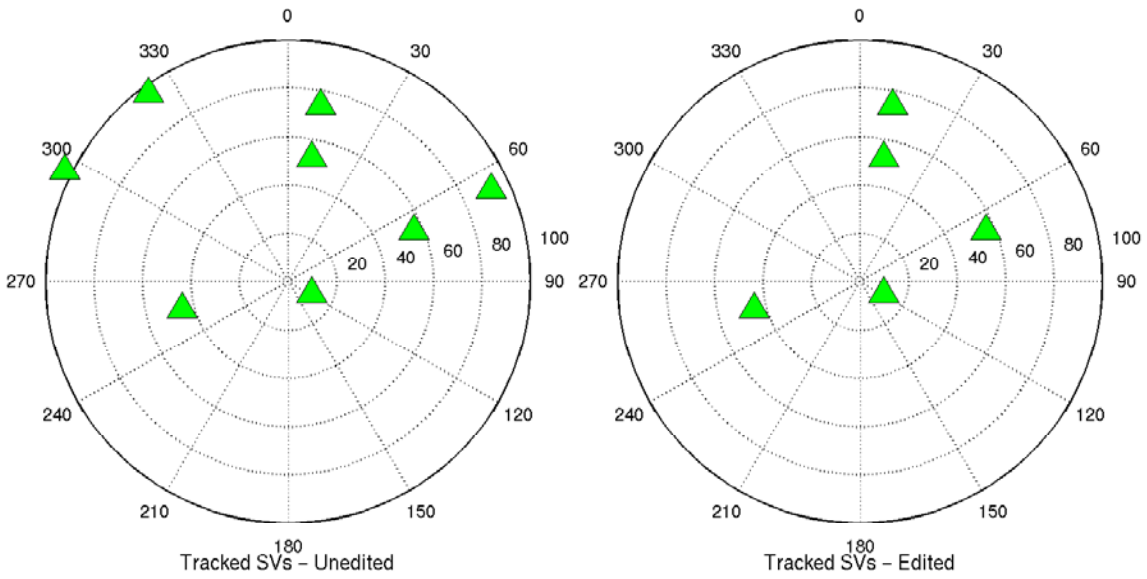

Figure 6.16: Example of GPS satellite sky distribution before and after data editing. Day of year 148, 2001, 30.2389 hours.

6.2.3. Results and Analysis of UNB CHAMP Processing

CHAMP data provided by the CHAMP Information System and Data Center [ISDC 2001] was processed for the period of the IGS LEO Orbit Comparison Campaign [ESOC

2001]: day of year 140 to 150, 2001. The resulting UNB solutions were compared against JPL solutions. Each 24 hour CHAMP data arc required less than 30 minutes for processing with UNB unoptimised computer code on an 85 MHz Sun server running Solaris 7.

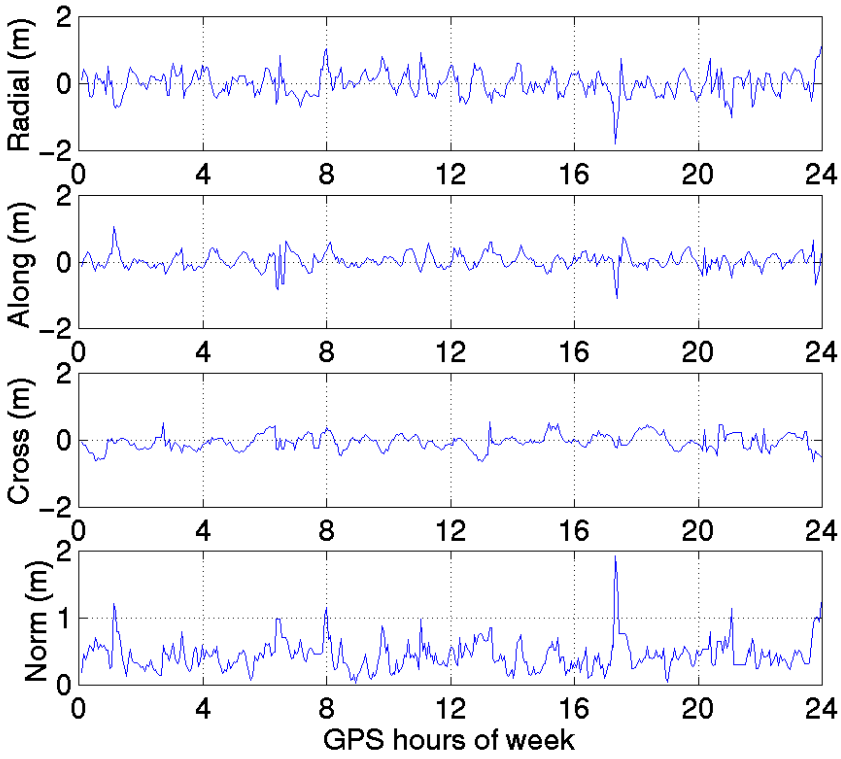

Figure 6.17: Position component differences between UNB and JPL for day of year 143, 2001.

Figure 6.17 shows the position component differences for day 143 – a typical day. The radial, along-track, cross-track, and norm r.m.s. (in cm) are 36, 25, 24, and 50, respectively. The forward filter post-fit residual r.m.s. for the ionosphere-free pseudorange is 105 cm and for the time-difference, ionosphere-free phase is 9 cm. The

spikes and much of the noise in the positions are due to data gaps and remaining poor-quality measurements. This is also evident from the relatively large post-fit residuals.

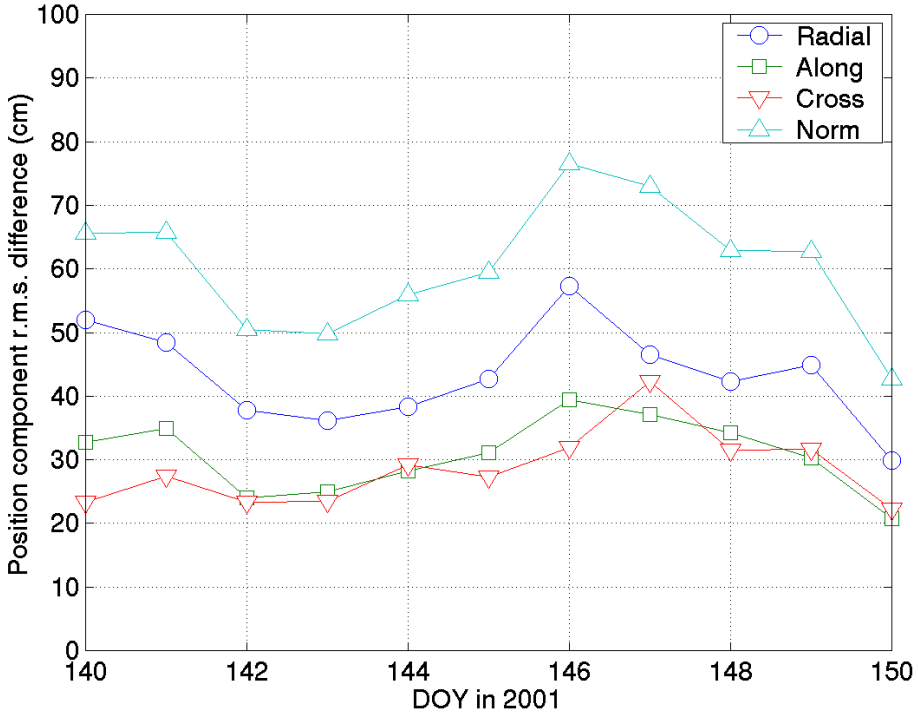

Figure 6.18: Daily position component r.m.s. differences between UNB and JPL.

Figure 6.18 illustrates the daily differences between UNB and JPL 24 hour arcs. The position difference r.m.s. ranges from: 30 cm to 57 cm in the radial direction; 21 cm to 39 cm along-track; 22 cm to 42 cm cross-track; and 43 cm to 76 cm for the norm. Notice the larger error difference in the radial component. The CHAMP radial component represents the nominal "up" component in the topocentric sense, and of course suffers from the GPS geometry predicament of having no transmitters below the receiver. The poor overall repeatability is again caused by the lack of continuous, quality GPS measurements. An indication of near-optimum solution comparison can be observed

during periods of good continuous data, *e.g.*, between hours 2 and 3 of day of year 150. For this short arc, the r.m.s. differences between UNB and JPL are as small as: 13 cm, 10 cm, 7 cm; in the radial, along-track, and cross-track directions, respectively, and 18 cm in the norm.

6.2.4. IGS Analysis Results

The European Space Agency was kind enough to maintain all of the AAC orbits, develop comparison routines, and perform the comparisons. Comparisons of each AAC's orbit solutions and laser ranging was also performed to estimate orbit accuracy. Table 6.4 gives the results presented during the January 2002 CHAMP Conference [ESOC, 2001].

AAC	r.m.s. (cm)
CSR (Univ. of Texas)	11.0
GRGS, (European Space Agency)	12.4
GFZ	13.9
JPL	16.2
CNES	22.8
NCL, (Newcastle Univ.)	23.8
ESA	27.8
UNB	45.0
AIUB, (Univ. of Berne)	52.1
UCAR, (Univ. Consortium for Atmospheric Research)	112.5

Table 6.4: Associated Analysis Center CHAMP orbit error derived from satellite laser ranging (SLR) results for CHAMP orbit campaign [ESOC, 2001].

Note that the Astronomical Institute of the University of Berne (AIUB) was the only other AAC producing geometric orbits in a similar fashion to UNB. All other solutions had the added benefit and complexity of dynamic models.

6.3. IMPROVED QUALITY CHAMP DATASET PROCESSING

Two specific limitations of the CHAMP data were uncovered in the previous section: noisy low elevation angle phase measurements, as compared to those from conventional terrestrial geodetic receivers; and a GPS satellite tracking selection algorithm that exacerbates the phase noise problem by having the receiver track GPS satellites to low elevation angles, rather than switch to higher ones. Given the geometric strategy total reliance on measurements, the above problems had a significant, negative impact on the CHAMP orbits that were generated for the IGS campaign.

From the launch of CHAMP, the BlackJack receiver underwent numerous firmware upgrades to both fix problems and improve performance [Meehan, 2002]. By the end of 2001, it was observed that the tracking algorithm had been altered [Hugentobler, 2002], which provided for a much larger percentage of low noise pseudorange and carrier phase data for processing of each orbital revolution as compared with the pre-2002 datasets. Therefore to evaluate the effectiveness of the developed technique, a more recent dataset was selected for processing. The first week (days 1-7) of January 2002 was selected, since these data reflected the firmware changes in the BlackJack receiver, and precise orbits had (by the time) been produced for comparison.

6.3.1. Results and Analysis of UNB CHAMP Processing of Improved Quality Dataset

The 2002 dataset was processed in a similar fashion to the 2001 dataset presented in section 6.2. The analysis is distributed between: an examination of the processing results

from one day; summary results from all of the days; and summary results from portions of all of the days.

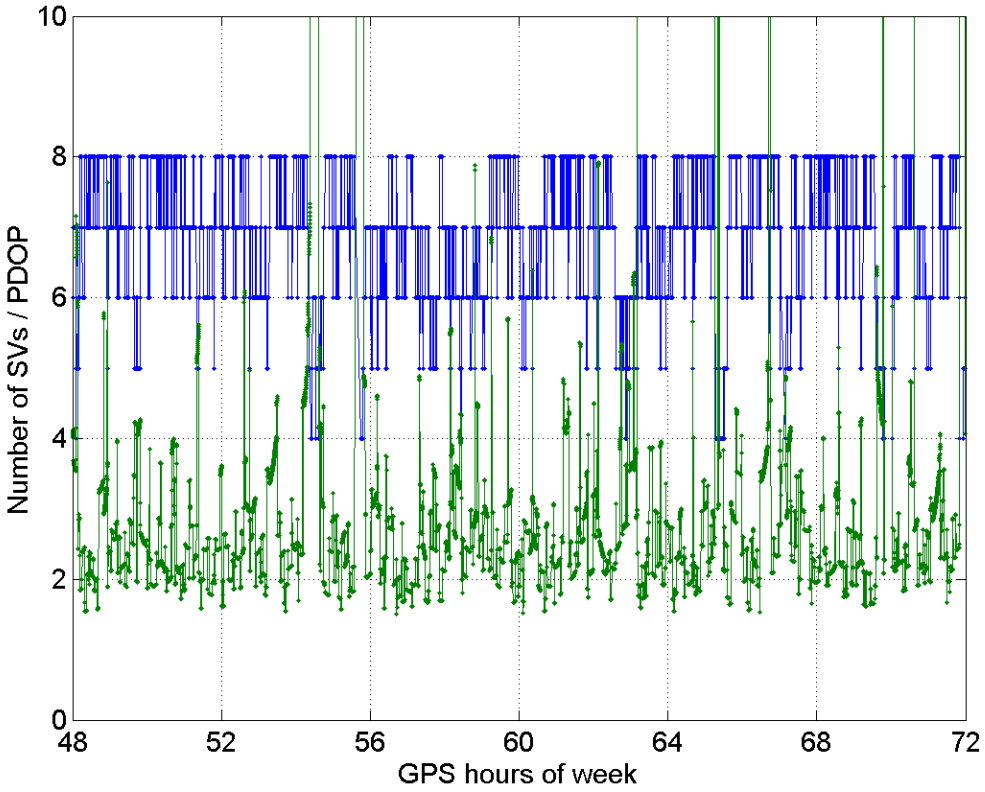

Figure 6.19: Number of SVs and PDOP for the CHAMP dataset, DOY 001, 2002.

Figure 6.19 illustrates the measurements available for day of year (DOY) 001, 2002 after outlier removal. The mean number of SVs used in the processing is 6.9 and the mean resulting PDOP is 3.2. Even though the number of tracked GPS satellites is relatively high, as was the situation in the 2001 dataset, the tracking distribution is such that relatively poor PDOPs are still produced. Also, there are a number of complete data outages (as observed in the 2001 dataset) lasting a few minutes, presumably due to

routine CHAMP operations. However, given these concerns, compared with the 2001 data (see Figure 6.8), the data availability in 2002 is much more consistent.

The data (CHAMP RINEX observation file and IGS precise ephemeris and clock files) were processed as described in Chapter 5. The appropriate CHAMP attitude file was applied to reduce the geometric strategy orbit from CHAMP GPS antenna phase centre to CHAMP centre of mass. The resulting SP3 file was compared against the JPL reduced-dynamic orbit of the same date using the ESA orbit comparison routine supplied for the 2001 CHAMP Orbit Comparison Campaign [ESOC, 2001]. JPL orbits were used in the 2002 comparison because they proved quite accurate in the 2001 IGS orbit comparison, and because they were available at the time of data processing / solution evaluation. It was estimated that the proved JPL orbits were accurate to better than 1 decimetre each component (1σ), as compared with satellite laser ranging results [Kuang, 2002].

The results of the comparison of the UNB and JPL CHAMP orbits for DOY 001, 2002 are given in Figure 6.20. Note that to reduce the effects of filtering and interpolation error at the extremities of the time series, 30 minutes have been removed from either end of the time series of results. At first glance the results appear similar to those from 2001 (see Figure 6.17). Spikes exist in the 2002 results, most noticeably at 49.5 and 66.5 hours, and the radial differences are greater than the along-track and cross-track differences. The reasons for these two phenomena remain the same: data gaps cause filter re-initialisations in the geometric strategy, and as with terrestrial GPS data processing, since there are no range measurements from beneath the receiver, the vertical positioning component precision is not as good as that of the horizontal components.

However, the differences are smaller (note the change in Y-axis scale); in terms of r.m.s., the comparison differences between the UNB and JPL orbits are approximately 50% smaller for DOY 001, 2002 than for DOY 143, 2001. This is a direct result of more useful data (specifically carrier-phase measurements) available in the 2002 data processing. Table 6.5 summarises the statistics for DOY 001, 2002. Therefore the technique produces approximately 15 cm orbits in the along-track and cross-track components and 25 cm in the radial component, as compared to the JPL orbit, which are accurate to ~10 cm in all three components. Also, no significant trends are observed in the difference time series.

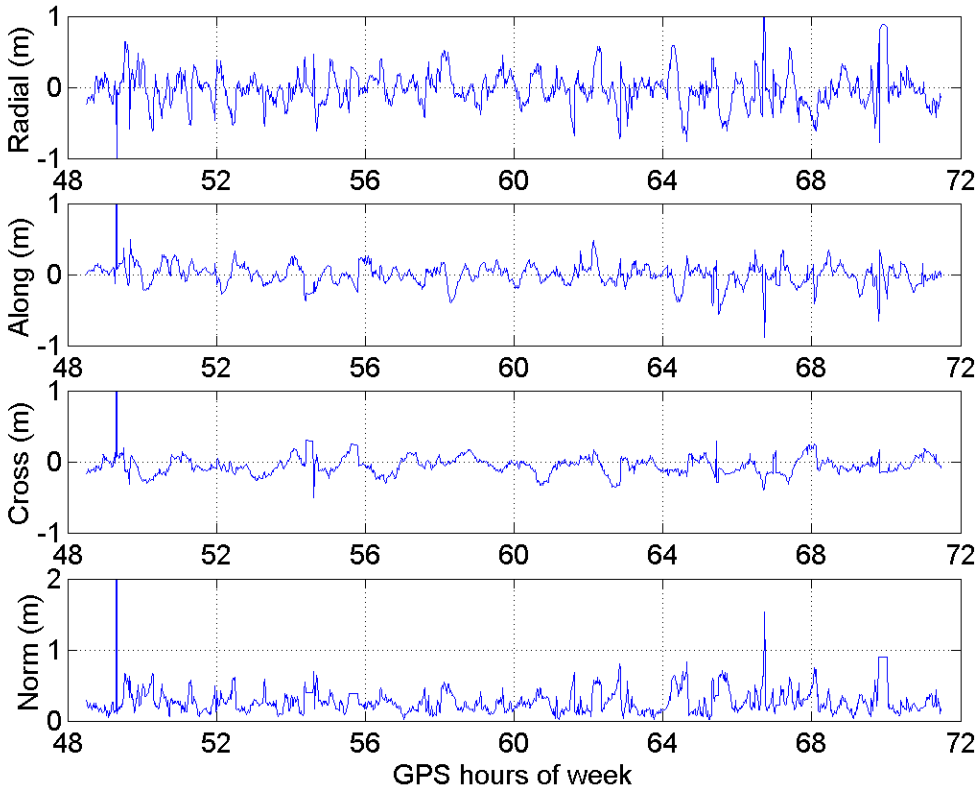

Figure 6.20: CHAMP orbit position component differences between UNB and JPL for 24 hour arc of DOY 001, 2002.

Component diff. (cm)	Max.	Bias	r.m.s.
Radial	120.3	-2.2	25.1
Along-track	309.3	-0.1	16.9
Cross-track	177.0	-5.2	14.0
Norm	372.7	27.4	33.3

Table 6.5: Summary statistics of CHAMP orbit position component differences between UNB and JPL for 24 hour arc of DOY 001, 2002.

A more revealing set of statistics is presented in Table 6.6. These summary values represent the statistics computed for the 3 hour arc (GPS hours of week: 57-60) from DOY 001, 2002. For this arc there were few data gaps, data outliers, or poor satellite tracking geometries, and hence the arc represents a period of *realistic* performance of the geometric POD strategy with *geodetic-quality* GPS receiver measurements. As can be seen, the r.m.s. errors have been reduced to 20 cm, 13 cm, and 8 cm, radial, along-track, and cross-track, respectively.

Component diff. (cm)	Max.	Bias	r.m.s.
Radial	51.5	3.9	19.7
Along-track	40.3	-0.9	12.8
Cross-track	16.5	0.9	7.9
Norm	54.4	21.9	24.8

Table 6.6: Summary statistics of CHAMP orbit position component differences between UNB and JPL for 3 hour arc (hrs: 57-60) of DOY 001, 2002.

The ionosphere-free pseudorange and ionosphere-free, time-differenced carrier-phase residuals for DOY 001 are shown in Figure 6.21. A number of few-minute data gaps can be readily observed. Outliers are present for both observables, particularly the noisy pseudoranges. The major phase outliers can be attributed to filter initialisation epochs when pseudorange measurements carry significant weight in the filtering process, such as after a data gap. The minor phase outliers are a result of isolated noisy measurements.

The r.m.s. of the residuals are 95 cm and 40 mm for the derived pseudorange and time-differenced carrier-phase observables, respectively. The time-differenced carrier phase value appears high for the quality of the undifferenced phase measurements from the BlackJack receiver, but computation of the residual r.m.s. over the 57-60 hours arc results in values of 96 cm and 15 mm for code and phase, respectively. Therefore, it can be stated that the phase measurements fit the mathematical model of the least-squares filter well.

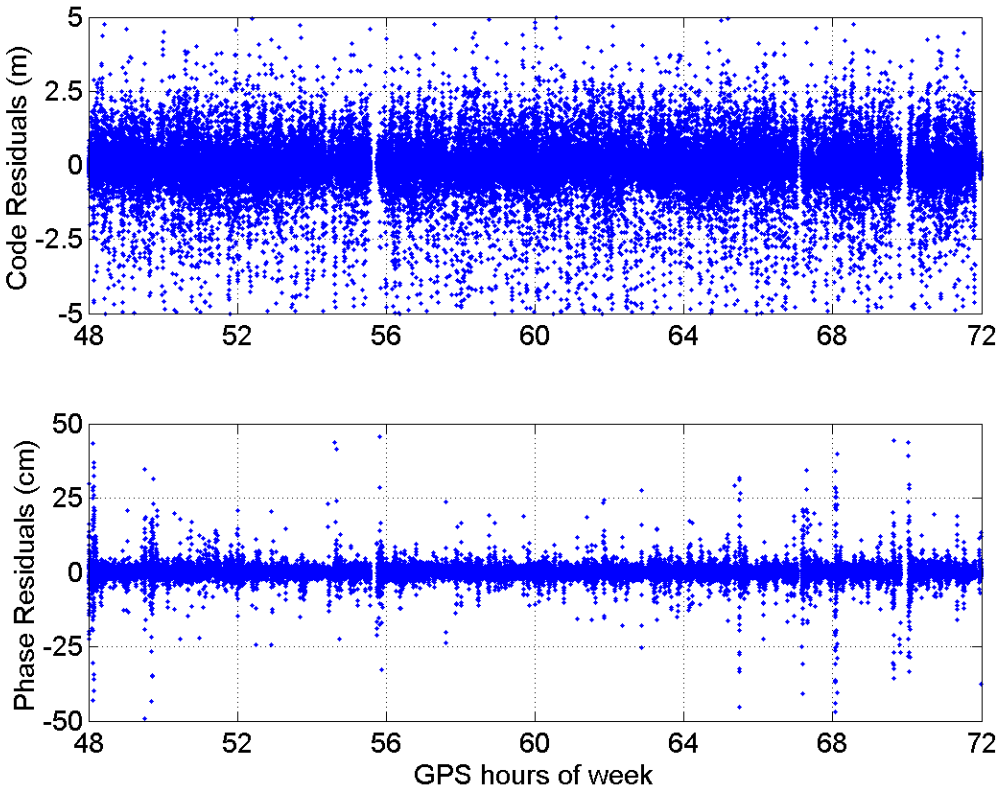

Figure 6.21: Forward filter observable residuals for UNB CHAMP solution for DOY 001, 2002.

Figure 6.22 shows the performance of the geometric strategy through the first week of 2002, as compared with the JPL orbits. The day-to-day results are quite similar, varying

by only a few centimetres. The r.m.s. difference for the radial, along-track, and cross-track components is approximately 25 cm, 15 cm, and 15 cm, respectively. This few decimetre performance therefore represents the precision level of the geometric strategy for this level of quality CHAMP data, as compared to reduced dynamic orbits.

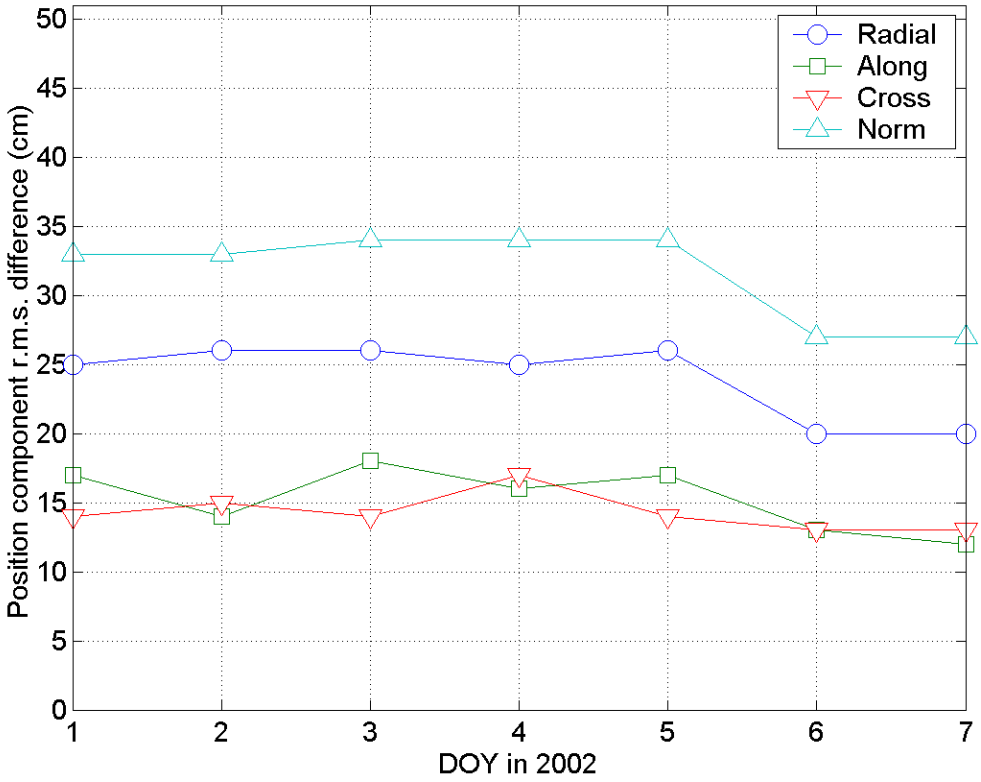

Figure 6.22: CHAMP orbit position r.m.s. component differences between UNB and JPL for 24 hour arcs of DOY 001 through 007, 2002.

The effectiveness of the strategy when good (*i.e.*, geodetic) quality measurements are available from CHAMP is illustrated in Figure 6.23. The r.m.s. difference values for day-to-day best three hour arcs is as consistent as that for the full day arcs, and as expected is smaller: 18 cm, 10 cm, and 11 cm, radial, along-track, and cross-track,

respectively. Even though it may be argued that these results do not represent typical results for the CHAMP mission, it can be said that for the CHAMP receiver, during periods of *expected performance*, the geometric strategy consistently provides near-decimetre positioning precision. And given that the reference JPL orbits are known to the decimetre level [Kuang, 2002], the magnitude of the r.m.s. differences presented here is even less significant.

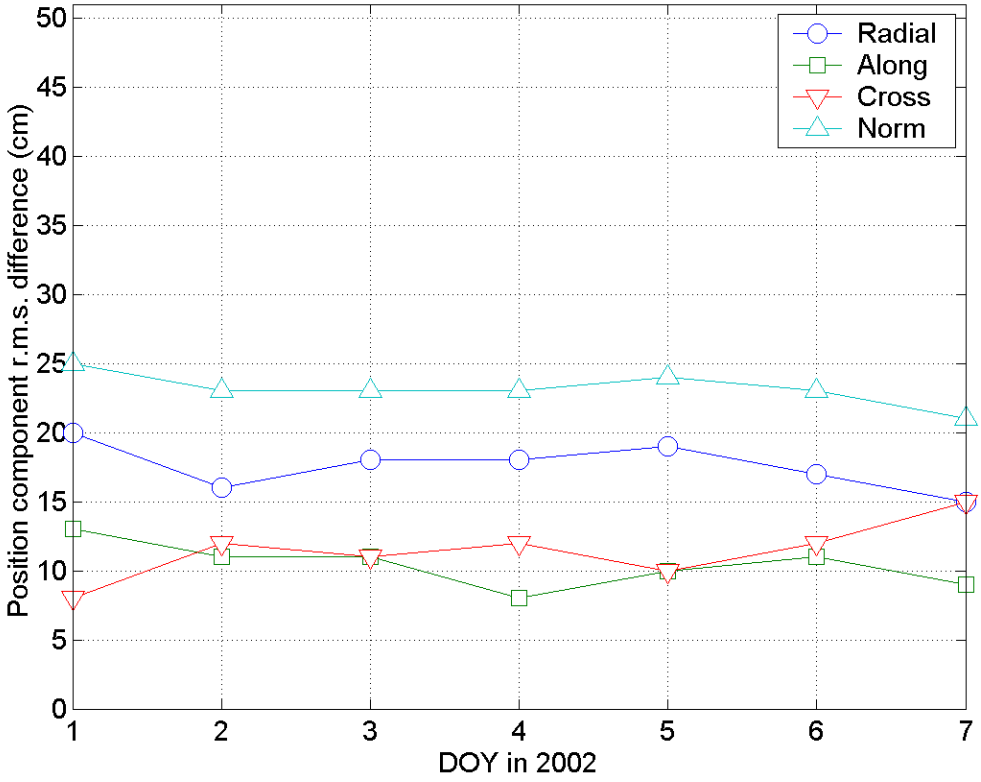

Figure 6.23: CHAMP orbit position r.m.s. component differences between UNB and JPL for 3 hour arc of DOY 001 through 007, 2002.

For completeness, the r.m.s. values of the observable residuals are given in Figure 6.24. Of note, aside from an outlier on DOY 004, the 3 hour arc iono-free, difference-in-time, phase residual noise level is extremely consistent at the 15 mm level.

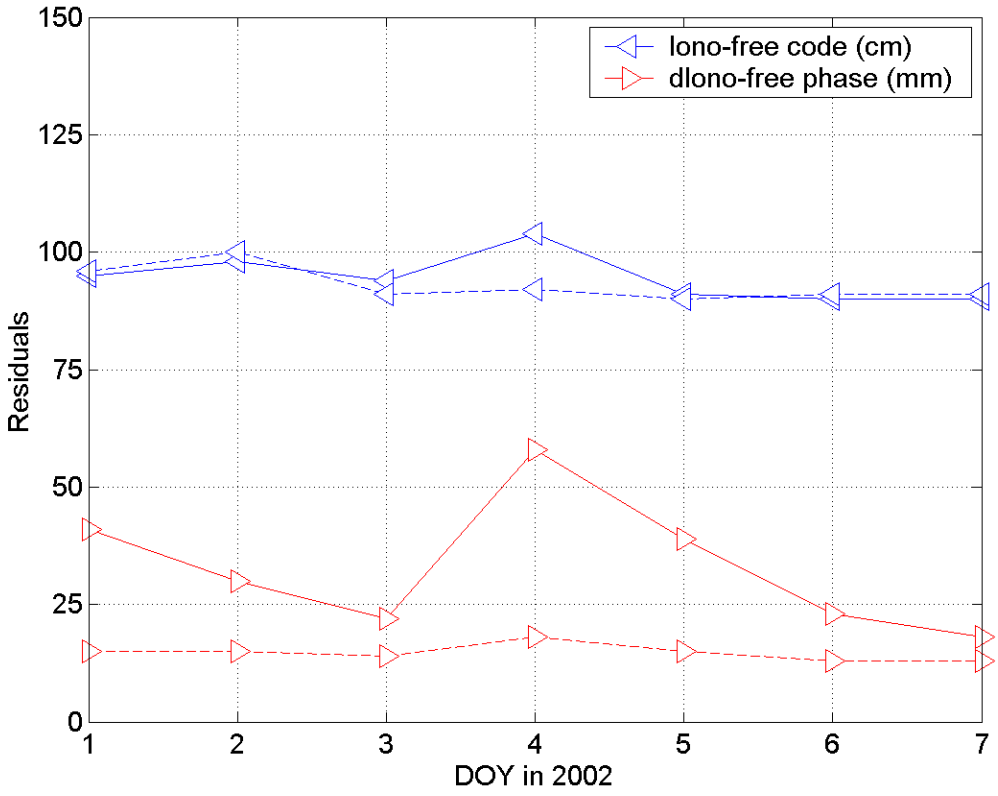

Figure 6.24: Forward filter observable residuals for UNB CHAMP solution for 24 hour arc (-) and 3 hour arc (--) of DOY 001 through 007, 2002.

7. CONCLUSIONS, RECOMMENDATIONS, AND FUTURE PROSPECTS

The research carried out for this dissertation is now summarised and pertinent conclusions are given in the context of the thesis question: Is POD of LEOs possible with a GPS-only solution and a single spaceborne GPS receiver, and if so, how accurate could the solutions be? Recommendations are put forth for the usage of a processing strategy such as the one developed, as well as for continuing research in this field. Finally, some thoughts are provided as to the future prospects of this processing strategy in the overall precise positioning and navigation industry.

7.1. CONCLUSIONS OF THIS RESEARCH

The initial fundamental goal of this research was the development of a practical and precise GPS-only LEO orbit determination procedure. Such a straightforward technique was seen as unique but complementary to existing POD techniques, which require core complex dynamic modelling. Were spaceborne GPS measurements precise, accurate and sufficiently abundant to produce useful orbits? A GPS measurement-only filter was devised, based on algorithms developed for various other purposes. Simulation software was constructed and the results indicated that under ideal conditions – good-quality, continuous GPS measurements and low signal noise – near-decimetre orbits determination was attainable.

With the removal of the intentional GPS satellite clock degradation of SA by the U.S. government, double-differencing of SGPS measurements and terrestrial reference station measurements was no longer necessary for the elimination of GPS satellite clock terms in

the estimation process; these terms could now be modelled by IGS GPS satellite clock products. Therefore the object of this research effort became the POD of LEOs with a GPS-only solution using only a single SGPS receiver.

The novel processing algorithm devised is based on two principles: dynamics-free processing, and single-receiver processing. The dynamics-free nature of the processing strategy arises from the fact that the pseudorange measurements are basically used to supply position information, while the carrier phase measurements essentially provide position change (or state transition) information. This is analogous to a Kalman filter, but the algorithm is presented in a kinematic, sequential least-squares filter form.

To practically test the ideas put forth, a complete processing package was created in FORTRAN 77 code based on the UNB static processing software DIPOP. A preprocessor was designed to import RINEX SGPS files and SP3 GPS satellite ephemerides and clock offset files. The pre-processor edits the data for outliers and reformats the output. The main processor executes the phase-connected, point positioning algorithm, applying all of the pertinent modelling. Each processor requires only tens of seconds to run 24 hours of 10 second CHAMP data on a 1.2 MHz Pentium 4 processor. This processing speed bodes well for potential real-time and near-real-time applications.

The thesis question has been answered positively: LEO POD with a GPS-only solution utilising a single GPS receiver is possible. The latest process results show that near-decimetre-level accuracy is attainable when compared against high-calibre reduced-dynamic orbits. Specifically for the CHAMP satellite, the average radial, along-track,

and cross-track accuracies for 7 consecutive 24 hour arcs was: 24, 15, and 14 cm, respectively. When 3 hour arcs without data gaps were analysed these statistics improved to 18, 10, and 11 cm, respectively. These values give a clear indication of the positional quality of orbits derived by the geometric strategy using the phase-connected, point positioning algorithm. Even though these results are not at the sub-decimetre level, as is the case for the reference GPS / dynamic solutions, they approach these accuracies and are valuable for real-time and near-real-time applications due to the extremely low processing cost. A key final point is that the GPS /dynamic orbits only reached the sub-decimetre accuracy level after significant processing, analysis, and tuning of the dynamic models. For example, a new gravity field model was developed for and from the reduced-dynamic CHAMP orbits, which allowed for these orbit accuracies. The geometric-strategy-based orbits required none of this analysis and extensive tuning.

A number of caveats are attached to these results. The accuracies quoted are associated only with the CHAMP data processed in January 2002. Older CHAMP data will definitely produce degraded orbits and newer data may produce enhanced orbits. This statement relies on the quantity and quality of observed CHAMP pseudorange and particularly carrier-phase measurements. Other LEOs in differing orbits, carrying equivalent GPS receivers would observe comparable segments of the GPS constellation and would therefore have similar data availability during processing. Therefore these CHAMP results can be generalized for all LEOs carrying high-quality, dual-frequency receivers: near-decimetre POD is attainable with the geometric strategy. The other major caveat is that high-quality IGS GPS ephemerides and clock-offset products be available for the corresponding SGPS data.

7.2. RECOMMENDATIONS FOR FURTHER RESEARCH

A number of refinements and additions can be made to the algorithms and software created to improve upon the accuracy and practicality of the work done for this dissertation. In terms of improved mathematical modelling, the effect of phase-windup, albeit small, can be added, and for terrestrial and airborne data processing estimation of the residual tropospheric delay would be a priority. An area where additional improvement may lie is in stochastic modelling. Implementation of a pseudorange multipath plus noise weighting scheme and more realistic carrier-phase weighting may provide an additional few centimetres improvement. The usage, that is the interpolation, of the IGS orbit and clock products can be further investigated and perhaps more accurate interpolation schemes can be applied.

Five major advances can be made to the software. The first is the implementation of some form of residual analysis to overcome problems with anomalous GPS measurement data or IGS orbit and clock information, similar to that performed by Bock *et al*. [2003]. The second is the importation of predicted IGS orbit and clock products for real-time or near-real-time POD, as is done by Muellerschoen *et al.* [2002] and Kouba and Héroux [2001]. The third is the addition of velocity estimation by either interpolation of the POD positions, estimating velocity directly from the time-differenced phases, or augmentation of the filter to incorporate Doppler measurements and velocity states, such as indicated by Kwon *et al.* [2002]. The fourth advancement would be in the form of faster filter convergence period from tens of minutes to minutes, for example by altering the mathematical and stochastic models, as suggested by Gao and Shen [2001], or incorporating other measurements from, *e.g*., atomic clocks, inertial systems, *etc*. The

fifth future addition is the optimization for speed of the FORTRAN code. The code was written for ease in construction and readability. No significant attempts were made to improve processing speed.

With such algorithm and software enhancements, the geometric strategy can potentially provide more accurate orbits than presented here. And equally as important, orbits can be generated for practically any LEO, with similar results, and with little or no modifications to the processing software or processing procedure. This strategy can therefore be used in a number of situations including those requiring near-decimetre orbits, where rapid solutions are necessary, for an independent verification of dynamic models in dynamic solutions, or to use GPS-only orbits as pseudo-observations in dynamic solutions by providing high-quality states for limited dynamic smoothing.

In terms of generic applications, the phase-connected, point positioning filter encapsulated in this processing package would be ideal for static and kinematic positioning of any platform for which requirements call for near-decimetre-level precision and the platform is significantly distant from any GPS base stations as to limit or prevent other forms of phase-based positioning. The caveats here are that copious obstructions would cause the filter to continually re-initialise, greatly degrading the solution, and that geodetic-quality, dual-frequency receiver data would be required. Also real-time, or near-real-time processing could be accomplished with access to near-term predicted IGS orbits and clock products.

7.3. Future Prospects For this Variant of GPS Data Processing

The last two paragraphs of the previous section described a number of general uses for varying applications. As a final commentary, it is worth considering what impact future planned and proposed changes to GPS and other GNSSs will have on this form of GPS data processing. The major structural changes include a civilian code on GPS L2 and a third GPS frequency, L5; replenishment GLONASS satellites; and perhaps most significant, the evolving Galileo constellation – a new GNSS. Given that the developed algorithm is completely measurement-based, improvements to measurement quantity and quality will have a direct, positive effect on solution availability, accuracy, precision, and integrity. Combined with advances in mathematical and stochastic modelling, RTK-like solutions could potentially be produced – that is, ambiguity-resolved point positioning: real-time, few-centimetre positioning with a single GPS receiver and some correction signal. This could also mark the coalescing of range-based WADGPS corrections and state-based point-positioning corrections. This convergence is already taking place in the commercial arena with the StarFire and SkyFix XP services (see NavCom [2003], Thales [2003] and Bisnath *et al*. [2003]).

8. REFERENCES

Ackermann, F. (1993). "GPS for photogrammetry." *Bollettino di Geodesia e Scienze Affini*, Vol. 56, No. 4, pp. 387-406.

Beutler, G. (1998). "GPS satellite orbits." In *GPS for Geodesy*, Eds. P.J.G. Teunissen and A. Kleusberg, Springer, Berlin, pp. 37-101.

Bierman, G.J. (1977). *Factorization Methods for Discrete Sequential Estimation*. Academic Press, New York, 241 pp.

Birmingham, W.P., B.L. Miller, and W.L. Stein (1983). "Experimental results of using the GPS for Landsat 4 onboard navigation," *Navigation*, Vol. 30, No. 3, pp. 244-251.

Bisnath, S.B. (1999). "Spaceborne GPS information site." [On-line] March 1999. http://gauss.gge.unb.ca/grads/ sunil/sgps.htm

Bisnath, S.B. (2000). "Efficient, automated cycle-slip correction of dual-frequency kinematic GPS data." *Proceedings of ION GPS 2000, the 13th International Technical Meeting of The Institute of Navigation*, Salt Lake City, Utah, USA, 19-22 September 2000, pp. 145-154.

Bisnath, S.B., T. Beran, and R.B. Langley (2002). "Precise platform positioning with a single GPS receiver." *GPS World*, Vol. 13, No. 4, pp. 42-49.

Bisnath, S., D. Dodd, and D. Wells (2003). "Evaluation of recent developments in high-precision GPS correction services." *Proceedings of The U.S. Hydrographic Conference*, 24-27 March, Biloxi, Mississippi, U.S.A.

Bisnath, S.B., D. Kim, and R.B. Langley (2001). "A new approach to an old problem: carrier phase cycle slips." *GPS World.* Vol. 12, No. 5, pp. 46-51.

Bisnath, S.B. and R.B. Langley (1996). "Assessment of the GPS/MET TurboStar GPS receiver for orbit determination of a future CSA micro/small-satellite mission." Final report by the Department of Geodesy and Geomatics Engineering, University of New Brunswick, Fredericton, N.B. for the Directorate of Space Mechanics, Space Technology Branch of the Canadian Space Agency, St-Hubert, Que. July, 188 pp.

Bisnath, S.B. and R.B. Langley (1999a). "Precise, efficient GPS-based geometric tracking of Low Earth Orbiters." *Proceedings of the 55th Annual Meeting of The Institute of Navigation*, Cambridge, Massachusetts, U.S.A., 28-30 June, pp. 751-760.

Bisnath, S.B. and R.B. Langley (1999b). "Precise a posteriori geometric tracking of Low Earth Orbiters with GPS." *Canadian Aeronautics and Space Journal*, Vol. 45, No. 3, pp. 245-252.

Bisnath, S.B. and R.B. Langley (2001a). "Precise orbit determination of Low Earth Orbiters with GPS point positioning." *Proceedings of The Institute of Navigation National Technical Meeting*, Long Beach, California, U.S.A., 22-24 January, pp. 725-733.

Bisnath, S.B. and R.B. Langley (2001b). "Pseudorange multipath mitigation by means of multipath monitoring and de-weighting." *Proceedings of the International Symposium on Kinematic Systems in Geodesy, Geomatics and Navigation*, Banff, Alberta, 5-8 June, pp. 392-400.

Bisnath, S.B. and R.B. Langley (2002a). "Precise orbit determination of the CHAMP satellite with stand-alone GPS." Presented at The European Navigation Conference – GNSS 2002, 27-30 May, Copenhagen, Denmark.

Bisnath, S.B. and R.B. Langley (2002b). "High-precision, kinematic positioning with a single GPS receiver." *Navigation*, Vol. 49, No. 3, pp. 161-169.

Bisnath, S.B. and R.B. Langley (2003). "CHAMP orbit determination with GPS phase-connected precise point positioning." In *First CHAMP Mission Results for Gravity, Magnetic and Atmospheric Studies*, Eds. C. Reigber, H. Lür, P. Schwintzer, Springer, Berlin, pp. 59-64.

Blaha, G. (1974). "Influence de l'incertitude des parametres tenus fixes dans une compensation sur la propagation des variances-covariances," *Bulletin Géodésique* No.113, pp. 307-315.

Blewitt, G. (1990). "An automatic editing algorithm for GPS data," *Geophysical Research Letters*, Vol. 17, No. 3, pp. 199-202.

Bock, H., G. Beutler, and U. Hugentobler (2001). "Kinematic orbit determination for Low Earth Orbiters," IAG Scientific Assembly, Budapest, Hungary, 2-7 September.

Bock, H., U. Hugentobler, and G. Beulter (2003). "Kinematic and dynamic determination of trajectories for low earth satellites using GPS." In *First CHAMP mission results for gravity, magnetic and atmospheric studies*, Eds. C. Reigber, H. Lür, P. Schwintzer, Springer, Berlin, pp. 65-69.

Boomkamp, H. (2001). Personal communication. European Space Operations Centre, Munich, Germany, December.

Braasch, M.S. (1994). "Isolation of GPS multipath and receiver tracking errors." *Navigation*. Vol. 41, No. 4, pp. 415-434.

CHAMP (2001). "CHAMP home page." GeoForschungsZentrum. [On-line] January 2001. http://op.gfz-potsdam.de/champ/index_CHAMP.html

Collins, J.P. (1999). *Assessment and Development of a Tropospheric Delay Model for Aircraft Users of the Global Positioning System.* M.Sc.E. dissertation. Department of Geodesy and Geomatics Engineering, Technical Report No. 203, University of New Brunswick, Fredericton, New Brunswick, 174 pp.

Collins, J.P. and R.B. Langley (1999). *Possible Weighting Schemes for GPS Carrier Phase Observations in the Presence of Multipath.* Contract report for the United States Army Corps of Engineers Topographic Engineering Center, No. DAAH04-96-C-0086 / TCN 98151, 33 pp.

Collins, J.P. (2002). Personal communication. Geodetic Survey Division, Natural Resources Canada, Ottawa, September.

Davis, G.W., K.L. Gold, P. Axelrad, G. H. Born, and T.V. Martin (1997). "A low cost, high accuracy automated GPS-based orbit determination system for low earth satellites." *Proceedings of the 10th International Technical Meeting of the Satellite Division of The Institute of Navigation*, Kansas City, Missouri, U.S.A., 16-19 September, Vol.1, pp.723-733.

Escobal, P.R. (1976). *Methods of Orbit Determination* (reprint). Robert E. Krieger, Inc., Malabar, Florida, U.S.A., 479 pp.

ESOC (2001). "IGS LEO orbit comparison campaign 2001." [On-line] October 2001. http://nng.esoc.esa.de/gps/campaign.html

El-Rabbany, A. (2002). *Introduction to GPS: The Global Positioning System.* Artech House, Boston, 176 pp.

Gao, Y. (1994). "GPS positioning accuracy using precise real-time ephemeris and clock correction." *Marine Geodesy*, Vol. 17, No. 4.

Gao, Y., K. Chen, and K. Shen (2003). "Real-time kinematic positioning based on undifferenced carrier phase data processing." *Proceedings of The Institute of Navigation National Technical Meeting*, 22-24 January, Anaheim, California, U.S.A., pp. 362-368.

Gao, Y. and X. Shen (2001). "Improving ambiguity convergence in carrier phase-based precise point positioning." *Proceedings of the 14th International Technical Meeting of the Satellite Division of The Institute of Navigation,* 11-14 September, Salt Lake City, Utah, U.S.A., pp. 1532-1539.

Gelb, A. (Ed.) (1974). *Applied Optimal Estimation.* Massachusetts Institute of Technology, Cambridge, 374 pp.

Gendt, G. (1998). "IGS combination of tropospheric estimates – experience from pilot experiment." In *Proceedings of IGS 1998 Analysis Center Workshop*, Darmstadt, Germany, 9-11 February, 1998, International GPS Service, pp. 205-216.

Gerrits, D. and R.B. Langley (1998). *GPS Line of Sight and Signal Occultations Determination for the BOLAS Spacecraft.* Internship project, Department of Geodesy and Geomatics Engineering, University of New Brunswick, Fredericton, N.B., 33 pp.

Gerrits, D. (2000). Personal communications. Department of Aerospace Engineering, Delft University of Technology.

Grejner-Brzezinska, D.A., C.K. Shum, and J.H. Kwon (2002). "A practical algorithm for LEO orbit determination." *Navigation*, Vol. 49, No. 3, pp. 127-135.

Hatch, R. (1982), "The synergism of GPS code and carrier measurements." *Proceedings of the Third International Geodetic Symposium on Satellite Doppler Positioning*", DMA, NOS, Las Cruces, N.Mex., 8-12 February, Physical Science Laboratory, New Mexico State University, Las Cruces, N.Mex., Vol. II, pp.1213-1232.

Héroux, P. and J. Kouba (1995). "GPS precise point positioning with a difference." Presented at Geomatics '95, 13-15 June, Ottawa, Ontario.

Héroux, P., J. Kouba, P. Collins, and F. Lahaye (2001). "GPS carrier-phase point positioning with precise orbit products." *Proceedings of the International Symposium on Kinematic Systems in Geodesy, Geomatics and Navigation 2001*, Banff, Alberta, 5-8 June.

Hofmann-Wellenhof, B., H. Lichtenegger, and J. Collins (2001). *Global Positioning System: Theory and Practice.* (5^{th} edition) Springer-Verlag, New York, 382 pp.

Hugentobler, U. (2002). Personal communication. Astronomical Institute, University of Bern, January.

ICD (2003). *Interface Control Document GPS-200C: Navstar GPS Space Segment / Navigation User Interface*. Version IRN-200C-005R1. ARINC Research Corporation, 164 pp.

IGEB (2003). "GPS fluctuations over time on May 2, 2000." Interagency GPS Executive Board. [On-line] January 2003. http://www.igeb.gov/sa/diagram.shtml

IGS (2001). "Working group on Low-Earth Orbiters." [On-line] October 2001. http://igscb.jpl.nasa.gov/projects/low-ear.html

ISDC (2001). "CHAMP information system and data center." [On-line] October 2001. http://isdc.gfz-potsdam.de/champ/

James, H.G. (1997). *BOLAS Phase A Final Report*. Report to the Canadian Space Agency, Ottawa, December.

Kleusberg, A., Y. Georgiadou, F. van den Heuvel, and P. Héroux (1993). *GPS Data Preprocessing with DIPOP 3.0*. Internal technical memorandum, Department of Surveying Engineering (now Department of Geodesy and Geomatics Engineering), University of New Brunswick, Fredericton, 84 pp.

Kleusberg, A. (1986). "Kinematic relative positioning using GPS code and carrier beat phase observations," *Marine Geodesy*, Vol. 10, No. 3/4, pp. 257-274.

Koenig, R. (2001). Personal communication. GeoForschungsZentrum, Potsdam, Germany, April.

Kouba, J. and P. Héroux (2001). "Precise point positioning using IGS orbit and clock products." *GPS Solutions*, Vol. 5, No. 2, pp. 12-28.

Kuang, D. (2002). Personal communication. Jet Propulsion Laboratory, Pasadena, California, U.S.A., March.

Kunze, H. (1997). Personal communication. Allen Osborne Associates, Inc., West Lake Village, California, U.S.A., December.

Kwon, J.H., D. Grejner-Brzezinska, and C.-K. Hong (2002). "Kinematic orbit determination of Low Earth Orbiters using triple differences." *Proceedings of The Institute of Navigation National Technical Meeting*, 28-30 January, San Diego, California, U.S.A., pp. 762-770.

Lachapelle, G., R. Klukas, D. Roberts, W. Qiu, and C. MacMillian (1994). "One-meter level kinematic point positioning using precise orbit and timing information." *Proceedings of the 7th International Technical Meeting of the Satellite Division of The Institute of Navigation*, 20-23 September, Salt Lake City, Utah, U.S.A., pp. 1435-1443.

Leick, A., (1995). *GPS Satellite Surveying.* Wiley, New York, 560 pp.

Meehan, T.K. (2002). Personal communication. Jet Propulsion Laboratory, January.

Melbourne, W.G., E.S. Davis, and T.P. Yunck (1994). "The GPS flight experiment on TOPEX/POSEIDON," *Geophysical Research Letters*, Vol. 21, No. 19, pp. 2171-2174.

Misra, P. and P. Enge (2001). *Global Positioning System: Signals, Measurements, Performance.* Ganga-Jamuna Press, Lincoln, Mass., 390 pp.

Montenbruck, O. (2002). Personal communication. Deutschen Zentrum für Luft-und Raumfahrt (DLR), Munich, Germany, January.

Montenbruck, O. and E. Gill (2000). *Satellite Orbits: Models, Methods, Applications*. Springer Verlag, Berlin, 369 pp.

Muellerschoen, R. J., W.I. Bertiger, and M.F. Lough (2000). "Results of an Internet-based dual-frequency global differential GPS system." *Proceedings of IAIN World Congress*, June, San Diego, California, U.S.A.

NavCom (2003). "StarFire network global GPS service." [On-line] April 2003, http://www.navcomtech.com/products/starfirenetwork.cfm

Neilan, R.E., J.F. Zumberge, G. Beutler, and J. Kouba (1997). "The International GPS Service: A global resource for GPS applications and research." *Proceedings of the 10th International Technical Meeting of the Satellite Division of The Institute of Navigation*, Kansas City, Missouri, U.S.A., 16-19 September, Part 1, pp. 883-889.

OSTP (2003). "Statement by the president regarding the United States' decision to stop degrading Global Positioning System accuracy." Office of Science and Technology Policy. [On-line] January 2003. http://www.ostp.gov/html/0053_2.html

Parkinson, B.W., and J.J. Spilker Jr. (Eds.). *Global Positioning System: Theory and Applications.* Progress in Astronautics and Aeronautics Volume 164, American Institute of Aeronautics and Astronautics, Inc., Washington, 1436 pp.

Quiles-Blanco, A. and M. Martin-Neira (1999). "Performance comparison between a dynamic-free navigation filter and the carrier smoothing algorithm." *Proceedings of the 12th International Technical Meeting of the Satellite Division of The Institute of Navigation*, Nashville, Tennessee, U.S.A., 14-17 September, pp.1597-1607.

Remondi, B. W. (1989). Extending the National Geodetic Survey Standard Orbit Formats, National Oceanic and Atmospheric Administration Technical Report National Ocean Service 133, National Geodetic Survey 46, 85 pp.

Roy, A. E. (1982). *Orbital Motion* (2nd ed.). Adam Hilger Ltd., Bristol, 495 pp.

Santos, M.C. (1995). *On Real-Time Orbit Improvement for GPS Satellites.* Doctoral dissertation. Department of Geodesy and Geomatics Engineering, Technical Report No. 178, University of New Brunswick, Fredericton, New Brunswick, 100 pp.

Seeber, G. (1993). *Satellite Geodesy*. de Gruyter, Berlin, 531 pp.

Schutz, B.E., B.D. Tapley, P.A.M. Abusali, and H.J. Rim (1994). "Dynamic orbit determination using GPS measurements from TOPEX/POSEIDON," *Geophysical Research Letters*, Vol. 21, No. 19, pp. 2179-2182.

Strang, G. and K. Borre (1997). *Linear Algebra, Geodesy, and GPS*. Wellesley-Cambridge Press, Wellesley, Mass., 640 pp.

Švehla, D. and M. Rothacher (2003). "CHAMP double-difference kinematic POD with ambiguity resolution." In *First CHAMP Mission Results for Gravity, Magnetic and Atmospheric Studies*, Eds. C. Reigber, H. Lür, P. Schwintzer, Springer, Berlin, pp. 70-77.

Tapley, B.D. (1989). "Fundamentals of orbit determination." In *Theory of Satellite Geodesy and Gravity Field Determination*, Eds. F. Sansò and R. Rummel, Lecture Notes in Earth Sciences 25, Eds. S. Bhattacharji, G. M. Friedman, H. J. Neugebauer, and A. Seilacher, Springer-Verlag, Berlin, pp. 235-260.

Teunissen, P.J.G. and A. Kleusberg, (eds.) (1998). *GPS for Geodesy*. Springer, Berlin, 650 pp.

Thales (2003). "SkyFix XP." [On-line] April 2003, http://www.thales-geosolutions.com/skyfix/skyfixxp.html

Unwin, M. (1995). *The Design and Implementation of a Small Satellite Navigation Unit Based on a Global Positioning System Receiver*. Doctoral thesis, Centre for Satellite Engineering Research, University of Surrey, Surrey, U.K., 304 pp.

Van Leeuwen, A., E. Rosen and L. Carrier (1980). "The Global Positioning System and its application in spacecraft navigation." In *Global Positioning System Papers Published in Navigation.* Janiczek, P.M. (Ed.). The Institute of Navigation, Washington, 796 pp.

Wells, D. (1997). *Lecture Notes in Approximation and Estimation*. Department of Geodesy and Geomatics Engineering, University of New Brunswick, Fredericton, N.B., 86 pp.

Wells, D., N. Beck, D. Delikaraoglou, A Kleusberg, E.J. Krakiwsky, G. Lachapelle, R.B. Langley, M. Nakiboglu, K.-P. Schwarz, J.M. Tranquilla, and P. Vaníček (1987). *Guide to GPS Positioning*. Canadian GPS Associates, Fredericton, N.B.

Wu, J.T., S.-C. Wu, G.A. Hajj, W.I. Bertiger, and S.M. Lichten (1993). "Effects of antenna orientation on GPS carrier phase," *Manuscripta Geodaetica*, Vol. 18, pp. 705-727.

Wu, S.-C. and W.G. Melbourne (1993). "An optimal GPS data processing technique for precise positioning," *IEEE Transactions on Geoscience and Remote Sensing*, Vol. 31, No. 1, pp.146-152.

Wu, S.-C., T. P. Yunck, and C. L. Thornton (1991). "Reduced-dynamic technique for precise orbit determination of Low Earth Satellites," *Journal of Guidance, Control, and Dynamics*, Vol. 14, No. 1, pp. 24-30.

Yunck, T. P. (1996). "Orbit determination." In *Global Positioning System: Theory and Applications Volume 2*, B.W. Parkinson, J.J. Spilker Jr. (Eds.), Progress in Astronautics and Aeronautics Volume 164, American Institute of Aeronautics and Astronautics, Inc., Washington, pp. 559-592.

Yunck, T.P. and S.-C. Wu (1986). "Non-dynamic decimeter tracking of earth satellites using the Global Positioning System." *American Institute of Aeronautics and Astronautics 24th Aerospace Sciences Meeting*, 6-9 January, Reno, Nevada, U.S.A., AIAA-86-0404.

Yunck, T. P., S.-C. Wu, and J.-T. Wu (1986). "Strategies for sub-decimeter satellite tracking with GPS," *Proceedings of IEEE Position, Location, and Navigation Symposium 1986*, Las Vegas, Nevada, U.S.A., 4-7 November, pp. 122-128.

Zumberge, J.F., M.B. Heflin, D.C. Jefferson, M.M. Watkins, and F.H. Webb (1997). "Precise point positioning for the efficient and robust analysis of GPS data from large networks." *Journal of Geophysical Research*, Vol. 102, No. B3, pp. 5005-5017.

APPENDIX A THE LEAST-SQUARES FILTER AS A SUBSET OF THE KALMAN FILTER

Batch least-squares can be represented in sequential (or recursive) form as (*e.g.*, Strang and Borre [1997], Wells [1997])

$$\hat{\mathbf{x}}_{\text{new}} = \mathbf{L}\hat{\mathbf{x}}_{\text{old}} + \mathbf{K}\ell_{\text{new}} \tag{A.1}$$

or

$$\hat{\mathbf{x}}_{\text{new}} = \hat{\mathbf{x}}_{\text{old}} + \mathbf{K}\left(\ell_{\text{new}} - \mathbf{A}_{\text{new}}\hat{\mathbf{x}}_{\text{old}}\right), \text{ i.e., } \mathbf{L} = \mathbf{I} - \mathbf{K}\mathbf{A}_{\text{new}} \tag{A.2}$$

That is, a new estimate $\hat{\mathbf{x}}_{\text{new}}$ is equal to a factor $\mathbf{L}$ multiplied by the old estimate $\hat{\mathbf{x}}_{\text{old}}$ plus a factor $\mathbf{K}$ multiplied by the observations ℓ_{new}. $\mathbf{L}$ can be reformulated as in (A.2), where $\mathbf{A}_{\text{new}}$ is the matrix of measurement partials with respect to $\hat{\mathbf{x}}_{\text{old}}$. This equation is intuitive: the new estimate $\hat{\mathbf{x}}_{\text{new}}$ is equal to the old estimate plus a correction. This correction consists of the weighting by $\mathbf{K}$ of the difference (the innovation) of new observations ℓ_{new} and a prediction based on old estimates $\mathbf{A}_{\text{new}}\hat{\mathbf{x}}_{\text{old}}$. The sequential least-squares filter with Kalman filter notation is

$$\hat{\mathbf{x}}_{t|t} = \hat{\mathbf{x}}_{t-1|t} + \mathbf{K}_t\left(\ell_t - \mathbf{A}_t\hat{\mathbf{x}}_{t-1|t}\right), \tag{A.3}$$

$$\mathbf{K}_t = \mathbf{P}_{t|t}\mathbf{A}_t^{\mathrm{T}}\mathbf{C}_t^{-1}, \text{ and} \tag{A.4}$$

$$\mathbf{P}_{t|t}^{-1} = \mathbf{P}_{t-1|t-1}^{-1} + \mathbf{A}_t^{\mathrm{T}}\mathbf{C}_t^{-1}\mathbf{A}_t, \tag{A.5}$$

where the subscript "a|b" represents the estimate at epoch "a" with measurements up to and including epoch "b", $\hat{\mathbf{x}}$ is the vector of estimated parameters, $\mathbf{A}$ is the matrix of

measurement partials with respect to the parameters, ℓ is the vector of observations, **C** is the associated variance-covariance matrix of the estimated parameters, and **K** is the filter gain matrix.

The equivalent equations for the Kalman filter are

$$\hat{\mathbf{x}}_{t|t-1} = \mathbf{\Phi}_{t-1}\hat{\mathbf{x}}_{t-1|t-1}, \tag{A.6}$$

$$\hat{\mathbf{x}}_{t|t} = \hat{\mathbf{x}}_{t-1|t} + \mathbf{K}_t\left(\ell_t - \mathbf{A}_t\hat{\mathbf{x}}_{t-1|t}\right), \tag{A.7}$$

$$\mathbf{P}_{t|t-1} = \mathbf{\Phi}_{t-1}\mathbf{P}_{t-1|t-1}\mathbf{\Phi}_{t-1}^{T} + \mathbf{Q}_t, \tag{A.8}$$

$$\mathbf{K}_t = \mathbf{P}_{t|t-1}\mathbf{A}_t^{T}\left(\mathbf{A}_t\mathbf{P}_{t|t-1}\mathbf{A}_t^{T} + \mathbf{C}_t\right)^{-1}, \text{ and} \tag{A.9}$$

$$\mathbf{P}_{t|t}^{-1} = \left(\mathbf{I} - \mathbf{K}_t\mathbf{A}_t\right)\mathbf{P}_{t|t-1}, \tag{A.10}$$

where the additional terms are the matrix $\mathbf{\Phi}_{t-1}$ relating $\hat{\mathbf{x}}_{t-1|t-1}$ to $\hat{\mathbf{x}}_{t|t-1}$, and the matrix $\mathbf{Q}_t$ is its associated system noise. (A.6) and (A.8) represent the Kalman time update or prediction, and (A.7), (A.9) and (A.10) represent the measurement update or correction.

The Kalman filter is equivalent to the sequential least squares filter when $\mathbf{\Phi}_{t-1} = \mathrm{I}$ and $\mathbf{Q}_t = 0$, that is, $\mathbf{x}_{t-1} = \mathbf{x}_t$. (A.6) becomes

$$\hat{\mathbf{x}}_{t|t-1} = \hat{\mathbf{x}}_{t-1|t-1}. \tag{A.11}$$

From (A.11), (A.7) becomes

$$\hat{\mathbf{x}}_{t|t} = \hat{\mathbf{x}}_{t-1|t-1} + \mathbf{K}_t\left(\ell_t - \mathbf{A}_t\hat{\mathbf{x}}_{t-1|t-1}\right), \tag{A.12}$$

which is equivalent to the least-squares parameter estimate (A.3) as long as the gain matrices are equivalent.

(A.8) becomes

$$\mathbf{P}_{t|t-1} = \mathbf{P}_{t-1|t-1}. \tag{A.13}$$

From (A.13), (A.10) becomes

$$\mathbf{P}_{t|t} = \mathbf{P}_{t-1|t-1} - \mathbf{K}_t \mathbf{A}_t \mathbf{P}_{t-1|t-1}. \tag{A.14}$$

Introducing and applying the following matrix lemma (*e.g.*, Wells [1997])

$$\left(\mathbf{S}^{-1} + \mathbf{T}^{\mathrm{T}}\mathbf{R}^{-1}\mathbf{T}\right)^{-1} = \mathbf{S} - \mathbf{S}\mathbf{T}^{\mathrm{T}}\left(\mathbf{R} + \mathbf{T}\mathbf{S}\mathbf{T}^{\mathrm{T}}\right)^{-1}\mathbf{T}\mathbf{S} \tag{A.15}$$

results in

$$\mathbf{P}_{t|t} = \left(\mathbf{P}_{t-1|t-1}^{-1} + \mathbf{A}_t^{\mathrm{T}}\mathbf{C}_t^{-1}\mathbf{A}_t\right)^{-1}, \tag{A.16}$$

which is equivalent to the least squares parameter covariance estimate (A.5). Finally, from (A.13), (A.9) becomes

$$\mathbf{K}_t = \mathbf{P}_{t-1|t-1}\mathbf{A}_t^{\mathrm{T}}\left(\mathbf{A}_t\mathbf{P}_{t-1|t-1}\mathbf{A}_t^{\mathrm{T}} + \mathbf{C}_t\right)^{-1}. \tag{A.17}$$

Introducing and applying the following matrix lemma (again, *e.g.*, Wells [1997])

$$\left(\mathbf{S}^{-1} + \mathbf{T}^{\mathrm{T}}\mathbf{R}^{-1}\mathbf{T}\right)^{-1}\mathbf{T}^{\mathrm{T}}\mathbf{R}^{-1} = \mathbf{S}\mathbf{T}^{\mathrm{T}}\left(\mathbf{R} + \mathbf{T}\mathbf{S}\mathbf{T}^{\mathrm{T}}\right)^{-1} \tag{A.18}$$

results in

$$\mathbf{K}_t = \left(\mathbf{P}_{t-1|t-1}^{-1} + \mathbf{A}_t^T \mathbf{C}_t^{-1} \mathbf{A}_t^T\right)^{-1} \mathbf{A}_t^T \mathbf{C}_t^{-1}. \tag{A.19}$$

Applying (A.5) gives

$$\mathbf{K}_t = \mathbf{P}_{t|t} \mathbf{A}_t^T \mathbf{C}_t^{-1}, \tag{A.20}$$

which is equivalent to the least-squares gain (A.4).

APPENDIX B DERIVATION OF AUGMENTED LEO POSITION COVARIANCE

A number of key derivations are presented in this appendix. The equations developed here are not only used for the error study, but also form the basis of the actual position filter processor described in Chapter 5. The extended solution covariance model is given first for the general parametric least-squares case and then specifically for the LEO error estimator. The required design matrices and covariance matrices are then derived.

APPENDIX B.1 DERIVATION FOR GENERIC PARAMETRIC LEAST-SQUARES CASE

The basic linearised parametric least-squares mathematical observation model is represented by

$$\mathbf{w} + \mathbf{A}\boldsymbol{\delta} - \mathbf{r} = 0; \qquad \mathbf{C}_\ell, \tag{B.1}$$

where $\boldsymbol{\delta}$ is the vector of corrections to the approximate parameters (that is, $\hat{\mathbf{x}} = \mathbf{x}^{\mathbf{o}} + \boldsymbol{\delta}$), $\mathbf{A}$ is the matrix of measurement partials with respect to the parameters, $\mathbf{w}$ is the vector of misclosures, $\mathbf{r}$ is the vector of residuals ($\hat{\ell} = \ell^{\mathbf{o}} + \mathbf{r}$), and $\mathbf{C}_\ell$ is the (usually diagonal) covariance matrix of the observations. Using matrix partitioning this model can be expanded (*e.g.*, Strang and Borre [1997]) to include additional information

$$\begin{bmatrix} \mathbf{w} \\ \mathbf{w_o} \end{bmatrix} + \begin{bmatrix} \mathbf{A} & \mathbf{A_o} \\ 0 & \mathbf{I} \end{bmatrix} \begin{bmatrix} \boldsymbol{\delta} \\ \boldsymbol{\delta_o} \end{bmatrix} - \begin{bmatrix} \mathbf{r} \\ \mathbf{r_o} \end{bmatrix} = 0; \quad \begin{bmatrix} \mathbf{C}_\ell & 0 \\ 0 & \mathbf{C}_{\ell_\mathbf{o}} \end{bmatrix}, \tag{B.2}$$

where $\boldsymbol{\delta}_\mathbf{o}$ is the vector of corrections to additional unknowns (terms to be considered in the adjustment as per Bierman [1977] terminology), $\mathbf{A_o}$ is the matrix of measurement

partials with respect to the considered parameters, and $\mathbf{w_o}$, $\mathbf{r_o}$ and $\mathbf{C}_{\ell_o}$ are the misclosure vector, residual vector and covariance matrix, respectively associated with the considered parameters. The unknown $\boldsymbol{\delta}_\mathbf{o}$ could contain, for example, the coordinates of a control monument used in a geodetic network adjustment. If a least squares adjustment were carried-out on all of (B.2), new estimates for $\boldsymbol{\delta}_\mathbf{o}$ would be obtained. This estimate would be using new observations in $\mathbf{w_o}$ to obtain estimates for $\hat{\mathbf{x}}$ which is required, but also estimates for $\boldsymbol{\delta}_\mathbf{o}$ which are not required nor desired. It is assumed that the published values of $\boldsymbol{\delta}_\mathbf{o}$ are the most accurate and should not be altered, but the error attached to these values should be propagated through the adjustment. Hence as described in, *e.g.*, Blaha [1974] and Strang and Borre [1997], the additional residual vector $\mathbf{r_o}$ is set to zero, which prevents any adjustment of $\boldsymbol{\delta}_\mathbf{o}$ and $\mathbf{w}_\mathbf{o} = -\boldsymbol{\delta}_\mathbf{0}$, making the elements of $\boldsymbol{\delta}_\mathbf{o}$ so-called *pseudo-observations*

$$\mathbf{w} - \mathbf{A}_\mathbf{o}\boldsymbol{\delta}_\mathbf{o} + \mathbf{A}\boldsymbol{\delta} - \mathbf{r} = 0;\ \begin{bmatrix} \mathbf{C}_\ell & 0 \\ 0 & \mathbf{C}_{\ell_\mathbf{0}} \end{bmatrix}, \tag{B.3}$$

and the least-squares solution is given by

$$\hat{\mathbf{x}} = \mathbf{x}^\mathbf{o} - \left(\mathbf{A}^\mathrm{T}\mathbf{C}_\ell^{-1}\mathbf{A}\right)^{-1}\mathbf{A}^\mathrm{T}\mathbf{C}_\ell^{-1}\left(\mathbf{w} - \mathbf{A}_\mathbf{o}\boldsymbol{\delta}_\mathbf{o}\right). \tag{B.4}$$

As can be seen in (B.3) and (B.4) the affect of adding the pseudo-observations has been really to only modify the observation vector. The effect on the parameter covariance though is quite profound. Applying the law of error propagation gives

$$\mathbf{C}_{\hat{\mathbf{x}}} = \begin{bmatrix} \dfrac{\partial \hat{\mathbf{x}}}{\partial \mathbf{w}} & \dfrac{\partial \hat{\mathbf{x}}}{\partial \mathbf{w_o}} \end{bmatrix} \begin{bmatrix} \mathbf{C}_{\ell} & 0 \\ 0 & \mathbf{C}_{\ell_o} \end{bmatrix} \begin{bmatrix} \dfrac{\partial \hat{\mathbf{x}}}{\partial \mathbf{w}} & \dfrac{\partial \hat{\mathbf{x}}}{\partial \mathbf{w_o}} \end{bmatrix}^{\mathrm{T}}. \tag{B.5}$$

Given that

$$\begin{bmatrix} \dfrac{\partial \hat{\mathbf{x}}}{\partial \mathbf{w}} & \dfrac{\partial \hat{\mathbf{x}}}{\partial \mathbf{w_o}} \end{bmatrix} = \begin{bmatrix} \left(\mathbf{A}^{\mathrm{T}}\mathbf{C}_{\ell}^{-1}\mathbf{A}\right)^{-1}\mathbf{A}^{\mathrm{T}}\mathbf{C}_{\ell}^{-1} & -\left(\mathbf{A}^{\mathrm{T}}\mathbf{C}_{\ell}^{-1}\mathbf{A}\right)^{-1}\mathbf{A}^{\mathrm{T}}\mathbf{C}_{\ell}^{-1}\mathbf{A}_{\mathbf{o}} \end{bmatrix}, \tag{B.6}$$

$$\mathbf{C}_{\hat{\mathbf{x}}} = \left(\mathbf{A}^{\mathrm{T}}\mathbf{C}_{\ell}^{-1}\mathbf{A}\right)^{-1} + \left(\mathbf{A}^{\mathrm{T}}\mathbf{C}_{\ell}^{-1}\mathbf{A}\right)^{-1}\mathbf{A}^{\mathrm{T}}\mathbf{C}_{\ell}^{-1}\mathbf{A}_{\mathbf{o}}\mathbf{C}_{\ell_{\mathbf{o}}}\mathbf{A}_{\mathbf{o}}^{\mathrm{T}}\mathbf{C}_{\ell}^{-1}\mathbf{A}\left(\mathbf{A}^{\mathrm{T}}\mathbf{C}_{\ell}^{-1}\mathbf{A}\right)^{-1}. \tag{B.7}$$

The first term of (B.7) is sometimes (*e.g.*, Strang and Borre [1997]) referred to as the internal error – the error resulting from direct measurement noise, and the second term as the external error – the error resulting from other sources, *e.g.*, control monument coordinate variances. Therefore (B.7) can be represented by

$$\mathbf{C}_{\hat{\mathbf{x}}} = \begin{bmatrix} \dfrac{\partial \hat{\mathbf{x}}}{\partial \mathbf{w}} \end{bmatrix} \begin{bmatrix} \mathbf{C}_{\ell} \end{bmatrix} \begin{bmatrix} \dfrac{\partial \hat{\mathbf{x}}}{\partial \mathbf{w}} \end{bmatrix}^{\mathrm{T}} + \begin{bmatrix} \dfrac{\partial \hat{\mathbf{x}}}{\partial \mathbf{w_o}} \end{bmatrix} \begin{bmatrix} \mathbf{C}_{\ell_o} \end{bmatrix} \begin{bmatrix} \dfrac{\partial \hat{\mathbf{x}}}{\partial \mathbf{w_o}} \end{bmatrix}^{\mathrm{T}} = \mathbf{C}_{\hat{\mathbf{x}}_{\mathbf{internal}}} + \mathbf{C}_{\hat{\mathbf{x}}_{\mathbf{external}}}. \tag{B.8}$$

Bierman [1997] refers to (B.7) in slightly different terms. The total covariance is referred to as the consider covariance $\mathbf{C}_{\hat{\mathbf{x}}_{\mathbf{con}}}$, and the constituent error sources as the commission error $\mathbf{C}_{\hat{\mathbf{x}}_{\mathbf{com}}}$ and the omission error $\mathbf{C}_{\hat{\mathbf{x}}_{\mathbf{om}}}$ (*e.g.*, Yunck [1996]):

$$\mathbf{C}_{\hat{\mathbf{x}}_{\mathbf{con}}} = \mathbf{C}_{\hat{\mathbf{x}}_{\mathbf{com}}} + \mathbf{S}\mathbf{C}_{\hat{\mathbf{x}}_{\mathbf{om}}}\mathbf{S}^{\mathrm{T}}, \tag{B.9}$$

where $\mathbf{C}_{\hat{\mathbf{x}}_{\mathbf{con}}} = \mathbf{C}_{\hat{\mathbf{x}}}$, $\mathbf{C}_{\hat{\mathbf{x}}_{\mathbf{com}}} = \left(\mathbf{A}^{\mathrm{T}}\mathbf{C}_{\ell}^{-1}\mathbf{A}\right)^{-1}$, $\mathbf{C}_{\hat{\mathbf{x}}_{\mathbf{om}}} = \mathbf{C}_{\ell_{\mathbf{o}}}$, and $\mathbf{S} = \left(\mathbf{A}^{\mathrm{T}}\mathbf{C}_{\ell}^{-1}\mathbf{A}\right)^{-1}\mathbf{A}^{\mathrm{T}}\mathbf{C}_{\ell}^{-1}\mathbf{A}_{\mathbf{o}}$. This last matrix is referred to as the sensitivity matrix and describes the response of the

estimate $\hat{\mathbf{x}}$ to the parameters $\boldsymbol{\delta}_o$. A final matrix $\mathbf{P}$ – the perturbation matrix, can be produced

$$\mathbf{P} = \mathbf{S}\,\mathrm{sqrt}\left(\mathrm{diag}\left(\mathbf{C}_{\hat{\mathbf{x}}_{\mathbf{om}}}\right)\right), \tag{B.10}$$

which describes the effects of a 1σ error in an element of $\boldsymbol{\delta}_o$ on the estimated parameters $\hat{\mathbf{x}}$. In this formalism $\boldsymbol{\delta}_o$, the vector of corrections to the omission error parameters, are referred to as bias parameters. That is, *e.g.*, uncertainties in control monument coordinates *bias* the results using these coordinates. However, as is shown in the above derivation, it is known formal random errors that are propagated through the adjustment process.

APPENDIX B.2 DERIVATION OF TOTAL LEO POSITION ERROR COVARIANCE ESTIMATOR

This derivation requires applying the parameter covariance estimator (B.7) to the kinematic, sequential, least-squares positioning filter model (A.19). To begin, the filter model can be expressed in the form of (B.3)

$$\begin{bmatrix} \mathbf{w}_{t-1} \\ \mathbf{w}_t \end{bmatrix} = \begin{bmatrix} 0 & \mathbf{D}_t & 0 & \mathbf{E}_t \\ \mathbf{D}_{t-1} & \mathbf{D}_t & \mathbf{E}_{t-1} & \mathbf{E}_t \end{bmatrix} \begin{bmatrix} \boldsymbol{\delta}\mathbf{stn}_{t-1} \\ \boldsymbol{\delta}\mathbf{stn}_t \\ \boldsymbol{\delta}\mathbf{sv}_{t-1} \\ \boldsymbol{\delta}\mathbf{sv}_t \end{bmatrix}$$

$$+ \begin{bmatrix} 0 & \mathbf{A}_t \\ -\mathbf{A}_{t-1} & \mathbf{A}_t \end{bmatrix} \begin{bmatrix} \boldsymbol{\delta}\mathbf{x}_{t-1} \\ \boldsymbol{\delta}\mathbf{x}_t \end{bmatrix} - \begin{bmatrix} \mathbf{r}_1 \\ \mathbf{r}_2 \end{bmatrix}; \begin{bmatrix} \mathbf{C}_{\mathbf{P}} & 0 & 0 & 0 \\ 0 & \mathbf{C}_{\boldsymbol{\Phi}} & 0 & 0 \\ 0 & 0 & \mathbf{C}_{\mathbf{stn}} & 0 \\ 0 & 0 & 0 & \mathbf{C}_{\mathbf{sv}} \end{bmatrix} \tag{B.11}$$

Therefore

$$\partial \mathbf{w} = \begin{bmatrix} \partial \mathbf{w_1} \\ \partial \mathbf{w_2} \end{bmatrix} = \begin{bmatrix} 0 & \mathbf{A}_t \\ -\mathbf{A}_{t-1} & \mathbf{A}_t \end{bmatrix} \begin{bmatrix} \partial \mathbf{x}^{\mathbf{o}}_{t-1} \\ \partial \mathbf{x}^{\mathbf{o}}_{t} \end{bmatrix}$$

$$+ \begin{bmatrix} 0 & \mathbf{D}_t & 0 & \mathbf{E}_t \\ \mathbf{D}_{t-1} & \mathbf{D}_t & \mathbf{E}_{t-1} & \mathbf{E}_t \end{bmatrix} \begin{bmatrix} \boldsymbol{\delta}\mathbf{stn}_{t-1} \\ \boldsymbol{\delta}\mathbf{stn}_{t} \\ \boldsymbol{\delta}\mathbf{sv}_{t-1} \\ \boldsymbol{\delta}\mathbf{sv}_{t} \end{bmatrix} - \begin{bmatrix} \partial \ell^{\mathbf{o}}_1 \\ \partial \ell^{\mathbf{o}}_2 \end{bmatrix}. \tag{B.12}$$

From (A.19),

$$\partial \hat{\mathbf{x}} = \begin{bmatrix} \boldsymbol{\delta}\hat{\mathbf{x}}_{t-1} \\ \boldsymbol{\delta}\hat{\mathbf{x}}_{t} \end{bmatrix} = \begin{bmatrix} \mathbf{x}^{\mathbf{0}}_{t-1} \\ \mathbf{x}^{\mathbf{0}}_{t} \end{bmatrix}$$

$$+ \begin{bmatrix} \mathbf{A}^{\mathrm{T}}_{t-1}\mathbf{C}^{-1}_{\boldsymbol{\Phi}}\mathbf{A}_{t-1} + \mathbf{C}^{-1}_{\hat{\mathbf{x}}_{t-1}} & -\mathbf{A}^{\mathrm{T}}_{t-1}\mathbf{C}^{-1}_{\boldsymbol{\Phi}}\mathbf{A}_{t} \\ -\mathbf{A}_{t}\mathbf{C}^{-1}_{\boldsymbol{\Phi}}\mathbf{A}_{t-1} & \mathbf{A}^{\mathrm{T}}_{t}\left(\mathbf{C}^{-1}_{\mathbf{P}} + \mathbf{C}^{-1}_{\boldsymbol{\Phi}}\right)\mathbf{A}_{t} \end{bmatrix}^{-1} \begin{bmatrix} -\mathbf{A}^{\mathrm{T}}_{t-1}\mathbf{C}^{-1}_{\boldsymbol{\Phi}}\partial \mathbf{w}_{t} \\ \mathbf{A}^{\mathrm{T}}_{t}\mathbf{C}^{-1}_{\mathbf{P}}\partial \mathbf{w}_{t-1} + \mathbf{A}_{t}\mathbf{C}^{-1}_{\boldsymbol{\Phi}}\partial \mathbf{w}_{t} \end{bmatrix}. \tag{B.13}$$

Let the inverted term in (B.13) be equal to $\mathbf{R}^{-1}$ and

$$\mathbf{R}^{-1} = \mathbf{S} = \begin{bmatrix} \mathbf{S}_{11} & \mathbf{S}_{12} \\ \mathbf{S}_{21} & \mathbf{S}_{22} \end{bmatrix}. \tag{B.14}$$

Substituting (B.12) and (B.14) into (B.13) and multiplying through gives

$$\partial \hat{\mathbf{x}}_{t-1} = \partial \mathbf{x}^{\mathbf{o}}_{t-1} + \mathbf{S_{11}}\mathbf{A}^{\mathrm{T}}_{t-1}\mathbf{C}^{-1}_{\boldsymbol{\Phi}}\mathbf{A}_{t-1}\partial \mathbf{x}^{\mathrm{o}}_{t-1} - \mathbf{S_{11}}\mathbf{A}^{\mathrm{T}}_{t-1}\mathbf{C}^{-1}_{\boldsymbol{\Phi}}\mathbf{A}_{t}\partial \mathbf{x}^{\mathbf{o}}_{t}$$

$$- \mathbf{S_{11}}\mathbf{A}^{\mathrm{T}}_{t-1}\mathbf{C}^{-1}_{\boldsymbol{\Phi}}\mathbf{D}_{t-1}\partial \boldsymbol{\delta}\mathbf{stn}_{t-1} - \mathbf{S_{11}}\mathbf{A}^{\mathrm{T}}_{t-1}\mathbf{C}^{-1}_{\boldsymbol{\Phi}}\mathbf{D}_{t}\partial \boldsymbol{\delta}\mathbf{stn}_{t} - \mathbf{S_{11}}\mathbf{A}^{\mathrm{T}}_{t-1}\mathbf{C}^{-1}_{\boldsymbol{\Phi}}\mathbf{E}_{t-1}\partial \boldsymbol{\delta}\mathbf{sv}_{t-1}$$

$$- \mathbf{S_{11}}\mathbf{A}^{\mathrm{T}}_{t-1}\mathbf{C}^{-1}_{\boldsymbol{\Phi}}\mathbf{E}_{t}\partial \boldsymbol{\delta}\mathbf{sv}_{t} + \mathbf{S_{11}}\mathbf{A}^{\mathrm{T}}_{t-1}\mathbf{C}^{-1}_{\boldsymbol{\Phi}}\partial \ell^{\mathbf{o}}_{\mathbf{2}}$$

$$+\mathbf{S}_{12}\mathbf{A}_t^{\mathrm{T}}\mathbf{C}_{\mathbf{P}}^{-1}\mathbf{A}_t\partial\mathbf{x}_t^{\mathbf{o}}+\mathbf{S}_{12}\mathbf{A}_t^{\mathrm{T}}\mathbf{C}_{\mathbf{P}}^{-1}\mathbf{D}_t\partial\boldsymbol{\delta}\mathbf{stn}_t+\mathbf{S}_{12}\mathbf{A}_t^{\mathrm{T}}\mathbf{C}_{\mathbf{P}}^{-1}\mathbf{E}_t\partial\boldsymbol{\delta}\mathbf{sv}_t$$

$$-\mathbf{S}_{12}\mathbf{A}_t^{\mathrm{T}}\mathbf{C}_{\mathbf{P}}^{-1}\partial\ell_{\mathbf{1}}^{\mathbf{o}}$$

$$-\mathbf{S}_{12}\mathbf{A}_t\mathbf{C}_{\boldsymbol{\Phi}}^{-1}\mathbf{A}_{t-1}\partial\mathbf{x}_{t-1}^{\mathbf{o}}+\mathbf{S}_{12}\mathbf{A}_t\mathbf{C}_{\boldsymbol{\Phi}}^{-1}\mathbf{A}_t\partial\mathbf{x}_t^{\mathbf{o}}+\mathbf{S}_{11}\mathbf{A}_t\mathbf{C}_{\boldsymbol{\Phi}}^{-1}\mathbf{D}_{t-1}\partial\boldsymbol{\delta}\mathbf{stn}_{t-1}$$

$$+\mathbf{S}_{12}\mathbf{A}_t\mathbf{C}_{\boldsymbol{\Phi}}^{-1}\mathbf{D}_t\partial\boldsymbol{\delta}\mathbf{stn}_t+\mathbf{S}_{12}\mathbf{A}_t\mathbf{C}_{\boldsymbol{\Phi}}^{-1}\mathbf{E}_{t-1}\partial\boldsymbol{\delta}\mathbf{sv}_{t-1}+\mathbf{S}_{12}\mathbf{A}_t\mathbf{C}_{\boldsymbol{\Phi}}^{-1}\mathbf{E}_t\partial\boldsymbol{\delta}\mathbf{sv}_t$$

$$-\mathbf{S}_{12}\mathbf{A}_t\mathbf{C}_{\boldsymbol{\Phi}}^{-1}\partial\ell_{\mathbf{2}}^{\mathbf{o}}, \tag{B.15a}$$

$$\partial\hat{\mathbf{x}}_t=\partial\mathbf{x}_t^{\mathbf{o}}+\mathbf{S}_{21}\mathbf{A}_{t-1}^{\mathrm{T}}\mathbf{C}_{\boldsymbol{\Phi}}^{-1}\mathbf{A}_{t-1}\partial\mathbf{x}_{t-1}^{\mathbf{o}}-\mathbf{S}_{21}\mathbf{A}_{t-1}^{\mathrm{T}}\mathbf{C}_{\boldsymbol{\Phi}}^{-1}\mathbf{A}_t\partial\mathbf{x}_t^{\mathbf{o}}$$

$$-\mathbf{S}_{21}\mathbf{A}_{t-1}^{\mathrm{T}}\mathbf{C}_{\boldsymbol{\Phi}}^{-1}\mathbf{D}_{t-1}\partial\boldsymbol{\delta}\mathbf{stn}_{t-1}-\mathbf{S}_{21}\mathbf{A}_{t-1}^{\mathrm{T}}\mathbf{C}_{\boldsymbol{\Phi}}^{-1}\mathbf{D}_t\partial\boldsymbol{\delta}\mathbf{stn}_t-\mathbf{S}_{21}\mathbf{A}_{t-1}^{\mathrm{T}}\mathbf{C}_{\boldsymbol{\Phi}}^{-1}\mathbf{E}_{t-1}\partial\boldsymbol{\delta}\mathbf{sv}_{t-1}$$

$$-\mathbf{S}_{21}\mathbf{A}_{t-1}^{\mathrm{T}}\mathbf{C}_{\boldsymbol{\Phi}}^{-1}\mathbf{E}_t\partial\boldsymbol{\delta}\mathbf{sv}_t+\mathbf{S}_{21}\mathbf{A}_{t-1}^{\mathrm{T}}\mathbf{C}_{\boldsymbol{\Phi}}^{-1}\partial\ell_{\mathbf{2}}^{\mathbf{o}}$$

$$+\mathbf{S}_{22}\mathbf{A}_t^{\mathrm{T}}\mathbf{C}_{\mathbf{P}}^{-1}\mathbf{A}_t\partial\mathbf{x}_t^{\mathbf{o}}+\mathbf{S}_{22}\mathbf{A}_t^{\mathrm{T}}\mathbf{C}_{\mathbf{P}}^{-1}\mathbf{D}_t\partial\boldsymbol{\delta}\mathbf{stn}_t+\mathbf{S}_{22}\mathbf{A}_t^{\mathrm{T}}\mathbf{C}_{\mathbf{P}}^{-1}\mathbf{E}_t\partial\boldsymbol{\delta}\mathbf{sv}_t$$

$$-\mathbf{S}_{22}\mathbf{A}_t^{\mathrm{T}}\mathbf{C}_{\mathbf{P}}^{-1}\partial\ell_{\mathbf{1}}^{\mathbf{o}}$$

$$-\mathbf{S}_{22}\mathbf{A}_t\mathbf{C}_{\boldsymbol{\Phi}}^{-1}\mathbf{A}_{t-1}\partial\mathbf{x}_{t-1}^{\mathbf{o}}+\mathbf{S}_{22}\mathbf{A}_t\mathbf{C}_{\boldsymbol{\Phi}}^{-1}\mathbf{A}_t\partial\mathbf{x}_t^{\mathbf{o}}+\mathbf{S}_{22}\mathbf{A}_t\mathbf{C}_{\boldsymbol{\Phi}}^{-1}\mathbf{D}_{t-1}\partial\boldsymbol{\delta}\mathbf{stn}_{t-1}$$

$$+\mathbf{S}_{22}\mathbf{A}_t\mathbf{C}_{\boldsymbol{\Phi}}^{-1}\mathbf{D}_t\partial\boldsymbol{\delta}\mathbf{stn}_t+\mathbf{S}_{22}\mathbf{A}_t\mathbf{C}_{\boldsymbol{\Phi}}^{-1}\mathbf{E}_{t-1}\partial\boldsymbol{\delta}\mathbf{sv}_{t-1}+\mathbf{S}_{22}\mathbf{A}_t\mathbf{C}_{\boldsymbol{\Phi}}^{-1}\mathbf{E}_t\partial\boldsymbol{\delta}\mathbf{sv}_t$$

$$-\mathbf{S}_{22}\mathbf{A}_t\mathbf{C}_{\boldsymbol{\Phi}}^{-1}\partial\ell_{\mathbf{2}}^{\mathbf{o}}, \tag{B.15b}$$

Factoring out the parameters in (B.15) gives

$$\partial\hat{\mathbf{x}} = \begin{bmatrix} \mathbf{1a} & \mathbf{1b} & \mathbf{1c} & \mathbf{1d} & \mathbf{1e} & \mathbf{1f} & \mathbf{1g} & \mathbf{1h} \\ \mathbf{2a} & \mathbf{2b} & \mathbf{2c} & \mathbf{2d} & \mathbf{2e} & \mathbf{2f} & \mathbf{2g} & \mathbf{2h} \end{bmatrix} \begin{bmatrix} \partial\ell_{\mathbf{1}}^{\mathbf{o}} \\ \partial\ell_{\mathbf{2}}^{\mathbf{o}} \\ \partial\mathbf{x}_{t-1}^{\mathbf{o}} \\ \partial\mathbf{x}_{t}^{\mathbf{o}} \\ \partial\boldsymbol{\delta}\mathbf{stn}_{t-1} \\ \partial\boldsymbol{\delta}\mathbf{stn}_{t} \\ \partial\boldsymbol{\delta}\mathbf{sv}_{t-1} \\ \partial\boldsymbol{\delta}\mathbf{sv}_{t} \end{bmatrix}, \tag{B.16}$$

where

$$\mathbf{1a} = -\mathbf{S}_{12}\mathbf{A}_t^{\mathrm{T}}\mathbf{C}_{\mathbf{P}}^{-1} \tag{B.16a}$$

$$\mathbf{2a} = -\mathbf{S}_{22}\mathbf{A}_t^{\mathrm{T}}\mathbf{C}_{\mathbf{P}}^{-1} \tag{B.16b}$$

$$\mathbf{1b} = \mathbf{S}_{11}\mathbf{A}_{t-1}^{\mathrm{T}}\mathbf{C}_{\boldsymbol{\Phi}}^{-1} - \mathbf{S}_{12}\mathbf{A}_t\mathbf{C}_{\boldsymbol{\Phi}}^{-1} \tag{B.16c}$$

$$\mathbf{2b} = \mathbf{S}_{21}\mathbf{A}_{t-1}^{\mathrm{T}}\mathbf{C}_{\boldsymbol{\Phi}}^{-1} - \mathbf{S}_{22}\mathbf{A}_t\mathbf{C}_{\boldsymbol{\Phi}}^{-1} \tag{B.16d}$$

$$\mathbf{1c} = \mathbf{I} + \mathbf{S}_{11}\mathbf{A}_{t-1}^{\mathrm{T}}\mathbf{C}_{\boldsymbol{\Phi}}^{-1}\mathbf{A}_{t-1} - \mathbf{S}_{12}\mathbf{A}_t\mathbf{C}_{\boldsymbol{\Phi}}^{-1}\mathbf{A}_{t-1} \tag{B.16e}$$

$$\mathbf{2c} = \mathbf{S}_{21}\mathbf{A}_{t-1}^{\mathrm{T}}\mathbf{C}_{\boldsymbol{\Phi}}^{-1}\mathbf{A}_{t-1} - \mathbf{S}_{22}\mathbf{A}_t\mathbf{C}_{\boldsymbol{\Phi}}^{-1}\mathbf{A}_{t-1} \tag{B.16f}$$

$$\mathbf{1d} = -\mathbf{S}_{11}\mathbf{A}_{t-1}^{\mathrm{T}}\mathbf{C}_{\boldsymbol{\Phi}}^{-1}\mathbf{A}_t + \mathbf{S}_{12}\mathbf{A}_t^{\mathrm{T}}\mathbf{C}_{\mathbf{P}}^{-1}\mathbf{A}_t + \mathbf{S}_{12}\mathbf{A}_t\mathbf{C}_{\boldsymbol{\Phi}}^{-1}\mathbf{A}_t \tag{B.16g}$$

$$\mathbf{2d} = \mathbf{I} - \mathbf{S}_{21}\mathbf{A}_{t-1}^{\mathrm{T}}\mathbf{C}_{\boldsymbol{\Phi}}^{-1}\mathrm{A}_t + \mathbf{S}_{22}\mathbf{A}_t^{\mathrm{T}}\mathbf{C}_{\mathbf{P}}^{-1}\mathbf{A}_t + \mathbf{S}_{22}\mathbf{A}_t\mathbf{C}_{\boldsymbol{\Phi}}^{-1}\mathbf{A}_t \tag{B.16h}$$

$$\mathbf{1e} = -\mathbf{S}_{11}\mathbf{A}_{t-1}^{\mathrm{T}}\mathbf{C}_{\boldsymbol{\Phi}}^{-1}\mathbf{D}_{t-1} + \mathbf{S}_{12}\mathbf{A}_t\mathbf{C}_{\boldsymbol{\Phi}}^{-1}\mathbf{D}_{t-1} \tag{B.16i}$$

$$\mathbf{2e} = -\mathbf{S}_{21}\mathbf{A}_{t-1}^{\mathrm{T}}\mathbf{C}_{\boldsymbol{\Phi}}^{-1}\mathbf{D}_{t-1} + \mathbf{S}_{22}\mathbf{A}_t\mathbf{C}_{\boldsymbol{\Phi}}^{-1}\mathbf{D}_{t-1} \tag{B.16j}$$

$$\mathbf{1f} = -\mathbf{S_{11}}\mathbf{A}_{t-1}^{T}\mathbf{C}_{\mathbf{\Phi}}^{-1}\mathbf{D}_t + \mathbf{S_{12}}\mathbf{A}_t^{T}\mathbf{C}_{\mathbf{P}}^{-1}\mathbf{D}_t + \mathbf{S_{12}}\mathbf{A}_t\mathbf{C}_{\mathbf{\Phi}}^{-1}\mathbf{D}_t \tag{B.16k}$$

$$\mathbf{2f} = -\mathbf{S_{21}}\mathbf{A}_{t-1}^{T}\mathbf{C}_{\mathbf{\Phi}}^{-1}\mathbf{D}_t + \mathbf{S_{22}}\mathbf{A}_t^{T}\mathbf{C}_{\mathbf{P}}^{-1}\mathbf{D}_t + \mathbf{S_{22}}\mathbf{A}_t\mathbf{C}_{\mathbf{\Phi}}^{-1}\mathbf{D}_t \tag{B.16l}$$

$$\mathbf{1g} = -\mathbf{S_{11}}\mathbf{A}_{t-1}^{T}\mathbf{C}_{\mathbf{\Phi}}^{-1}\mathbf{E}_{t-1} + \mathbf{S_{12}}\mathbf{A}_t\mathbf{C}_{\mathbf{\Phi}}^{-1}\mathbf{E}_{t-1} \tag{B.16m}$$

$$\mathbf{2g} = -\mathbf{S_{21}}\mathbf{A}_{t-1}^{T}\mathbf{C}_{\mathbf{\Phi}}^{-1}\mathbf{E}_{t-1} + \mathbf{S_{22}}\mathbf{A}_t\mathbf{C}_{\mathbf{\Phi}}^{-1}\mathbf{E}_{t-1} \tag{B.16n}$$

$$\mathbf{1h} = -\mathbf{S_{11}}\mathbf{A}_{t-1}^{T}\mathbf{C}_{\mathbf{\Phi}}^{-1}\mathbf{E}_t + \mathbf{S_{12}}\mathbf{A}_t^{T}\mathbf{C}_{\mathbf{P}}^{-1}\mathbf{E}_t + \mathbf{S_{12}}\mathbf{A}_t\mathbf{C}_{\mathbf{\Phi}}^{-1}\mathbf{E}_t \tag{B.16o}$$

$$\mathbf{2h} = -\mathbf{S_{21}}\mathbf{A}_{t-1}^{T}\mathbf{C}_{\mathbf{\Phi}}^{-1}\mathbf{E}_t + \mathbf{S_{22}}\mathbf{A}_t^{T}\mathbf{C}_{\mathbf{P}}^{-1}\mathbf{E}_t + \mathbf{S_{22}}\mathbf{A}_t\mathbf{C}_{\mathbf{\Phi}}^{-1}\mathbf{E}_t \tag{B.16p}$$

Therefore the internal and external covariances can now be determined, as well as the covariances attributed to each considered term:

$$\mathbf{C}_{\hat{\mathbf{x}}\,\mathbf{int}} = \begin{bmatrix} \mathbf{1a} & \mathbf{1b} & \mathbf{1c} & \mathbf{1d} \\ \mathbf{2a} & \mathbf{2b} & \mathbf{2c} & \mathbf{2d} \end{bmatrix} \begin{bmatrix} \mathbf{C_P} & 0 & 0 & 0 \\ 0 & \mathbf{C_\Phi} & 0 & 0 \\ 0 & 0 & \mathbf{C}_{\hat{\mathbf{x}}_{t-1}} & 0 \\ 0 & 0 & 0 & 0 \end{bmatrix} \begin{bmatrix} \mathbf{1a} & \mathbf{1b} & \mathbf{1c} & \mathbf{1d} \\ \mathbf{2a} & \mathbf{2b} & \mathbf{2c} & \mathbf{2d} \end{bmatrix}^{T}, \tag{B.17a}$$

$$\mathbf{C}_{\hat{\mathbf{x}}_{\mathbf{ext}}} = \begin{bmatrix} \mathbf{1e} & \mathbf{1f} & \mathbf{1g} & \mathbf{1h} \\ \mathbf{2e} & \mathbf{2f} & \mathbf{2g} & \mathbf{2h} \end{bmatrix} \times \begin{bmatrix} \mathbf{C}_{\mathbf{stn}_{t-1}} & 0 & 0 & 0 \\ 0 & \mathbf{C}_{\mathbf{stn}_t} & 0 & 0 \\ 0 & 0 & \mathbf{C}_{\mathbf{sv}_{t-1}} & 0 \\ 0 & 0 & 0 & \mathbf{C}_{\mathbf{sv}_t} \end{bmatrix}$$

$$\times \begin{bmatrix} \mathbf{1e} & \mathbf{1f} & \mathbf{1g} & \mathbf{1h} \\ \mathbf{2e} & \mathbf{2f} & \mathbf{2g} & \mathbf{2h} \end{bmatrix}^{T}. \tag{B.17b}$$

APPENDIX B.3 DERIVATION OF DESIGN MATRICES

As per (B.11) the following design matrices of the measurement partials are needed: **A**, **D**, **E**, **F**, and **G**. The epoch subscripts are not included and each matrix contains x, y, and z elements for each observation equation. (Only the x component is described here.)

The ionosphere-free pseudorange observation model (A.12) between receiver "i" and GPS satellite "k" is again

$$P_i^k = \rho_i^k + c\left(dT_i^k - dt_i^k\right) + dtrop_i^k + e_i^k . \tag{B.18}$$

The double–difference observation model between two receivers: "i" (terrestrial reference receiver) and "j" (LEO receiver) and two GPS satellites: "k" and "l" is then

$$P_{ij}^{kl} = \rho_{ij}^{kl} + dtrop_{ij}^{kl} + e_{ij}^{kl} , \tag{B.19}$$

where

$$\rho_{ij}^{kl} = \rho_i^k - \rho_j^k - \left(\rho_i^l - \rho_j^l\right), \tag{B.20}$$

and similarly

$$dtrop_{ij}^{kl} = dtrop_i^k - dtrop_j^k - \left(dtrop_i^l - dtrop_j^l\right). \tag{B.21}$$

From (B.19), (B.20) and (B.21) the elements of the design matrices can be assembled:

$$\frac{\partial P_{ij}^{kl}}{\partial x_j} = +\frac{\left(x^k - x_j\right)}{\rho_j^k} - \frac{\left(x^l - x_j\right)}{\rho_j^l} \qquad \text{for design matrix } \mathbf{A}, \tag{B.22}$$

$$\frac{\partial P_{ij}^{kl}}{\partial x^k} = +\frac{\left(x^k - x_i\right)}{\rho_i^k} - \frac{\left(x^k - x_j\right)}{\rho_j^k} \qquad \text{and} \tag{B.23}$$

$$\frac{\partial P_{ij}^{kl}}{\partial x^l} = -\frac{\left(x^l - x_i\right)}{\rho_i^l} + \frac{\left(x^l - x_j\right)}{\rho_j^l} \text{ for design matrix } \mathbf{D}, \tag{B.24}$$

$$\frac{\partial P_{ij}^{kl}}{\partial x_i} = -\frac{\left(x^k - x_i\right)}{\rho_i^k} + \frac{\left(x^l - x_i\right)}{\rho_i^l} \qquad \text{for design matrix } \mathbf{E}, \tag{B.25}$$

and

$$\frac{\partial P_{ij}^{kl}}{\partial dtrop_i^k} = +1 \text{ and} \tag{B.26}$$

$$\frac{\partial P_{ij}^{kl}}{\partial dtrop_i^l} = -1 \tag{B.27}$$

for design matrices **F** and **G**.

APPENDIX B.4 DERIVATION OF COVARIANCE MATRICES

The pseudorange double-difference covariance $\mathbf{C_P}$ can be represented by

$$\mathbf{C_P} = \sigma_P^2 \mathbf{Q}\mathbf{Q}^T, \tag{B.28}$$

where σ_P^2 is the variance of the pseudorange observation, and

$$\mathbf{Q} = \begin{bmatrix} 1 & -1 & 0 & 0 & -1 & 1 & 0 & 0 \\ 0 & 1 & -1 & 0 & 0 & -1 & 1 & 0 \\ 0 & 0 & 1 & -1 & 0 & 0 & -1 & 1 \end{bmatrix}. \tag{B.29}$$

The example of **Q** is for two receivers observing four GPS satellites.

The carrier phase triple-difference covariance $\mathbf{C}_{\mathbf{\Phi}}$ can be represented by

$$\mathbf{C}_{\mathbf{\Phi}} = \sigma_{\Phi}^2 \mathbf{TQ}(\mathbf{QT})^{\mathrm{T}}, \tag{B.30}$$

where σ_{Φ}^2 is the variance of the carrier phase observation, **Q** is as defined in (B.29), and

$$\mathbf{T} = \begin{bmatrix} -1 & 0 & 0 & 1 & 0 & 0 \\ 0 & -1 & 0 & 0 & 1 & 0 \\ 0 & 0 & -1 & 0 & 0 & 1 \end{bmatrix}. \tag{B.31}$$

Note that for both the double-difference pseudorange and the triple-difference carrier phase, a reference GPS satellite "book-keeping" approach is not used. That is, a reference satellite is not chosen to form the per-epoch differences with all other satellite observations, but rather adjacently recorded satellite observations in the RINEX files are differenced.

The terrestrial reference station and GPS satellite positions covariance matrices are represented in celestial coordinates with no dependence between matrix elements. Also, these values are time invariant. The reference station covariance matrix is

$$\mathbf{C}_{\mathbf{stn}} = \begin{bmatrix} \sigma_{\mathrm{stn}}^2 & 0 & 0 \\ 0 & \sigma_{\mathrm{stn}}^2 & 0 \\ 0 & 0 & \sigma_{\mathrm{stn}}^2 \end{bmatrix}, \tag{B.32}$$

where σ_{stn}^2 is the variance of each Cartesian component of the station position.

The GPS satellite covariance matrix is

$$\mathbf{C_{sv}} = \begin{bmatrix} \sigma_{sv}^2 & 0 & \cdots & 0 \\ 0 & \sigma_{sv}^2 & \cdots & 0 \\ \vdots & \vdots & \ddots & 0 \\ 0 & 0 & 0 & \sigma_{sv}^2 \end{bmatrix}, \tag{B.33}$$

where σ_{sv}^2 is the variance of each Cartesian component of each satellite's position.

Finally, the tropospheric noise terms can be represented by the zenith delay multiplied by the simple mapping function cosecant of the GPS satellite elevation angle. Therefore for the four GPS satellite, one epoch case

$$\mathbf{C_{tropP}} = \begin{bmatrix} \sigma_{trop}^2 / \sin\left(el_1^1\right) & 0 & 0 & 0 \\ 0 & \sigma_{trop}^2 / \sin\left(el_1^2\right) & 0 & 0 \\ 0 & 0 & \sigma_{trop}^2 / \sin\left(el_1^3\right) & 0 \\ 0 & 0 & 0 & \sigma_{trop}^2 / \sin\left(el_1^4\right) \end{bmatrix} \text{ and} \tag{B.34}$$

$$\mathbf{C_{trop\Phi}} = \begin{bmatrix} C_{tropP_{t-1}} & 0 \\ 0 & C_{tropP_t} \end{bmatrix}, \tag{B.35}$$

where σ_{trop}^2 is the residual zenith tropospheric variance and el_a^b is the elevation angle of GPS satellite "b" with respect to terrestrial receiver "a".

VITA

Candidate's full name: Sunil Balkaran Bisnath

Universities attended:

University of Toronto at Mississauga
3359 Mississauga Road North
Mississauga, Ontario, L5L 1C6
1989-1993
Hons. B.Sc., 1993, Surveying Science

University of Toronto at Mississauga
3359 Mississauga Road North
Mississauga, Ontario, L5L 1C6
1993-1995
M.Sc., 1995, Geography and Planning

University of New Brunswick
Post Office Box 4400
Fredericton, New Brunswick, E3B 5A3
1996-2002

Publications:

Bisnath, S., D. Wells, S. Howden, D. Dodd, D. Wiesenburg and G. Stone (2004). "Development of an operational RTK GPS-equipped buoy for tidal datum determination." *International Hydrographic Review*, Vol. 5, No. 1, pp. 76-86.

Bisnath, S.B. and R.B. Langley (2003). "CHAMP orbit determination with GPS phase-connected, precise point positioning." In *First CHAMP Mission Results for Gravity, Magnetic and Atmospheric Studies*, Eds. C. Reigber, H. Lür, P. Schwintzer, Springer, Berlin, pp. 59-64.

Bisnath, S.B. and R.B. Langley (2002). "High-precision platform-independent positioning with a single GPS receiver." *Journal of Navigation*, Vol. 29, No. 3, pp. 161-169.

Bisnath, S.B., T. Beran, R.B. Langley (2002). "Precise platform positioning with a single GPS receiver." *GPS World*, Vol. 13, No. 4, pp. 42-49.

Bisnath, S.B., D. Kim, and R.B. Langley (2001). "A new approach to an old problem: carrier-phase cycle slips." *GPS World*, Vol. 12, No. 5, pp. 46-51.

Bisnath, S.B. and R.B. Langley (1999). "Precise *a posteriori* geometric tracking of Low Earth Orbiters with GPS." *Canadian Aeronautics and Space Journal*, Vol. 45, No. 3, pp. 245-252.

Bisnath, S.B. and R.B. Langley (1999). *A Comparison of the Kinematic GPS and Aerotriangulation Results Completed for the New Brunswick Colour Softcopy Orthophotomap Data Base Project.* A study commissioned by WaterMark Industries Inc, March, 30 pp.

Bisnath, S.B. and R.B. Langley (1997). *Development of Specifications for the BOLAS GPS Receivers and Assessment of Feasibility of Phase Synchronizing an HF Interferometer Using GPS.* A study commissioned by Bristol Aerospace Limited, December, 38 pp.

Bisnath, S.B., J.P. Collins, and R.B. Langley (1997). *GPS Multipath Assessment of the Hibernia Oil Platform.* A study commissioned by Cougar Helicopters Ltd., July, 34 pp.

Bisnath, S.B. and R.B. Langley (1996). *Assessment of the GPS/MET TurboStar GPS Receiver for Orbit Determination of a Future CSA Micro/Small-Satellite Mission.* Final report for Space Technology Branch of the Canadian Space Agency, St-Hubert, Que. July, 188 pp.

Bisnath, S.B. (1995). *The Use of Positional Data from the Global Positioning System in Geographical Information System Applications.* M.Sc. dissertation, Programme in Geomatics, Department of Geography and Planning, University of Toronto.

Kingston, L.A. and S.B. Bisnath (1995): "Appendix B: Geodetic Monument Maintenance Report," In Wassef, A.M. and G. Gracie. *The Need for Geodetic Monument Maintenance in Metropolitan Toronto*, Programme in Geomatics, University of Toronto.

Conference presentations:

Bisnath, S., D. Wells, S. Howden, and G. Stone (2003). "The use of a GPS-equipped buoy for water level determination." *Proceedings of OCEANS 2003*, 22-26 September, San Diego, California, MTS / IEEE. p. 1241-1246.

Bisnath, S., D. Wells and D. Dodd (2003). "Evaluation of commercial carrier phase-based WADGPS services for marine applications." *Proceedings of The Institute of Navigation International Technical Meeting ION GPS / GNSS 2003*, 9-12 September, Portland, Oregon, The Institute of Navigation. p. 17-27.

Bisnath, S., D. Wells, S. Howden, D. Dodd, D. Wiesenburg and G. Stone (2003). "Development of an operational RTK GPS-equipped buoy for water level recovery." *Proceedings of The Institute of Navigation International Technical Meeting ION GPS / GNSS 2003*, 9-12 September, Portland, Oregon, The Institute of Navigation. p. 59-66.

Bisnath, S., D. Dodd and D. Wells (2003). "Evaluation of recent developments in high-precision GPS correction services." *Proceedings of the U.S. Hydrographic Conference 2003*, 24-27 March, Biloxi, Mississippi, The Hydrographic Society of America.

Bisnath, S., D. Dodd, D. Wells, S. Howden, D. Wiesenburg and G. Stone (2003). "Water level recovery with an RTK GPS-equipped buoy." *Proceedings of the U.S. Hydrographic Conference 2003*, 24-27 March, Biloxi, Mississippi, The Hydrographic Society of America.

Bisnath, S.B. and R.B. Langley (2001). "High-precision platform positioning with a single GPS Receiver." *Proceedings of ION GPS 2001, The 14th International Technical Meeting of The Institute of Navigation*, Salt Lake City, Utah, 11-14 September 2001, pp. 2585-2593.

Bisnath, S.B. and R.B. Langley (2001). "GPS phase-connected, precise point positioning of Low Earth Orbiters." *Proceedings of the GNSS 2001 Global Navigation Satellite Systems Conference*, Spanish Institute of Navigation, 8-11 May, Seville, Spain.

Bisnath, S.B. and R.B. Langley (2001). "Pseudorange multipath mitigation by means of multipath monitoring and de-weighting." *Proceedings of the International Symposium on Kinematic Systems in Geodesy, Geomatics and Navigation (KIS 2001)*, Banff, Alberta, 5-8 June 2001, pp. 392-400.

Bisnath, S.B. and R.B. Langley (2001). "Precise Orbit Determination of Low Earth Orbiters with GPS point positioning." *Proceedings of The Institute of Navigation National Technical Meeting 2001*, Institute of Navigation, 22-24 January, Long Beach, Calif., U.S.A., pp. 725-733.

Bisnath, S.B. (2000). "Efficient, automated cycle-slip correction of dual-frequency kinematic GPS data." *Proceedings of ION GPS 2000*, the 13th International Technical Meeting of The Institute of Navigation, Salt Lake City, Utah, 19-22 September 2000, pp. 145-154.

Langley, R.B., H. Jannasch, B. Peeters, and S. Bisnath (2000). "The GPS broadcast orbits: An accuracy analysis." *Proceeding of the 33rd COSPAR Scientific Assembly*, Warsaw, 16-23 July 2000.

Bisnath, S.B. and R.B. Langley (2000). "Automated cycle-slip correction of dual-frequency kinematic GPS data." *Proceedings of the 47th Annual Conference of the Canadian Aeronautics and Space Institute*, Ottawa, 30 April - 3 May 2000, pp. 121-125.

Bisnath, S.B. and R.B. Langley (1999). "Precise, efficient GPS-based geometric tracking of Low Earth Orbiters." *Proceedings of the 55th Annual Meeting of the Institute of Navigation*, Institute of Navigation, 28-30 June, Cambridge, Mass., U.S.A., pp. 751-760.

Bisnath, S.B. and R.B. Langley (1998). "Precise *a posteriori* geometric tracking of Low Earth Orbiters with GPS." *Proceedings of the 45th Annual Conference of the Canadian Aeronautics and Space Institute*, 10-13 May, Calgary, Alta.

Bisnath, S.B. and R.B. Langley (1997). "An introduction to the proposed BOLAS mission for ionospheric research." Presented at the *IGS Analysis Center Workshop*, Jet Propulsion Laboratory, Pasadena, Calif., U.S.A., 12-14 March.

Bisnath, S.B., V.B. Mendes and R.B. Langley (1997). "Effects of tropospheric mapping functions on space geodetic data." Prepared for the *IGS Analysis Center Workshop*, Jet Propulsion Laboratory, Pasadena, Calif., U.S.A., 12-14 March.